Shear flow instabilities in pipes and channels

a thesis presented for the degree of

Doctor of Philosophy of Imperial College London

and the

Diploma of Imperial College

by

Matthew Gipon

Department of Mathematics

Imperial College

180 Queen's Gate, London SW7 2BZ

March 2018

I certify that this thesis, and the research to which it refers, are the product of my own work, and that any ideas or quotations from the work of other people, published or otherwise, are fully acknowledged in accordance with the standard referencing practices of the discipline.

Copyright

The copyright of this thesis rests with the author and is made available under a Creative Commons Attribution Non-Commercial No Derivatives licence. Researchers are free to copy, distribute or transmit the thesis on the condition that they attribute it, that they do not use it for commercial purposes and that they do not alter, transform or build upon it. For any reuse or redistribution, researchers must make clear to others the licence terms of this work.

Thesis supervisor: Professor Professor Philip Hall Matthew Gipon

Shear flow instabilities in pipes and channels

Abstract

Two broad problems are considered in this thesis. The first investigation focuses on the spatial stability of pressure driven flow in a pipe, while the second problem is concerned with temporal stability of Couette flow in a parallel wall channel. A similar approach is taken with both halves of this thesis: an asymptotic analytical model is developed and this is then solved with numerical methods.

The prominent problem in the first chapter is Hagen-Poiseuille flow with suction and injection on the pipe wall boundary. The flow is fully developed in the axial direction and the suction acts radially at the wall while the other boundary conditions are no-slip. The flow is perturbed by a small non-axisymmetric disturbance and this configuration is solved in the radial-azimuthal plane. The results are provided for 2π-periodic suction and it is found that the non-parallel base flow is unstable in certain conditions. The suction coefficient is varied but the critical Reynolds number is found to be the same. A weakly nonlinear stability analysis reveals that there is a finite amplitude solution in the supercritical region.

The second chapter presents the vortex-wave interaction equations and a special case of the model is created to seek stationary, equilibrium solutions of the sinuous wave disturbance in Couette flow. The flow is initiated with an artificial forcing which has the sinusoidal symmetries embedded. From this initial condition the 'roll' problem is solved and the 'streak' can be found from this solution. The wave on this streak has Reynolds stresses which now force the 'roll'. The amplitude of the wave is varied and the system is iterated until the wave is neutral. This equilibrium configuration is then marched forward in time and studied. The solutions agree with numerical

Thesis supervisor: Professor Professor Philip Hall Matthew Gipon

calculations and experiments.

Acknowledgments

I would like to thank my supervisor Professor Philip Hall for his guidance throughout my studies and the opportunities he has provided to me. The time and help given to me by Dr Shahid Mughal has also been greatly appreciated.

I am grateful for the financial support to enable me to work on this research from the Engineering and Physical Sciences Research Council (EPSRC) and Airbus UK and EADS Innovation Works.

Contents

1 Introduction **1**

1.1 Transition to turbulence 1

1.2 Linear stability theory 3

1.3 Nonlinear stability theory 5

1.4 Large Reynolds number theory 6

1.5 Stability of shear flows 8

1.5.1 Pipe flow 9

1.5.2 Concentric cylinders and Taylor vortices 11

1.5.3 Introducing perturbations to flows 12

1.5.4 Triple deck theory 13

1.5.5 Vortex-wave interactions and self-sustained processes . 14

1.6 Thesis summary 18

2 Numerical methods **20**

2.1 Finite difference methods 20

2.2 Chebyshev and Fourier spectral methods 21

2.3 Cylindrical geometry and coordinate singularity 24

2.4 Linear and nonlinear systems of equations 26

2.5 Solving eigenvalue problems 27

2.6 Numerical convergence 28

3 Pipe flow problems **33**

3.1 Non-dimensionalised Navier-Stokes equations in cylindrical coordinates 35

3.2 Pipe flow with solid wall boundaries 37
3.2.1 Introduction and formulation 37
3.2.2 Linear spatial stability of circular pipe flow 39
3.2.3 Numerical method for the stability analysis 41
3.2.4 Stability results for circular pipe flow 42
3.2.5 Conclusions 47
3.3 Pipe flow with suction at the boundaries 49
3.3.1 Introduction 49
3.3.2 Formulation 50
3.3.3 Two-dimensional swirl flow in a pipe with suction . . . 52
3.3.4 Axial flow in a pipe with suction 56
3.3.5 Linear spatial stability of pipe flow with suction 59
3.3.6 Linear stability results for 2π-periodic suction 62
3.3.7 Weakly nonlinear spatial stability 69
3.3.8 Conclusions 81

4 Parallel wall channel flows **83**
4.1 Flow between concentric cylinders and Taylor vortices 86
4.1.1 Introduction and formulation 86
4.1.2 Numerical methods 90
4.1.3 Linear stability results 91
4.1.4 Nonlinear stability results 93
4.1.5 Conclusions 95
4.2 Three dimensional vortex-wave interaction equilibria 97
4.2.1 Introduction 97
4.2.2 Couette flow formulation 103
4.2.3 Vortex-wave interaction equations 105
4.2.4 Special case of the vortex-wave interaction equations . 111

4.2.5 The sinuous instability mode 116
4.2.6 Numerics of the vortex-wave interaction equations . . . 117
4.2.7 Solving the wave problem and correcting the wave amplitude 121
4.2.8 Results 123
4.2.9 Time periodic solutions 130
4.2.10 Conclusions 132

5 Conclusion **139**

Appendix A Weakly nonlinear equations **143**
A.1 The zeroth harmonic 146
A.2 The second harmonic 148
A.3 The first harmonic correction 149
A.4 The adjoint problem and the solvability condition 151

References **153**

List of figures

1.1 Reynolds'[41] sketches of flow in a pipe. The upper most version shows a streak of colour continues in a straight line at low velocity. The middle version reveals that at a greater velocity the colour will mix with the rest of the fluid downstream of the intake. The lowest version shows the eddies and curls that appear in the fluid before it's fully mixed. 8

1.2 Schematic of triple-deck structure. 13

1.3 Iso-contours at different positions in the longitudinal direction of the mean streamwise velocity in the wall normal-spanwise plane. Nine contours are plotted with velocities of $U/U_\infty, = 0.1, 0.2, ..., 0.9$. From Swearingen & Blackwelder[48]. 15

1.4 Vortex-wave interaction in plane Couette flow. The rolls in (a) drive the streak in (b). By linearizing the Navier-Stokes equations about the streak a solution to the wave problem can be found (c). The wave is forced to equilibrium by modifying the wave amplitude ρ and the Reynolds stresses of the wave (d) force the roll. From Blackburn, Hall & Sherwin[3]. 18

3.1 The streamwise velocity in circular pipe flow. 39

3.2 The eigenvalue solutions of circular pipe flow when $\omega = 1$ and $R = 2000$. The least stable eigenvalue, circled in red, is the $n = 1$ eigenmode. 43

3.3 Variation of growth rate and wavenumber for the least stable eigenvalue, mode $n = 1$, for circular pipe flow. Wavenumber (blue) and growth rate (green) when $\omega = 0.5$. Wavenumber (red) and growth rate (black) when $\omega = 1.0$. 44

3.4 Circular pipe flow least stable mode $n = 1$ eigenfunctions plotted against the radius. (V top left, W top right, U bottom left, P bottom right - real part (blue circles), imaginary part (red stars)). $R = 5000$, $\omega = 0.1$. 45

3.5 Disturbance profiles for Hagen-Poiseuille flow. Plots on the left when $\omega = 0.001$ and $R = 10000$, on the right $\omega = 0.1$ and $R = 20000$. 46

3.6 The velocity disturbance, the streamwise component (colour scale) and the streamlines of the radial and azimuthal components (arrows), when $\omega = 1.$ and $R = 20000$. The plot is focused in the area 0.35 radius lengths from the centre of the pipe. 47

3.7 Circular pipe flow $R = 10000$ with 2π-periodic and $\lambda = 5$ suction. $(v(1, \theta) = 5cos(\theta))$. 56

3.8 Circular pipe flow $R = 10000$ with 2π-periodic and $\lambda = 5$ suction. $(v(1, \theta) = 5cos(2\theta))$. 56

3.9 Circular pipe flow $R = 10000$ with $3\pi/2$-periodic and $\lambda = 5$ suction. $(v(1, \theta) = 5cos(3\theta))$. 57

3.10 The streamwise velocity in circular pipe flow with 2π-periodic suction. $v(1, \theta) = \lambda cos(\theta)$ on the pipe wall. (Same scales). . . 58

3.11 The streamwise velocity in circular pipe flow at $\theta = 0$ with varying λ. 58

3.12 The streamwise velocity in circular pipe flow with varying suction periodicity. $R = 10000$, $\lambda = 5$. Where $v(1, \theta) = \lambda cos(m\theta)$ is the non-zero boundary condition on the pipe wall. 59

3.13 Neutral curve plots for pipe flow with suction at varying suction coefficients. 63

3.14 Colour plot for growth rates and neutral curves (same scales). a) λ=0, b) λ=5, c) λ=7.5, d) λ=10. 64

3.15 Growth rate plotted against a) frequencies at $R = 6000$, b) Reynolds number at $\omega = 0.5$. $\lambda = 10$. 65

3.16 Comparison of streamwise disturbance profiles in pipe flow with 2π-periodic suction when $\omega = 0.4$, $\lambda = 10$. White line indicates where $\alpha_r u = \omega$. 66

3.17 Comparison of streamwise disturbance profiles in pipe flow with 2π-periodic suction when $R = 20000$, $\lambda = 10$. White line indicates where $\alpha_r u = \omega$. 67

3.18 Frequency against wavenumber on the neutral curve for pipe flow with 2π-periodic suction and $\lambda = 5$. 68

3.19 Streamwise velocity maximum (blue circles) and phase velocity (red dots) against suction coefficient λ for pipe flow with 2π-periodic suction. 69

3.20 Sketches for the behaviour of $|A|^2$. Blue is the case $\beta_{1r}R_1 > 0$, $\beta_{2r} < 0$, and the two variations of red are for the cases $\beta_{1r}R_1 < 0$, $\beta_{2r} > 0$. (When C is chosen to be positive.) 73

3.21 Weakly nonlinear stability of pipe flow with suction. Supercritical case, $R > R_c$. 78

3.22 Weakly nonlinear stability of pipe flow with suction. Subcritical case, $R < R_c$. 79

3.23 The ratio of $\beta_{1r}(R - R_c)$ to the growth rate from linear theory, over a range of disturbance frequencies, ω. 80

4.1 Critical Taylor number against wavenumber from the linear equations. 92

4.2 Radial disturbance velocity taken at π in the azimuthal direction. 92

4.3 Vector field plot of axially periodic Taylor vortices. 93

4.4 Maximum radial disturbance velocity against time for flow between concentric cylinders. (Linear stability analysis.) Blue: $T = 3389.9$; Green: $T = 3289.9$; Red: $T = 3489.9$. 94

4.5 Maximum radial disturbance velocity against time for flow between concentric cylinders. (Nonlinear stability analysis.) Green: $T = 3289.9$; Blue: $T = 3440.0$; Red: $T = 3489.9$; Cyan: $T = 3540.0$. . . 95

4.6 The vortex velocity field made up of a streak u and rolls v, w. The colour scale refers to the streak and rolls are depicted by arrows. $\alpha = 0.8, 1.0, 1.2$ in the top, middle and bottom plots respectively. $R = 10000$. 124

4.7 The equilibrium critical layers $y = f(z)$ where the streak velocity equals the wavespeed $u = c$, which equal zero in this situation. $\alpha = 0.8$ is the blue line, $\alpha = 1.0$ is the black line, and $\alpha = 1.2$ is the red line. $R = 10000$. 125

4.8 Convergence in time of the wave amplitude ρ for the lower branch steady solution. $\alpha = 1.0$, $R = 10000$. 126

4.9 Longitudinal (left), radial (middle) and spanwise (right) disturbance velocity components in half spanwise period. The arrows describe the vortex roll and the white line is the critical layer. . . . 127

4.10 Convergence in time of the wave amplitude ρ for the upper branch steady solution. $\alpha = 1.0$, $R = 10000$. 128

4.11 Panel (a) is the upper branch equilibrium solution for $\alpha = 0.8$. Panel (b) is the upper branch for $\alpha = 1.0$. Panel (c) is the lower branch for $\alpha = 0.8$. Panel (d) is the lower branch for $\alpha = 1.0$. Upper plots: vortex system, with the colour scale for the streak u and the arrows for the rolls v, w. Lower plots: magnitude of the wave Reynolds stress. $R = 10000$. 129

4.12 Plots of the magnitude of the wave Reynolds stress for converged lower branch equilibrium solutions with varying number of collocation points in the wall normal direction. From top to bottom: 46 points, 50, 54, 58. 24 points in the spanwise direction. $\alpha = 1.0$, $R = 10000$. 133

4.13 Plots of the magnitude of the wave Reynolds stress for converged lower branch equilibrium solutions with varying number of collocation points in the spanwise direction. From top to bottom: 20 points, 24, 28, 32. 50 points in the wall normal direction. $\alpha = 1.0$, $R = 10000$. 134

4.14 Plots of the magnitude of the wave Reynolds stress for converged upper branch equilibrium solutions with varying number of collocation points the wall normal direction. From top to bottom: 46 points, 50, 54, 58. 24 points in the spanwise direction. $\alpha = 1.0$, $R = 10000$. 135

4.15 Plots of the magnitude of the wave Reynolds stress for converged upper branch equilibrium solutions with varying number of collocation points the spanwise direction. From top to bottom: 20 points, 24, 28, 32. 50 points in the wall normal direction. $\alpha = 1.0$, $R = 10000$. 136

List of tables

2.1 The disturbance growth rate for non-parallel pipe flow with 2π-periodic suction boundary conditions. Reynolds number, $R = 10000$, wave frequency, $\omega = 0.5$, and the suction coefficient, $\lambda = 10$. 29

2.2 The converged value of the radial disturbance velocity for flow between concentric cylinders from the nonlinear stability equations when the system is at equilibrium. Taylor number, $T = 3440$. . . . 30

2.3 The converged wave amplitude, ρ, for the lower branch equilibrium solutions to the vortex-wave interaction equations against the number of collocation points in the wall normal and spanwise directions. Reynolds number, $R = 10000$, and wavenumber, $\alpha = 1.0$. 30

2.4 The converged wave amplitude, ρ, for the upper branch equilibrium solutions to the vortex-wave interaction equations against the number of collocation points in the wall normal and spanwise directions. Reynolds number, $R = 10000$, and wavenumber, $\alpha = 1.0$. 31

2.5 Time in seconds it takes on average to solve one iteration of the full vortex-wave interaction system for the special case numerically. 50 wall normal and 24 spanwise points were used to calculate the majority of solutions in Chapter 4. Reynolds number, $R = 10000$, and wavenumber, $\alpha = 1.0$. 32

4.1 Nonlinear amplitude effects. A comparison of Taylor number, equilibrium radial velocity and time taken to reach 99% of equilibrium velocity value. 96

4.2 The lower branch equilibrium amplitude ρ and the wall drag as a function of α calculated for this thesis compared to the wall drag calculated by Deguchi & Hall[9]. $R = 10000$. 125

4.3 The amplitude ρ and the wall drag for lower and upper branch vortex-wave interaction equilibrium solutions as a function of α. The results calculated for this thesis are compared against the wall drag calculated by Deguchi & Hall[9] which were shared in a private communication. $R = 10000$. 128

4.4 The converged amplitude ρ for the lower branch equilibrium solutions to the vortex-wave interaction equations against the Reynolds number. $\alpha = 1.0$. 131

1

Introduction

This thesis is concerned with understanding the stability properties of several shear flows but the broader context is the field of transition to turbulence. The first section in this introduction describes why transition is interesting mathematically, why it is a significant problem in the wider world and what is already known about the process. The following sections of the introduction cover some of the theoretical approaches used in this thesis. These topics are hydrodynamic linear stability theory, nonlinear stability theory and large Reynolds number asymptotics. This is followed by a description of the types of shear flows that are studied here and the interaction these flows have with wave disturbances. The introduction is completed by a summary of the thesis and the findings.

1.1 Transition to turbulence

Ultimately this thesis is concerned with adding to the body of work that is attempting to understand turbulence and transition to turbulence mathematically. It makes sense to begin with a section which describes the problem and previous literature before the mathematical framework for approaching

this problem is discussed.

Transition from streamline laminar to chaotic turbulent flow is of major interest in fluid dynamics research but also of practical importance in the marine, aerospace and biological industries. Drag is generally increased by turbulence and, taking the example of air flowing over a body such as an aeroplane wing, if the distance of laminar flow can be extended or the flow can be relaminarised then the amount of drag is reduced and efficiency increased. Turbulence is a highly nonlinear process and it is still not fully understood. It is believed that a better grasp of the underlying structures in wall-bounded turbulent flow, such as three-dimensional, nonlinear traveling wave solutions of the Navier-Stokes equations, will allow for progress to made in this field.

The process of transition to turbulence has been described several times before but it is worthwhile to review the stages here in the context of shear flows. The first phase is receptivity, where an external environmental disturbance excites a perturbation of the same frequency and scale. In a channel flow, for example, the perturbation will be triggered close to the channel wall, the viscous boundary layer. In many cases the disturbance is small and is called a primary mode. These disturbances are captured by linear stability theory and, although there are different types, the normal-mode instability will be the focus of much of the discussion in this thesis. This instability is a wave ansatz, where the disturbance profile is independent of time and the streamwise direction. In bounded shear flows this instability is often referred to as the Tollmien-Schlichting wave. These disturbances are known to play an important role in the transition of several interesting flows.

The primary perturbations are so small that they do not interact with the mean flow and therefore do not excite transition alone but if they grow in time or downstream in the flow then nonlinear behaviour can lead to secondary instabilities. This will quickly lead to a breakdown of the laminar flow into turbulence. Transition can also be initiated when the disturbances are large and distort the mean flow directly, and this is known as bypass transition.

Waleffe[52,54], in particular, approached the problem of understanding turbulent flow through dynamical systems. In this theory, which he demonstrated

with Couette flow but is applicable to all shear flows, there are structures that have a central role in turbulence but breakdown if the flow returns to a laminar state. These structures are exact equilibrium solutions of the Navier-Stokes equations and are called exact coherent structures. These structures are not small and are relevant to bypass transition, and these equilibrium systems are known as self-sustained processes. Waleffe's approach is concerned with understanding the structures that maintain turbulent flow.

These exact coherent states can be found computationally by direct numerical simulations but this method is inefficient it and neglects known asymptotic relationships. The challenge to fully describe these solutions of the Navier-Stokes equations with mathematical theory still exists. The subject of vortex-wave interactions reveals that fixed scalings exist for some shear flows and disturbances that can achieve equilibrium. For Couette flow these scalings have been found to show good agreement to the coherent structures.

1.2 Linear stability theory

The starting point for the mathematical framework to solve these problems is linear stability theory. Linear stability theory for hydrodynamic problems is rooted in the idea of perturbing the basic state of a flow and seeing how a small disturbance responds. These disturbances, or perturbations, are small compared to the size of the base flow and the stability is a question of whether or not these disturbances grow or decay. Small disturbances are an appropriate place to start an analysis of flow stability and the product of infinitesimal perturbations can be considered negligible. Being able to ignore the nonlinear terms in the Navier-Stokes equations about the base flow is what is termed linearization. Of course, small disturbances are not a valid assumption in all hydrodynamic problems but in this thesis the first, and sometimes the only, stability analysis is linear.

One limitation of linear stability theory is that it reveals nothing about the behaviour of the disturbance as it becomes large and therefore nothing about the nonlinear interaction with the mean flow. While disturbances are small the most dominant typically take a wave-like form, where each disturbance

has a particular frequency and wavelength. Consider a two-dimensional perturbation, δ, to a flow in a channel, where x is the streamwise direction and y is the wall normal direction,

$$\delta(x, y) = \Delta(y)e^{i\alpha(x-ct)} + c.c., \tag{1.1}$$

here the disturbance shape Δ is only a function of y, while there is a complex wavenumber α and a complex wave speed c, and '$c.c.$' denotes complex conjugate. For a base flow parallel to some wall boundary, where x is the streamwise direction, this disturbance is known as the Tollmien-Schlichting wave. The Tollmien-Schlichting wave appears in several flows as they transition from laminar to turbulent states. In disturbance problems of this type there can be a critical layer where the scaled streamwise velocity, u, is equal to the scaled wave speed and the growth rate is zero. Different modes have different critical layers and these play a role in understanding the stability of a flow. In the case of inviscid Rayleigh flows the neutral wave frequency will be a singularity in the mathematical theory because of the removal of the viscous terms, as can be seen in Hall & Horseman[21]. At this point it worth highlighting the Reynolds number, R, which has a central role in the nondimensionalised Navier-Stokes equations and it is defined as the dimensionless ratio of inertial forces to viscous forces,

$$R = \frac{\rho v L}{\mu}, \tag{1.2}$$

where ρ is the density of the fluid, v is the maximum velocity of the flow, L is the characteristic length scale and μ is the dynamic viscosity.

The wave-like type of disturbances discussed in this section generate the Orr-Sommerfeld equation when the flow is viscous and parallel. In that equation the spatial or temporal eigenvalue can be calculated while the other parameter is fixed. The relationship is known as a dispersion relation. For a fixed

α the Reynolds number determines the temporal growth rate, $Im(c)$, for all modes. When the growth rate is less than zero the solution is stable and for a positive growth rate the solution is unstable. If there is a least stable mode with zero growth, and therefore the flow is in equilibrium, this is said to be the critical Reynolds number. For Plane Poiseuille flow Orszag[36] showed the that critical Reynolds number for the Orr-Sommerfeld equation is $R = 5772.2$. This critical value would hold true if the model was extended to three-dimensions by virtue of Squire's theorem[44], which states that in boundary layers the least stable mode is two-dimensional. Interestingly, Hagen-Poiseuille flow in a circular pipe has not been shown to be linearly unstable for any Reynolds numbers. This result is contrary to what is found in experiments and reveals another limitation of linear theory and the need for nonlinear considerations. Poiseuille flow in a pipe is studied in this thesis and the subject is reviewed later in the introduction.

1.3 Nonlinear stability theory

Linear stability theory gives insight into the critical point about which a flow becomes unstable and the type of disturbances that cause this but to gain an understanding into transition to turbulence nonlinear terms must be considered. In an analytical investigation a full nonlinear stability analysis is unfeasible but there are several different approaches to nonlinear stability investigations. In this thesis the wave-like perturbation approach, similar to linear stability theory, is used. This type of nonlinear theory is only valid when the disturbance is still small and has been called weakly nonlinear theory. At the disturbance level the nonlinear terms in the Navier-Stokes equations are interactions between waves and therefore generate different harmonics. The zeroth harmonic, when the wave-like part of the disturbance is simply equal to 1, has the potential to interact and distort the mean flow if it has an amplitude term large enough, and this is the type of mechanism in that happens in transition.

This weakly nonlinear theory was initially postulated by Landau[32] and it states that near the linear stability neutral point a disturbance of finite size

has an amplitude $|A|$ which satisfies the following equation,

$$\frac{d|A|^2}{dt} = k_1|A|^2 + k_2|A|^4, \tag{1.3}$$

where k_1 and k_2 are constant coefficients.

Stuart[46] and Watson[56] solidified this theory and presented the nonlinear stability analysis of plane Poiseuille flow and Couette flow. Stuart[47] also delivered another paper concerned primarily with the nonlinear stability of Couette flow between concentric cylinders. In this paper Stuart attempts to gain a knowledge of the transition process by understanding the bifurcations from the laminar state to a more complicated but non-turbulent flow. It is possible to replicate these investigations for other shear flows and in this study a weakly nonlinear stability analysis of Poiseuille flow in a pipe with suction on the boundaries is conducted.

Nowadays it is possible to approach nonlinear problems with computational force. Instead of defining a perturbation which is wave-like the nonlinear disturbance problem can be solved completely numerically, typically using an iterative procedure. In this thesis the primary interests are stability rather than full transition and linear stability analysis is sufficient in most cases.

1.4 Large Reynolds number theory

Linear and weakly nonlinear stability are two methods for simplifing the analysis of flow stability but one approach for reducing the Navier-Stokes equations is to consider an asymptotically large Reynolds number. High Reynolds flows are common, such as airflow past an aircraft or water flowing past a ship, and when the Reynolds number is large the inertial forces are far greater than the viscous forces and the flow approaches the inviscid limit. In this limit the viscous terms can be dropped from the Navier-Stokes equations and when they are the resultant system is known as the Euler equations.

When the Reynolds number is large enough the flow away from a boundary or

wall is typically described by the inviscid equations but close to the boundary the viscosity has an important role in the dynamics. Prandtl[40] presented an analysis where the flow is separated into a region close to the wall, the boundary layer, and one in the far field. The boundary layer is dominated by viscous terms and most of the drag is generated here, and, as a consequence, the flow velocity is damped in this area. The advance by Prandtl is significant because it greatly reduces the Navier-Stokes equations in the boundary layer, while the outer region is simplified because it is inviscid. In the boundary layer the change in velocity and pressure in the wall normal direction is much faster than in the streamwise direction and to make the continuity equation balance the wall normal velocity must be small compared to the streamwise velocity.

When the streamwise component of a flow is much larger than in the other directions a reasonable assumption may seem to be parallel flow. A two-dimensional parallel flow combined with the wave-like linear instability of the last section leads to the Orr-Sommerfeld equation. Boundary layers are examples of where the mean flow can be approximated by a parallel flow because it is almost uni-directional but for most flows which approximate real-world siutions this simplification is invalid. For flows at large Reynolds numbers it is possible to scale the velocities using the Reynolds number, R. One of the scalings that occurs frequently for streamwise vortex flows is when the velocities in the wall normal direction, v, and spanwise direction, w, are proportional to the streamwise velocity, u, divided by the Reynolds number, or, $R(v, w) \propto u$.

These scales of the velocity components can result in equilibrium solutions such as in the work on Taylor vortices by Davey[5] and even Taylor's original investigations[49]. The scales were explored further in the many subsequent studies into Görtler vortices but the work of Hall & Smith[23,24,25,26] made significant strides in understanding these vortex-type flows and the interactions with wave-like disturbances. The scales of the longitudinal vortices are fairly straight forward to understand but the scales of the disturbance field are much more intricate. These relationships are covered in more detail in the vortex-wave interactions and self-sustained processes section but in these

problems the Reynolds number is always taken to be large.

Another feature of large Reynolds number flows is the localisation of the disturbance terms around the critical layer. As the critical layer is approached some linear disturbance terms become large and these are balanced with the viscous terms. In the study of vortex-wave interactions the disturbances drive the vortical flow and the critical layer is central to the interaction.

1.5 Stability of shear flows

A few approaches to the analysis and simplification of the Navier-Stokes equations have been discussed but the type of flows under consideration in this thesis have yet to be documented. Shear flows will be studied in the following chapters and these flows are driven by forces and can be characterised by adjacent layers of fluid moving with variable speeds. This class of flows includes Couette flow between parallel plates, which is driven by moving boundaries, and Hagen-Poiseuille flow in a circular pipe, which is driven by a pressure gradient. These two flows are studied in this thesis and both are linearly stable. However, it will be shown that instability occurs in these flows under certain conditions.

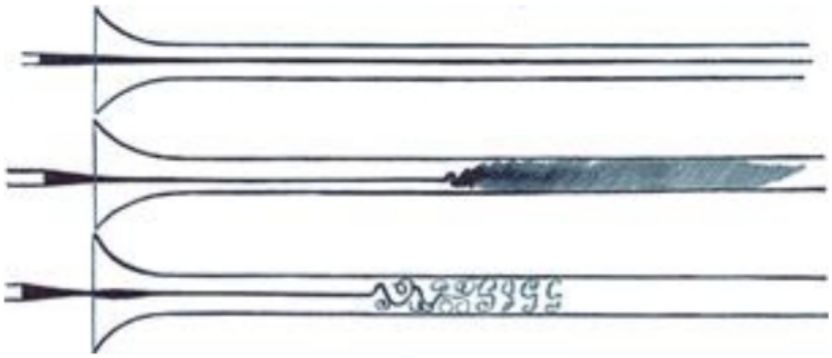


Figure 1.1: Reynolds'[41] sketches of flow in a pipe. The upper most version shows a streak of colour continues in a straight line at low velocity. The middle version reveals that at a greater velocity the colour will mix with the rest of the fluid downstream of the intake. The lowest version shows the eddies and curls that appear in the fluid before it's fully mixed.

Channel flows have been investigated since Reynolds[41] famously showed that fluid flow in a pipe becomes turbulent under certain conditions in an experiment, Figure 1.1. The mathematical theory explaining stability took a significant step forward when Taylor[49] used linear theory to demonstrate that flow between concentric cylinders could be unstable. In the following years research into channel flows covered stability of Taylor vortices, Görtler vortices, more sophisticated experiments and nonlinear theory. More recently these studies have been informative to the theories of vortex-wave interactions and self-sustained processes.

1.5.1 Pipe flow

Pipe flow is a major field of study in fluid dynamics today but the first rigorous research goes back to the 19th century. Hagen[17] and Poiseuille[39] almost simultaneously came up with the theoretical parallel flow in a pipe now known as Hagen-Poiseuille flow, which is an exact solution of the Navier-Stokes equations. A few years later Reynolds[41] conducted his famous experiments on flows in pipes, Figure 1.1. Reynolds noticed that flow in a pipe transitioned to turbulence under many conditions. This study led to the discovery of a dimensionless relationship between inertial and viscous forces that was key to the transition. The dimensionless ratio is now known as the Reynolds number.

The reason these flows are still studied today is because traditional linear stability theory for hydrodynamic problems suggests that Hagen-Poiseuille flow should always be stable. This traditional theory is the study of a flow as the sum of an $\mathcal{O}(1)$ base flow and an infinitesimal wave-like disturbance velocity field. A simple example of this theory is the Orr-Sommerfeld equation which is the resulting disturbance level equation for a viscous parallel flow. The main deficiency of the results from the Orr-Sommerfeld problem is the assumption of parallel flow, that the base flow uni-directional. It is clear that neglecting the nonlinear disturbance terms and the assumption of parallel flow simplify the stability analysis for pipe flow greatly.

Gill[16] presented an analysis of linear spatial and temporal stability of a vis-

cous incompressible fluid in a pipe and Davey & Drazin[7] conducted a similar study with their numerical approach. The results showed that infinitesimal axisymmetric disturbances were always stable in pipe flow and Garg & Rouleau[15] completed the analysis by concluding that non-axisymmetric disturbances are also always linearly spatially stable in pipe flow. The discussion in subsequent papers centred around finite-amplitude disturbances. At the forefront of this research were the papers by Davey & Nguyen[8], Itoh[28,29] and Davey[6]. The latter's paper was actually a review and comparison of the two former papers and found that there wasn't a conclusive theory that showed disturbances becoming unstable, although in certain situations eigenvalues could be shown to be unstable.

To broaden the study of pipe flows and attempt to find unstable solutions, Bansal[1] considered small suction solutions to the two-dimensional Navier-Stokes equations. Bansal found that for constant suction the axial flow component was damped and eventually reversed. This phenomenon can be attributed to the reduced mass of fluid in the pipe. Several other papers followed on the subject of pipe flows with alternative boundary conditions to the basic no-slip conditions and one interesting study was by Zaturska & Banks[58]. The authors combined suction with an accelerating wall and found an unstable region of conditions.

Moving away from analysis involving boundary conditions, Faisst & Eckhardt[12] used the ideas of self-sustained processes in the channel and applied them to pipe flow. Starting with a specific three dimensional flow initial condition in the pipe and imposing Tollmien-Schlichting type perturbations, the authors found a set of unstable three-dimensional travelling waves for Reynolds numbers greater than 1250. These wave solutions are claimed to be associated with intermittent transition to turbulence. Using a similar approach, Wedin & Kerswell[57] found a family of rotational symmetric travelling wave solutions. Using a numerical approach and an initial guess for the flow only can produce sporadic results, but Ozcakir[37] used fully numerical methods and the vortex-wave research of Hall & Sherwin[22] to set out a systematic process for finding vortex-wave solutions.

The method of Ozcakir[37] differed from the stimulated initial guesses of Faisst

& Eckhardt[12] and Wedin & Kerswell[57]. This method introduced alternate suction and injection at the boundary, which enabled the bifurcation from Poiseuille flow to other sustained states where the flow is neutrally stable. By scaling the suction on the Reynolds number the non-zero boundary condition becomes small as the R tends to infinity, and in this sense the flow is close Poiseuille flow. In a subsequent paper, Ozcakir et al[38] demonstrated that initializing the flow and wave solution with the suction and injection boundary condition, and then switching the wall condition to zero, they could recover the solutions of Wedin & Kerswell.

1.5.2 Concentric cylinders and Taylor vortices

The early work on shear flows focused on pipe flow but Taylor[49] decided to turn his interest to parallel channel flows in order to prove the idea of a critical flow velocity mathematically. He struggled to design a good channel flow model however and began to look at viscous incompressible flow between concentric cylinders. In this configuration one infinitely long cylinder sits inside another cylinder and one, or both, rotate with an angular velocity. Taylor managed to show that infinitesimal disturbances would grow under certain conditions. The perturbations formed cellular toroidal vortices spaced regularly along the axis of the cylinders. Taylor's experiments were successful too, confirming the same disturbance velocity arrangement but there were differences.

Taylor found that there is a critical velocity dependent on the relative sizes of the cylinders and type of fluid. This information is captured in the dimensionless quantity Taylor number, T, as it is now known. In the supercritical region of Taylor numbers the theory predicted that the disturbances would grow exponentially in time, while in subcritical conditions they would decay exponentially. According to Taylors experiments[49, 50] the subcritical cellular vortices would decay to zero, however the supercritical perturbations would reach a finite equilibrium rather than be continually amplified. The difference in results was attributed to the omission of the nonlinear disturbance terms.

Davey[5] used the nonlinear theory developed by Stuart[46] and Watson[56], a perturbation expansion including the harmonics, to study the concentric cylinders problem with nonlinear disturbances. He showed that mathematically it could be confirmed that the vortices attain a finite equilibrium amplitude in the supercritical case. Davey's study required that the amplification rate remains small but the results are valid for any gap width between the cylinders and any angular velocity.

Hall[18] specifically investigated the problem when the outer cylinder is static and the inner wall has an angular velocity, and the distance between the cylinders is small. In this study the angular velocity of the inner pipe is modulating by a small amount and this problem had been approached experimentally a few years earlier by Donnelly[11]. A key finding of Donnelly's was that the critical Taylor number at which Taylor vortex type flow appeared was higher than its unmodulated value. Hall's approach was theoretical in nature and he considered different asymptotic limits for the modulation. Some of Hall's results were contrary to Donnelly's findings but once again the nonlinear terms were found to play the crucial role in achieving finite amplitude equilibrium solutions.

The results of this classic problem are replicated in this thesis. The problem forms an appropriate bridge between pipe flows and parallel-wall channel flows as it did for Taylor. This problem is also a temporal problem and the stability analysis in the vortex-wave interactions is for the temporal eigenvalue. The method used in the investigation here is different to the ones previously mentioned. The linear problem is solved in a similar way to Hall[18] but the nonlinear analysis is a numerical iteration method rather than the analytical method of Hall. The details of the numerical approach are in subsection (4.1.2). The results of the model developed here confirm the critical Taylor number and the impact of including the nonlinear terms.

1.5.3 Introducing perturbations to flows

Taylor's work[49] and Davey's paper[5] highlighted some of the important relative scales that occur in the interactions between streamwise flows and

vortices. However, these systems crucially neglect the presence of a wave disturbance. Several experiments in the 1960s showed interactions between longitudinal vortices and waves, and later more experiments and numerical simulations followed. The phenomena has been seen in nature and is believed to be fundamental in the transition to turbulence. The longitudinal vortices are dominated by the longitudinal component, the $\mathcal{O}(1)$ 'streak', but are crucially combined with the small, $\mathcal{O}(R^{-1})$, where R is Reynolds number, 'roll'.

1.5.4 Triple deck theory

One problem which arose from the studies in the 1960s was the presence of singularities in boundary layer separation. Stewartson & Williams[45] and Neiland[35] first developed triple-deck analysis to handle these singularities but the theory has been used as a tool for solving many sophisticated flow problems since. The theory splits a flow into three tiers, with two inside the boundary layer and one outside, see Figure 1.2.

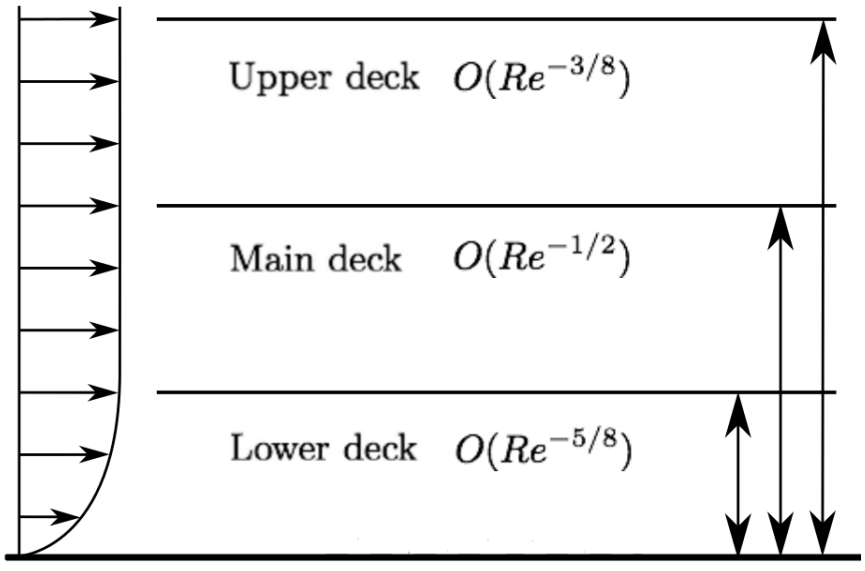


Figure 1.2: Schematic of triple-deck structure.

The bottom layer, the 'lower deck', is viscous and the relatively small velocity is subject to a displacement effect where pressure variations alter the flow

streamlines. The middle tier, the 'main deck', is the bulk of the boundary layer and is less responsive to pressure changes. The top layer, the 'upper deck', is an inviscid potential flow where a pressure force is induced by the deformed flow below. This pressure force in turn drives the velocity disturbances in the viscous flow below it. In this way triple-deck theory describes interactions between the boundary layer and the mean flow. The scaling of these layers is based on the Reynolds number, which has to be asymptotically large.

1.5.5 Vortex-wave interactions and self-sustained processes

The previous subsections have described historic approaches to solving shear flow problems in specific geometry. From this substantial collection of work came two theories: Vortex-wave interactions and self-sustained processes. These areas are still actively researched today and have shown promising results which could lead to a coherent explanation of instabilities and turbulence. These theories are also particularly useful for studying shear flow instabilities in pipes and channels.

Smith[43] revealed that Tollmien-Schlichting waves near the lower branch of the neutral stability curve are captured by an unsteady triple-deck model. This theory includes nonlinear effects, non-parallel flow and a mechanism for the mean flow to be altered, and compared to the Orr-Sommerfeld equation this triple-deck analysis was a real step forward.

This work was consolidated in the paper by Swearingen & Blackwelder[48]. The aim of that research was to experimentally model transition to turbulence and turbulent flat-wall boundary layer flows, with a particular focus on the structures which exist in the flow. The instabilities in the flow are introduced through a Görtler vortices generator. The authors found that the slow velocity at the wall is drawn up between the vortices and the instabilities scale with the shear-layer thickness and velocity difference, see Figure 1.3. Images of the secondary instabilities revealed horseshoe vortex and sinuous modes. Swearingen & Blackwelder commented that it is the sinuous oscillation mode which is the most pervasive and dominant in nature.

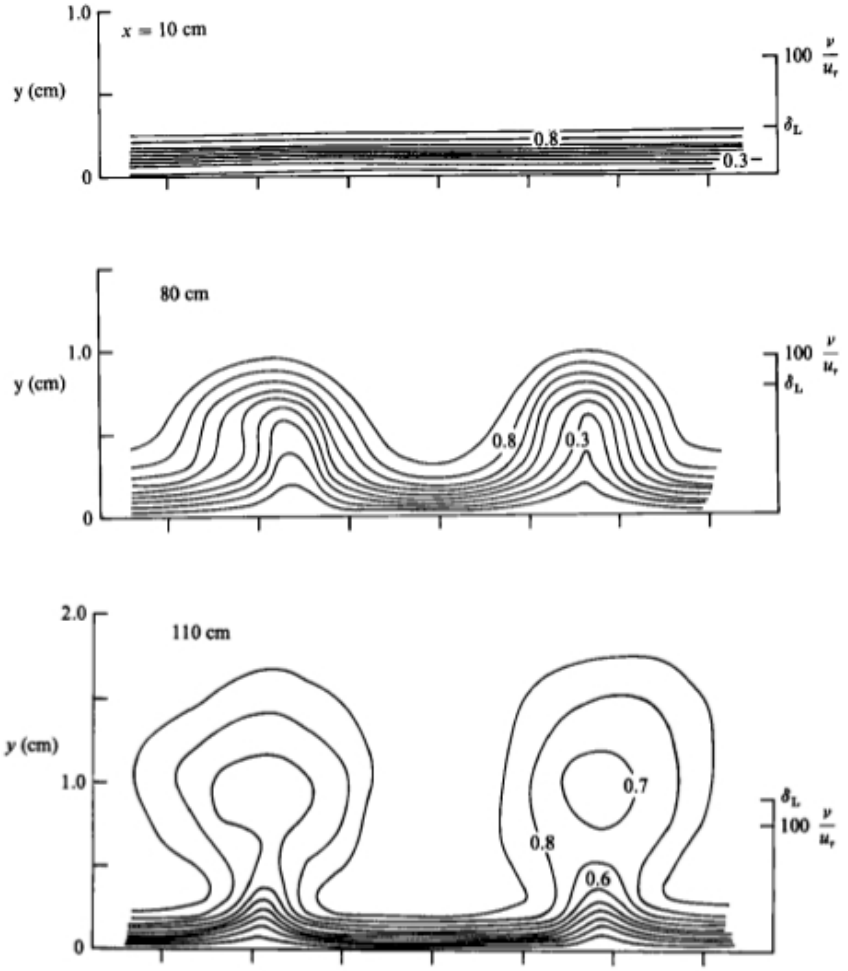


Figure 1.3: Iso-contours at different positions in the longitudinal direction of the mean streamwise velocity in the wall normal-spanwise plane. Nine contours are plotted with velocities of $U/U_\infty, = 0.1, 0.2, ..., 0.9$. From Swearingen & Blackwelder[48].

Following work of Swearingen & Blackwelder[48] was a paper by Hall & Smith[23] which considered the interaction between Tollmien-Schlichting instabilities and Görtler vortices in a curved channel. At initially low amplitudes the interaction caused the size of the instabilities to grow exponentially in finite time. Greater initial disturbance amplitudes lead to more complex evolution equations which are dependent on the orientation of the wavefronts. Crucially though, this interaction can take place in the absence of curvature, meaning that the vortices are completely driven by the wave.

Papers by Hall & Smith[23,24,25,26] presented a formal asymptotic framework for what is now called vortex-wave interaction theory. The framework is fully nonlinear, in that the mean flow is entirely changed from its unperturbed profile, and can be applied to both small amplitude inviscid Rayleigh waves and Tollmien-Schlichting waves, which interact with longitudinal vortices. These papers are concerned with boundary-layer flow and a triple-deck approach is used with a large Reynolds number assumed throughout. When these waves have neutral growth rate the system is in equilibrium in time. These waves are of the utmost interest because their interactions can be observed and followed in time. Using this theory the experiments of Swearingen & Blackwelder were verified mathematically in the work of Hall & Horseman[21].

Related computations were published by Waleffe[52], who focused on a sinusoidal shear flow. In this research the author found linearly stable self-sustaining states. The Reynolds number is taken to be finite and the production of the wave is generated by the linear instability of the streamwise velocity, the streak. The author noticed that the process was remarkably insensitive to the boundary conditions. Several other papers (Faisst & Eckhardt[12], Waleffe[54], Wedin & Kerswell[57]) on self-sustained processes at finite-R solutions followed.

Wang et al[55] confirmed numerically the relative scaling of the self-sustained processes for a plane Couette flow artificially forced initially and the importance of the linear stability of the streak. The paper concluded from numerical results that some equilibrium solutions have an exact coherent structure of $\mathcal{O}(1)$ streaks and $\mathcal{O}(R^{-1})$ rolls at large Reynolds numbers, and that the wave develops a critical layer where higher harmonics are infinitesimal. These solutions are the so-called 'lower branch' solutions, as there are further equilibrium states at higher Reynolds numbers, and it is claimed that these are edge states, where initial disturbances will either eventually become turbulent or stay laminar. These nonlinear equilibrium states are unstable and are located on a manifold. One side of the manifold is stable and here solutions decay to the laminar flow solution, while on the other side these states become turbulent. For smaller Reynolds numbers the edge state is larger and perturbed flows are more likely to be attracted to here than for

large Reynolds numbers.

Hall & Sherwin[22] managed to reconcile the theories of vortex-wave interactions and self-sustained processes. In theoretical half of that paper Couette flow was considered, as in Wang's work[55], with a sinusoidal neutral, stationary Rayleigh wave. The critical layer singularity was handled with asymptotic jump conditions. Hall & Sherwin followed previous work by having $\mathcal{O}(1)$ streaks and $\mathcal{O}(R^{-1})$ rolls and they found that when they adapted the theory described in Hall & Smith[26] the wave has amplitude of $R^{-7/6}$ away from the critical layer and amplitude of $R^{-5/6}$ at the critical layer. When these asymptotic limits for large Reynolds numbers were plotted against Wang's results the agreement was very good. This paper revealed that self-sustained equilibrium solutions were finite Reynolds number lower branch solutions of the vortex-wave interaction equations.

The paper by Blackburn, Hall & Sherwin[3] extended the work of Hall & Sherwin[22] to a range of spanwise wavenumbers and reveals that for small wavelengths the disturbances are localized to the centre of the flow. As these states feel no influence from the walls they are relevant to arbitrary shear flows. This paper also introduced the hybrid computational approach for calculating the forcing terms in the roll equations directly from the wave. For finite amplitude waves the averaged Reynolds stresses balance the dissipation in the rolls. Blackburn, Hall & Sherwin also elegantly described the interactions in their Figure 1. which has been reproduced here in Figure 1.4.

Up to this point the upper branch solutions have not been discussed. Wang[55] suggested that the lower branch equilibriums follow the $\mathcal{O}(R^{-1})$ vortex flow scaling at large Reynolds numbers but the upper branch states are not described. Hall & Sherwin[22] noted that the upper branch is usually inviscid but in this case the hybrid computational approach for the forcing may be able to capture the upper branch. Blackburn, Hall & Sherwin[3] called the upper branch equilibrium solutions 'organizing centres' about which the flow slowly cycles during the approach to turbulence. Deguchi & Hall[9] resolved the upper branch states with the same method as they did for the lower branch state. The authors found that the upper branch solution is of vortex-wave type, with the usual scalings, but where the wave is increasingly concen-

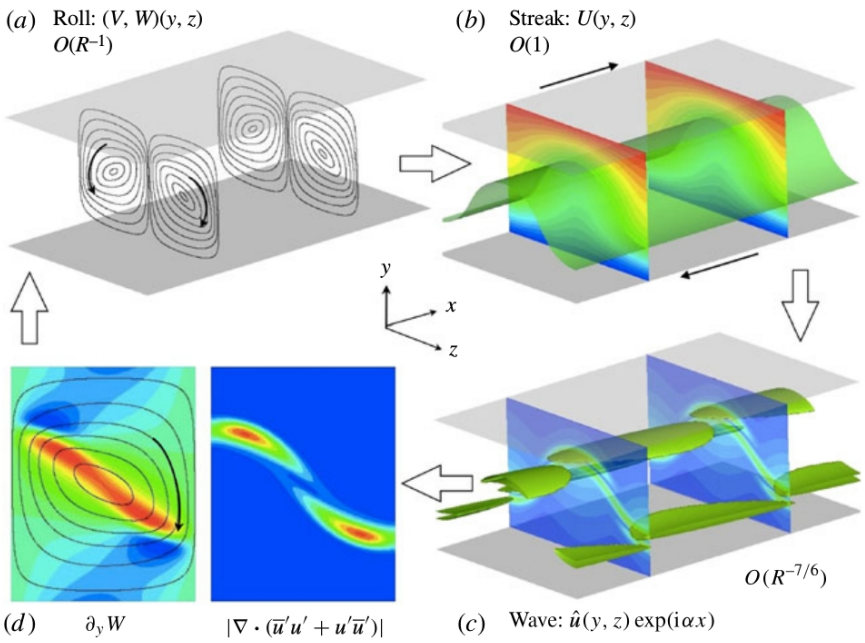


Figure 1.4: Vortex-wave interaction in plane Couette flow. The rolls in (a) drive the streak in (b). By linearizing the Navier-Stokes equations about the streak a solution to the wave problem can be found (c). The wave is forced to equilibrium by modifying the wave amplitude ρ and the Reynolds stresses of the wave (d) force the roll. From Blackburn, Hall & Sherwin[3].

trated vertically away from the critical layer rather than at the critical layer. Therefore the upper branch is also a steady solution and subject to the same symmetries as the lower branch.

1.6 Thesis summary

Thesis structure

This thesis has two main chapters. The first chapter is concerned with pipe flow problems and spatial stability analysis. This chapter has two sections and the first introduces the problem of Hagen-Poiseuille flow. This flow's stability properties are studied here, and the results are compared to previous literature. The second section in the first chapter considers Hagen-Poiseuille flow with suction on the pipe wall. This suction destabilises the flow and

several interesting results are documented.

The second chapter in this thesis tackles channel flow problems and considers temporal stability. The first problem investigated is Couette flow between two concentric cylinders. The disturbances to this flow are Taylor vortices and the solutions are followed to large time. The second problem in this chapter is also related to Couette flow but this time vortex-wave interaction theory is used to study the stability and equilibrium properties of the fluid flow.

The chapter immediately following this introduction describes the numerical methods developed for this thesis. In this chapter some preliminary results are discussed and the methods are validated.

Thesis objectives

This thesis seeks to establish new results in two broad problems of fluid dynamics: in non-parallel pipe flows and in vortex-wave interaction theory. These two problems are approached in similar ways in this thesis with a combination of asymptotic analysis and numerical methods. The first objective in each chapter is to develop and then validate a mathematical model on a relatively simple problem. This model will then be developed further to solve a more prominent problem.

In the first chapter the aim is to describe one reason why linear theory fails to predict that pipe flow becomes unstable under certain conditions. The approach taken here is two-fold: to use a base flow that does not conform to the parallel flow assumption and then use nonlinear stability theory to increase the understanding of the results.

The second chapter attempts to show that a special, reduced case of the vortex-wave interaction equations is sufficient to determine the main flow stability characteristics of Couette flow with a sinuous wave disturbance. The full vortex-wave interaction equations are described and then modifications are justified and applied. The results validate the model but are restricted to steady waves.

2

Numerical methods

Numerical methods have an important role in this thesis and modern mathematics. All of the problems tackled in this study require numerical methods at some point. This includes solving linear and nonlinear systems of equations, eigenvalue problems and more modest tasks such as integrating a vector. This section describes and validates the numerical methods used in this thesis.

For the differential problems there needs to be a method of expanding or approximating the functions and its derivatives. The two most common ways of doing this are called finite difference methods and spectral methods, and both of these ideas are used in this study. All the various techniques used in this thesis are outlined in the following subsections. In the following chapters, where a specific problem is under consideration, more details are given on how the numerical method was used in that situation.

2.1 Finite difference methods

In general, finite difference methods are not used extensively in this study. The common exception is when a solution is being 'stepped' forward in time

or space and there is a first order derivative in this variable. In some of the problems here a solution is sought at several spatial or temporal positions, the well-known Euler method for ordinary differential equations is used in these situations. The method is first-order, meaning that the error at each step is proportional to the square of the step size and the global error, at a specific time, is proportional to the step size. There are a number of variations on the Euler method and in this study the implicit, or backwards, Euler method is used. The scheme is described in equation (2.1),

$$y_{k+1} = y_k + hf\left(t_{k+1}, y_{k+1}\right), \tag{2.1}$$

where t is time, y is time dependent function, f is a function of t and y, h is the step size and k is the current step. The advantage of this scheme over the explicit method is that it removes the stability issues that affect the explicit Euler scheme. The implicit version is much more computationally costly as a coupled system of equations must be solved.

2.2 Chebyshev and Fourier spectral methods

Orszag[36] used Chebyshev polynomials to solve the Orr-Sommerfeld problem and argued that the method was superior to other numerical methods. The approach is more efficient in terms of time and memory than finite-difference schemes and increased accuracy can be gained with little extra effort. Orszag showed that Chebyshev polynomial approximations have an infinite order of accuracy, or, in other words, as the number of Chebyshev polynomials used, N, increases the errors tend to zero quicker than any power of $1/N$. This approach was used by Orszag for plane Poiseuille flow but he recommended it's use for all approximately parallel flows.

For the bulk of the differential problems in this thesis Chebyshev and Fourier spectral methods are employed. Boyd's text[4] gives a good summary of these methods and has been referred to several times in during this study. The concept of spectral methods is that an unknown function $y(x)$ can be expanded

and approximated by the sum of 'basis' functions $\Phi_n(x)$,

$$y(x) \approx y_N(x) = \sum_{n=0}^{N} c_n \Phi_n(x). \tag{2.2}$$

In the Chebyshev spectral method the basis functions are Chebyshev polynomials $T_n(x)$. These are a sequence of orthogonal polynomials which are subject to a three term recursive relationship. The first few terms and the general form of each term in the Chebyshev polynomials are described below,

$$\begin{aligned} T_0(x) &= 1, \\ T_1(x) &= x, \\ T_{n+1}(x) &= 2xT_n(x) - T_{n-1}(x). \end{aligned} \tag{2.3}$$

There are other, equivalent definitions of Chebyshev polynomials and they can be used in several ways for a wide range of problems. In this study a collocation, or pseudospectral, approach is used. The idea behind this approach is that the differential equation is solved exactly at these points. The larger N is the better the approximation of the function is away from these collocation points. These collocations points, x, can be chosen in different ways but here the Gauss-Lobatto points are used,

$$x = \cos\left(\frac{i\pi}{N-1}\right) \quad for \quad i = 0, ..., N-1. \tag{2.4}$$

These points are in the interval $[-1, 1]$ and clustered towards the end points, but they can be manipulated or redistributed if required. This is particularly useful when more accuracy is required in a specific area of the interval. Boundary conditions can be enforced in different ways with a Chebyshev spectral method. One choice, which is often used here, is to simply replace the equation at the boundary with the boundary condition. An alternative

choice is to modify the Chebyshev polynomials such that they automatically satisfy the conditions at the boundary. For example, if the boundary conditions are zero at each end point the Chebyshev polynomials can be multiplied by $(1 - x^2)$.

For the Fourier series the basis functions are trignometric. The general Fourier series is below,

$$y(x) = \sum_{n=-\infty}^{\infty} c_n \exp(inx) = a_0 + \sum_{n=1}^{\infty} a_n \cos(nx) + \sum_{n=1}^{\infty} b_n \sin(nx), \qquad (2.5)$$

with x in the interval $[-\pi, \pi]$ or $[0, 2\pi]$, which are equivalent because of periodicity. This property makes Fourier series ideal for solving problems with periodic boundary conditions, which are automatically satisfied by these basis functions. If $y(x)$ is symmetric then only the cosine terms are required and if $y(x)$ is antisymmetric only the sine terms are needed. If the basis functions are calculated at all the points in the interval the function expansions will be singular because of the periodicity. The remedy is to solve the problem in the half interval $x \in [0, \pi]$ and this has the favourable property of reducing the problem size by half.

These methods will be used to solve differential problems and the derivatives of the unknown functions must also be approximated. This is easy to do with spectral methods and the derivatives of the basis functions can be taken directly. The overall effect of this pseudospectral approach is to create a dense pseudospectral matrix for all the collocation points.

The most significant difference between spectral and finite difference methods is that the former uses global basis functions which are polynomials of high degree while the latter segments the interval into sub-intervals, where the basis functions are local and polynomials are of fixed degree.

Although the efficiency, in terms of accuracy versus computational time, of spectral and finite difference methods is similar, the spectral method has the great benefit that as N is increased the grid step size is decreased and the

order of the method is increased, giving it exponential convergence. To improve the accuracy of a finite difference method the step size can be decreased but to match spectral accuracy a higher order difference method needs to be implemented too. Furthermore the spectral method is memory minimising; Boyd[4] claims that for a crude calculation, where 5% error is acceptable, spectral methods use about half as many degrees of freedom in each dimension as a fourth order finite difference method.

Throughout this thesis the numerical methods used will be explained and justified. Broadly, Fourier series are used when the boundary conditions are periodic and Chebyshev methods are used elsewhere. Where functions are two dimensional, which is most of the time in this study, they can be decomposed in two directions with different, or the same, spectral approaches without hindrance. A two dimensional function might have the following sum of basis functions.

$$y(x,y) \approx \sum_{m=0}^{N} \sum_{n=-\infty}^{\infty} c_{m,n} T_m(x) \exp(iny). \tag{2.6}$$

2.3 Cylindrical geometry and coordinate singularity

Chapter 3 in this thesis is set in cylindrical geometry. To solve the issues that arise in these problems guidance is taken from Batchelor & Gill[2]. The authors of that paper formulate a version of the Navier-Stokes equations for a disturbance problem equivalent to the following set of equations here.

$$\begin{aligned} &i\alpha u U - i\omega U + V\frac{\partial u}{\partial r} + \frac{W}{r}\frac{\partial u}{\partial \theta} \\ &= -\alpha i P + \frac{1}{R}\left[\frac{1}{r}\frac{\partial U}{\partial r} + \frac{\partial^2 U}{\partial r^2} + \frac{1}{r^2}\frac{\partial^2 U}{\partial \theta^2} - \alpha^2 U\right], \end{aligned} \tag{2.7}$$

$$
\begin{aligned}
&i\alpha u V - i\omega V \\
&= -\frac{\partial P}{\partial r} + \frac{1}{R}\left[\frac{1}{r}\frac{\partial V}{\partial r} + \frac{\partial^2 V}{\partial r^2} + \frac{1}{r^2}\frac{\partial^2 V}{\partial \theta^2} - \frac{V}{r^2} - \frac{2}{r^2}\frac{\partial W}{\partial \theta} - \alpha^2 V\right], \qquad (2.8)
\end{aligned}
$$

$$
\begin{aligned}
&i\alpha u W - i\omega W \\
&= -\frac{1}{r}\frac{\partial P}{\partial \theta} + \frac{1}{R}\left[\frac{1}{r}\frac{\partial W}{\partial r} + \frac{\partial^2 W}{\partial r^2} + \frac{1}{r^2}\frac{\partial^2 W}{\partial \theta^2} - \frac{W}{r^2} + \frac{2}{r^2}\frac{\partial V}{\partial \theta} - \alpha^2 W\right], \qquad (2.9)
\end{aligned}
$$

$$
i\alpha U + \frac{1}{r}V + \frac{\partial V}{\partial r} + \frac{1}{r}\frac{\partial W}{\partial \theta} = 0, \qquad (2.10)
$$

where x is the distance in the axial direction, r is the distance in the radial direction, θ is the distance in the azimuthal direction, ($U(r,\theta)$,$V(r,\theta)$,$W(r,\theta)$) are the disturbance velocity components, $P(r,\theta)$ is the perturbation pressure, u is the axial base flow, α is the wavenumber, ω is the wave frequency and R is the Reynolds number.

Batchelor & Gill[2] described the boundary conditions for disturbances at the centre of a unidirectional flow in cylindrical geometry. A similar approach will be used for the boundary conditions here. At the pipe wall, $r = 1$, the conditions for the flow are the 'no-slip' conditions, and these can be written down directly:

$$
U(1,\theta), V(1,\theta), W(1,\theta) = 0. \qquad (2.11)
$$

At the centre of the pipe, $r = 0$, there is a coordinate singularity. The flow components can be expressed in terms of Fourier series in the azimuthal direction without limiting the form of the disturbance profile and each mode must be considered independently to obtain the correct solution,

$$U(0,\theta) = \sum_{n=-\infty}^{\infty} U_n(0)e^{in\theta},$$
$$V(0,\theta) = \sum_{n=-\infty}^{\infty} V_n(0)e^{in\theta}, W(0,\theta) = \sum_{n=-\infty}^{\infty} W_n(0)e^{in\theta}, \tag{2.12}$$
$$P(0,\theta) = \sum_{n=-\infty}^{\infty} P_n(0)e^{in\theta}.$$

The coordinate system requires that U and P should be independent of θ at $r = 0$. For that reason

$$U_n(0) = 0, \quad P_n(0) = 0 \quad for \quad n \neq 0. \tag{2.13}$$

For the Fourier mode $n = 0$, as $r \to 0$ the equation (2.7) has the unbounded term $\frac{1}{r}\frac{\partial U_0}{\partial r}$. To handle this issue the condition $\frac{\partial U_0}{\partial r} = 0$ is enforced for this mode. At $n = 0$, P_0 can be found in terms of the other disturbance profiles.

The coordinate system requires that V and W act sinusoidally at the centre of the pipe. The continuity equation (2.10) at the centre of the pipe where the Fourier mode is $n = 1$ has the following form

$$V_1(0) + iW_1(0) = 0. \tag{2.14}$$

Setting this as the boundary condition for V and W achives this sinusoidal behaviour. All other Fourier modes for the radial and azimuthal components at the centre of the pipe are simply zero, $V_n, W_n = 0$ for $n \neq 1$.

2.4 Linear and nonlinear systems of equations

For linear problems decomposed into basis functions the task becomes one of solving a pseudospectral matrix for a linear system of equations. In this study the LAPACK linear algebra package of routines was used to solve

these types of systems. The approach of these routines is to implement an LU decomposition and this is possible for real and complex systems.

Nonlinear problems are more complicated. The general approach is to approximate the nonlinear terms by some means. In this study nonlinear problems are approached with fixed point iteration. The nonlinear terms are approximated from previous iterations or previous time positions, and then the nonlinear equation is solved. This procedure is iterated upon until the solution converges. In the problems tackled here the linearized equations usually give a good approximation to the nonlinear solution. This results in few problems, and few iterations, for convergence.

2.5 Solving eigenvalue problems

The most important problems in this thesis require eigenvalues and eigenvectors to be found. Different eigenvalue solver routines were used in this thesis dependent on the size of the problem. Computational memory issues are common with large problems and parallel computing has been implemented on some occasions here. The details of these methods are given below for the following generalised problem,

$$Av = \lambda Bv, \tag{2.15}$$

with the pseudospectral approach the matrices A and B are square, nonsymmetric and dense. λ is the scalar eigenvalue and v is the right eigenvector. The first step to solving this problem is converting the matrices to a single nonsymmetric matrix $C = B^{-1}A$. The next step is dependent on the type of problem, however the step taken in most situations was to reduce C to upper Hessenburg form and all of the eigenvalues can be calculated from this point. The number of eigenfunctions to be calculated is decided at this stage too and usually it is sufficient to just calculate the eigenfunction associated to the least stable eigenvalue. Alternative methods include calculating all of the eigenfunctions from the matrix C or using an Arnoldi method. It was found that calculating all of the eigenfunctions for small sized problems

wasn't overly time intensive. The Arnoldi method for finding a few eigenvalues is quicker than the Hessenburg method but it was found to be less reliable. To make the Arnoldi method more reliable and accurate resulted in the method being just as time intensive as the Hessenburg method. Many of the routines used in this procedure come from LAPACK or the parallel computing equivalent library, ScaLAPACK.

2.6 Numerical convergence

In order to validate the results presented in this thesis a study into the numerical convergence of these solutions must be conducted. The following study will ensure that when the grid size and number of grid points used in the numerical scheme to solve these mathematical problems are changed the solutions are very similar and converging numerically. The approach of using spectral methods at collocation points means that as more grid points are used in the approximation of an unknown function the order of the method is increased also. This is because the numerical scheme is global, using all points in the entire grid for each approximation.

Pipe flow problems

In Chapter 3 a model is developed for a perturbed base flow in a pipe. The chapter begins with a simple parallel base flow and linear stability analysis but the study moves on to a non-parallel base flow and eventually nonlinear stability analysis. The nonlinear stability investigation is predominately a theoretical study and the most sophisticated problem from the viewpoint of numerical methods is the linear stability analysis of the non-parallel base flow. Several colour-plots are produced to depict the shape of the disturbances but the crucial metric in this problem is the disturbance growth rate.

The linear stability of non-parallel pipe flow is solved in the radial-azimuthal plane and the flow is fully developed axially. There are essentially two numerical parameters which can be varied, the number of points in the radial direction and the number of points in the azimuthal direction. Table 2.1

records the growth rate of the least stable eigenvalue when the number of grid points is varied.

Radial points	Azimuthal points	Growth rate
40	20	0.0206
40	24	0.0199
48	20	0.0215
48	24	0.0218
60	20	0.0212
60	24	0.0217

Table 2.1: The disturbance growth rate for non-parallel pipe flow with 2π-periodic suction boundary conditions. Reynolds number, $R = 10000$, wave frequency, $\omega = 0.5$, and the suction coefficient, $\lambda = 10$.

It is possible to use less points in the azimuthal direction than the radial direction for this problem because the changes in the base flow and disturbance velocities are much smaller in this direction. This is true for 2π-periodic suction but when the periodicity of the suction is decreased the changes in velocity in the azimuthal direction rapidly increase. The plots of the base flow and disturbance velocity appear to be very similar for all of these combinations of grid points from inspection.

Parallel wall channel flows

Chapter 4 begins by looking at the problem of Taylor vortices in concentric cylinders. To verify this model is numerically consistent the nonlinear stability results can be reproduced using a different number of collocation points. In the results presented in subsection 4.1.4 20 collocation points in the radial direction and 30 points in the axial direction were used. Table 2.2 presents the equilibrium radial velocity when several different number of points are used.

The second section of Chapter 4 is concerned with three dimensional vortex-wave interaction equilibria. To reduce the size of the problem but maximise the accuracy of the model the symmetries of the flow are exploited. As discussed in section 4.2.6 the equations can be solved in just half the spanwise

Wall normal points	Spanwise points	Equilibrium radial velocity
18	30	2.741
18	32	2.748
20	28	2.759
20	30	2.752
20	32	2.757
20	34	2.753
24	30	2.762
24	32	2.759

Table 2.2: The converged value of the radial disturbance velocity for flow between concentric cylinders from the nonlinear stability equations when the system is at equilibrium. Taylor number, $T = 3440$.

period. In the results presented in subsection 4.2.8 50 collocation points are used in the wall normal direction and 24 points in the spanwise direction, covering half the spanwise period.

In the vortex-wave interaction problem the key parameter of the equilibrium solution is the converged value of the wave amplitude, ρ, at large time, T. By solving this problem with a different grid size and comparing the converged values of ρ it will be possible to identify if the previous solutions were spurious.

Wall normal points	Spanwise points	ρ
46	24	0.92513
50	20	0.92380
50	24	0.92509
50	28	0.92664
50	32	0.92623
54	24	0.92588
58	24	0.92556

Table 2.3: The converged wave amplitude, ρ, for the lower branch equilibrium solutions to the vortex-wave interaction equations against the number of collocation points in the wall normal and spanwise directions. Reynolds number, $R = 10000$, and wavenumber, $\alpha = 1.0$.

Table 2.3 shows that the converged values of ρ are very similar for different numbers of collocation points. Even the plots of the magnitude of the wave

Reynolds stresses, figures 4.12 and 4.13, are virtually identical.

When the upper branch solutions are tested for numerical convergence the results are very similar again. Table 2.4 shows the converging value of ρ when the number of points is varied. Figures 4.14 and 4.15 depict the changes in the magnitude of the wave Reynolds stresses.

Wall normal points	Spanwise points	ρ
46	24	1.25327
50	20	1.24583
50	24	1.25358
50	28	1.24723
50	32	1.25019
54	24	1.24401
58	24	1.24736

Table 2.4: The converged wave amplitude, ρ, for the upper branch equilibrium solutions to the vortex-wave interaction equations against the number of collocation points in the wall normal and spanwise directions. Reynolds number, $R = 10000$, and wavenumber, $\alpha = 1.0$.

The results in Tables 2.3 and 2.4 for the value of ρ appear to be numerically converged to two decimal places. Table 2.5 shows how long it took on average to calculate one iteration of the full system for the given number of collocation points. Although it appears fewer than 50 wall normal and 24 spanwise points could have been used to produce sufficiently accurate results, using less points resulted in the model failing to converge to solutions on occasions.

Wall normal points	Spanwise points	Time
46	24	198
50	20	253
50	24	306
50	28	410
54	24	447
50	32	448
58	24	675

Table 2.5: Time in seconds it takes on average to solve one iteration of the full vortex-wave interaction system for the special case numerically. 50 wall normal and 24 spanwise points were used to calculate the majority of solutions in Chapter 4. Reynolds number, $R = 10000$, and wavenumber, $\alpha = 1.0$.

3

Pipe flow problems

The first investigation in this thesis considers viscous, incompressible fluid flow through a pipe. Research into pipe flows goes back to the 19th century but it is still of interest today because several problems remain unresolved. Recent progress in the areas of vortex-wave interactions and self-sustained processes have thrown up new results for pipe flow and further results are described here.

Hagen[17] and Poiseuille[39] first found an exact solution to the Navier-Stokes equations for parallel flow. The shear flow that they described is driven by a pressure gradient and it is this Hagen-Poiseuille flow that forms the basis for the research in this thesis. It has been shown in several studies that a flow of this type is linearly stable, this is to say, there is no critical value of the Reynolds number above which the disturbances have exponential growth. Gill[16] and, at the same time in a different paper, Davey & Drazin[7] presented their analyses of axisymmetric infinitesimal disturbances in a pipe and found them to be stable under all conditions. Garg & Rouleau[15] formalized the linear stability of flow in a pipe for non-axisymmetric perturbations and reviewed the axisymmetric findings and once again found all configurations to be stable. This result is at odds with experiments, which show that the

flow can be unstable to small disturbances.

Another significant finding in Garg & Rouleau's[15] investigation was that there is a consistent order of the least stable eigenmodes. When n is the azimuthal wavenumber, $n = 1$ is the least stable and the following sequential order of least stable eigenmodes is $n = 0, 2, 3, ...$ Garg & Rouleau also showed that for a fixed azimuthal mode increasing the wave frequency or the Reynolds number increases the wave's spatial growth rate and wavelength. These results are replicated here, partly to validate the model but also to prepare for more complicated flows. Even for non-axisymmetric disturbances Garg & Rouleau studied the reduced two-dimensional problem but in this thesis the three-dimensional problem is tackled. This will give more insight into the disturbance shapes and could even yield unstable solutions.

This chapter begins with the fundamental problem of Hagen-Poiseuille flow and linear spatial stability analysis, with non-axisymmetric disturbances. The analysis here is conducted in the radial and azimuthal plane and the wave problem is periodic in the axial direction with the wavenumber α. The next section in this chapter addresses the extended, non-parallel Hagen-Poiseuille problem. In the basic problem the pipe boundary conditions are no-slip on solid walls but the extended problem has periodic suction and injection on the pipe walls. The new boundary conditions result in a non-parallel flow that has an axial streak and vortical elements. It is shown that this flow is linearly unstable under certain conditions and the neutral curves are plotted in the results section, Figure 3.13b. The disturbance profiles are also studied and shown to be increasingly localised as the Reynolds number is increased, Figures 3.16 and 3.17.

For a more accurate portrayal of a real flow a weakly nonlinear stability analysis is also conducted on this non-parallel flow. Linear stability analysis is limited to infinitesimal disturbances that can either grow or decay exponentially but through nonlinear theory it is shown that small disturbances reach an equilibrium amplitude in space in the supercritical case.

3.1 Non-dimensionalised Navier-Stokes equations in cylindrical coordinates

In this section the system under consideration has a total dimensional flow $\mathbf{u}^* = (u^*, v^*, w^*)$ in the cylindrical coordinate system (x^*, r^*, θ). The incompressible form of the Navier-Stokes equations and the continuity equation will be used as a starting point,

$$\rho^* \left(\frac{\partial \mathbf{u}^*}{\partial t^*} + \mathbf{u}^* \cdot \nabla \mathbf{u}^* \right) = -\nabla p^* + \mu \nabla^2 \mathbf{u}^*, \tag{3.1}$$

$$\nabla \cdot \mathbf{u}^* = 0, \tag{3.2}$$

where star denotes dimensional terms and p^* is the pressure, t^* is the time variable, μ is the viscosity constant and ρ^* is the flow density. The Navier-Stokes equations are non-dimensionalised in the following way

$$\mathbf{u} = \frac{\mathbf{u}^*}{u_c^*}, \quad p = \frac{p^*}{\rho^* {u_c^*}^2}, \quad R = \frac{\rho^* r_w u_c^*}{\mu}. \tag{3.3}$$

In this case u_c is the streamwise velocity at the centre of the pipe and r_w is the radius of the pipe. $\mathbf{u} = (u, v, w)$ and R is the dimensionless Reynolds number. The cylindrical coordinate system is also changed to the new system of (x, r, θ), where $x = x^*/r_w$ and $r = r^*/r_w$. The time variable is transformed similarly, with $t = u^* t^*/r_w$. The resultant non-dimensional, incompressible Navier-Stokes equations are

$$\frac{\partial \mathbf{u}}{\partial t} + \mathbf{u} \cdot \nabla \mathbf{u} = -\nabla p + \frac{1}{R} \nabla^2 \mathbf{u}, \tag{3.4}$$

$$\nabla \cdot \mathbf{u} = 0. \tag{3.5}$$

In this section the pipe flow, $\mathbf{u}$, will be considered as the sum of an $\mathcal{O}(1)$ base, or mean, flow and some small, $\mathcal{O}(\epsilon)$ disturbance. In the following discussion the base flow terms will be denoted by lower case letters and the disturbance terms by upper case letters. All the flows in this section are studied at the large Reynolds number limit.

3.2 Pipe flow with solid wall boundaries

3.2.1 Introduction and formulation

The objective of this section is to validate a linear stability model for a simple viscous, incompressible flow in a circular pipe. This model can then be used for a more complicated, non-parallel pipe flow and as the basis for a nonlinear investigation. The pipe flow studied here was first described by Hagen[17] and Poiseuille[39] and is an exact solution of the Navier-Stokes equations (3.4) and (3.5).

The configuration for this flow problem is a pipe with normalised radius of 1 and infinite length in the axial direction. As mentioned before, the problem is solved in the radial-azimuthal plane and solved at an arbitrary axial position. This is possible as the $\mathcal{O}(1)$ base flow is parallel, steady and fully developed in the streamwise direction. The velocity at the solid pipe walls is zero and the flow is the result of a pressure gradient in the axial direction. This base flow is then subjected to a small, $\mathcal{O}(\epsilon)$, Tollmien-Schlichting wave perturbation. The disturbance shape is dependent on the radial and azimuthal directions but the streamwise part is wave-like and time periodic. The results in this chapter will show that the disturbance growth rate and wavenumber converges as the Reynolds number is increased, Figure 3.3.

The types of problems that must be solved in this section are linear systems of equations and generalized eigenvalue problems. The methods that were outlined in Chapter 2 will be used here. Specifically, the functions that are sought will be expanded in Chebyshev polynomials in the radial direction and Fourier series in the azimuthal direction. In the equations the spatial eigenvalue, α, is of power two and the disturbance equations will need to be rearranged such that the system can be solved as a generalized eigenvalue problem.

Circular pipe flow

The first task in this chapter is to derive the base, $\mathcal{O}(1)$, viscous, incompressible flow. The flow is taken to be parallel, $\mathbf{u} = (u, 0, 0)$, and the other assumptions are that the base flow is steady, ($\frac{\partial u}{\partial t} = 0$), and independent of x, ($\frac{\partial u}{\partial x}, \frac{\partial^2 u}{\partial x^2} = 0$). This second assumption can be interpreted as the flow being fully developed in the streamwise direction. Upon substitution of this flow into (3.4) and (3.5) the result of the assumptions is a vastly reduced form of the Navier-Stokes equations.

$$\frac{\partial^2 u}{\partial r^2} + \frac{1}{r}\frac{\partial u}{\partial r} = R\frac{\partial p}{\partial x}. \tag{3.6}$$

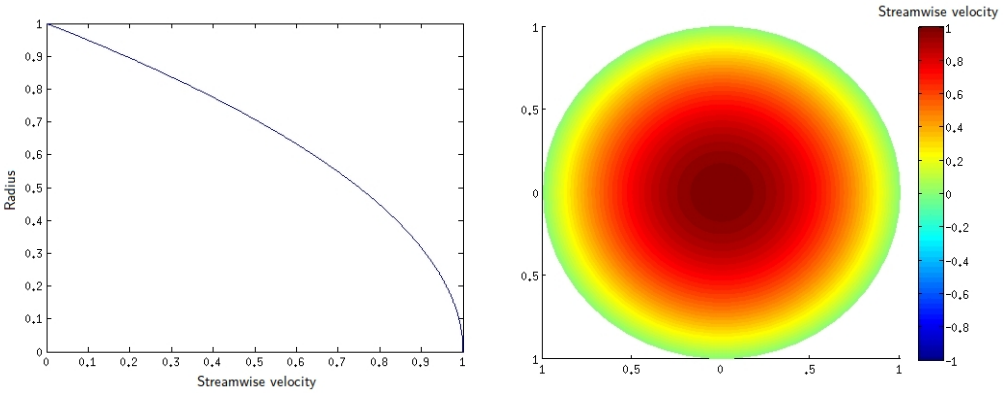
Now the flow is necessarily driven by a constant pressure gradient. For a non-trivial solution the pressure gradient can not be zero and because $u = u(r, \theta)$ is not dependent on x then neither is $\frac{\partial p}{\partial x}$ and therefore must be constant. The equation can be integrated twice and the boundary conditions can be used to find the solution,

$$u = \frac{R}{4}\frac{\partial p}{\partial x}r^2 + c_1 ln(r) + c_2, \tag{3.7}$$

where c_1 and c_2 are the constants of integration and R is the nondimensional Reynolds number. u must be finite at $r = 0$, meaning that $c_1 = 0$, and as the condition on the pipe wall boundary, $r = 1$, is the no-slip condition $u = 0$ then the flow is described by equation (3.8),

$$u = -\frac{R}{4}\frac{\partial p}{\partial x}\left(1 - r^2\right). \tag{3.8}$$

The choice of the pressure gradient is arbitrary and here it is chosen to be $\frac{\partial p}{\partial x} = -\frac{4}{R}$, ensuring that u is at maximum 1 and minimum zero. As shown in Figure 3.1, the flow is axisymmetric, zero on the pipe wall and 1 at the centre of the pipe. Both plots in Figure 3.1 are taken at an arbitrary x position as the base flow is independent of x.



(a) One-dimensional view of streamwise velocity in circular pipe flow.

(b) Two-dimensional view of streamwise velocity in circular pipe flow.

Figure 3.1: The streamwise velocity in circular pipe flow.

3.2.2 Linear spatial stability of circular pipe flow

To examine the flow's spatial stability a small disturbance field is imposed on the base flow and taken to be a non-axisymmetric, travelling wave velocity disturbance, $(U(r,\theta)$,$V(r,\theta)$, $W(r,\theta))$, with a corresponding pressure perturbation, $P(r,\theta)$. These small perturbations will take a similar form to those in traditional hydrodynamic linear stability theory. The total flow, the base and the disturbance, has the following form,

$$\begin{aligned}\mathbf{u} = (u &+ \epsilon(U(r,\theta)E(x,t) + c.c.),\\ &+\epsilon(V(r,\theta)E(x,t) + c.c.),\\ &+\epsilon(W(r,\theta)E(x,t) + c.c.)),\end{aligned} \tag{3.9}$$

$$\text{with} \quad E = e^{i(\alpha x - \omega t)}, \tag{3.10}$$

where ϵ is a small scalar and '$c.c.$' is the complex conjugate. In this fully developed basic flow in the streamwise direction there is no reason to make the disturbance profiles (U,V,W) dependent on x, as they are in parabolised stability theory. Instead, the disturbances follow the form of the Tollmien-Schlichting wave, which are the most dominant disturbance type, in the sense

that they are most likely to become unstable, in fully developed pipe flow. The partitioned disturbances account separately for the wave-like nature of the disturbance, E, and the profile of the disturbances.

The products of these small perturbations in the Navier-Stokes equations are infinitesimal and can be neglected, resulting in a linearised problem. The linearization argument for the disturbances is valid when the basic flow has been affected by small environmental perturbations which develop into the primary mode growth. The equations can be formed with nonlinear terms but the goal of this section is to prove the validity of the method by corroborating results, consequently the linearised problem is as far as this problem is taken here.

The Navier-Stokes equations, (3.4) and (3.5), at the disturbance level, ϵ, under these assumptions become

$$\begin{aligned} &i\alpha uU - i\omega U + V\frac{\partial u}{\partial r} + \frac{W}{r}\frac{\partial u}{\partial \theta} \\ &= -\alpha i P + \frac{1}{R}\left[\frac{1}{r}\frac{\partial U}{\partial r} + \frac{\partial^2 U}{\partial r^2} + \frac{1}{r^2}\frac{\partial^2 U}{\partial \theta^2} - \alpha^2 U\right], \end{aligned} \tag{3.11}$$

$$\begin{aligned} &i\alpha uV - i\omega V \\ &= -\frac{\partial P}{\partial r} + \frac{1}{R}\left[\frac{1}{r}\frac{\partial V}{\partial r} + \frac{\partial^2 V}{\partial r^2} + \frac{1}{r^2}\frac{\partial^2 V}{\partial \theta^2} - \frac{V}{r^2} - \frac{2}{r^2}\frac{\partial W}{\partial \theta} - \alpha^2 V\right], \end{aligned} \tag{3.12}$$

$$\begin{aligned} &i\alpha uW - i\omega W \\ &= -\frac{1}{r}\frac{\partial P}{\partial \theta} + \frac{1}{R}\left[\frac{1}{r}\frac{\partial W}{\partial r} + \frac{\partial^2 W}{\partial r^2} + \frac{1}{r^2}\frac{\partial^2 W}{\partial \theta^2} - \frac{W}{r^2} + \frac{2}{r^2}\frac{\partial V}{\partial \theta} - \alpha^2 W\right], \end{aligned} \tag{3.13}$$

$$i\alpha U + \frac{1}{r}V + \frac{\partial V}{\partial r} + \frac{1}{r}\frac{\partial W}{\partial \theta} = 0. \tag{3.14}$$

The boundary conditions for this problem are detailed in the Numerical methods chapter in subsection 2.3. At the pipe wall the disturbance velocity is zero but at the centre of the pipe the disturbance velocity and pressure is non-zero.

3.2.3 Numerical method for the stability analysis

If the equations (3.11-3.14) are to be solved numerically they are rearranged such that α is the complex eigenvalue of a generalised eigenvalue problem to be found. A sensible choice for the wave frequency, ω, is for it to be real, that is, neutral in growth and periodic in time. If ω is allowed to grow or decay then it would make it more difficult to understand the growth rate behaviour of the spatially related eigenvalue. The rearranged equations (3.11-3.14) have the form

$$\left(\begin{bmatrix} a_0 & a_1 \\ 0 & I \end{bmatrix} + \alpha \begin{bmatrix} 0 & a_2 \\ -I & 0 \end{bmatrix} \right) \begin{pmatrix} \boldsymbol{\delta} \\ \alpha\boldsymbol{\delta} \end{pmatrix} = \begin{pmatrix} 0 \end{pmatrix}, \tag{3.15}$$

where

$$a_0 = \begin{bmatrix} M & \frac{\partial u}{\partial r} & \frac{1}{r}\frac{\partial u}{\partial \theta} & 0 \\ 0 & \frac{1}{r^2 Re} + M & \frac{2}{r^2 Re}\frac{\partial}{\partial \theta} & \frac{\partial}{\partial r} \\ 0 & -\frac{2}{r^2 Re}\frac{\partial}{\partial \theta} & \frac{1}{r^2 Re} + M & \frac{1}{r}\frac{\partial}{\partial \theta} \\ 0 & \frac{1}{r} + \frac{\partial}{\partial r} & \frac{1}{r}\frac{\partial}{\partial \theta} & 0 \end{bmatrix}, \tag{3.16}$$

$$a_1 = \begin{bmatrix} iu & 0 & 0 & i \\ 0 & iu & 0 & 0 \\ 0 & 0 & iu & 0 \\ i & 0 & 0 & 0 \end{bmatrix}, \tag{3.17}$$

$$a_2 = \begin{bmatrix} \frac{1}{R} & 0 & 0 & 0 \\ 0 & \frac{1}{R} & 0 & 0 \\ 0 & 0 & \frac{1}{R} & 0 \\ 0 & 0 & 0 & 0 \end{bmatrix}, \tag{3.18}$$

$$M = -\omega i - \frac{1}{R}\left[\frac{1}{r}\frac{\partial}{\partial r} + \frac{\partial^2}{\partial r^2} + \frac{1}{r^2}\frac{\partial^2}{\partial \theta^2}\right], \tag{3.19}$$

and $\boldsymbol{\delta} = (U, V, W, P)$. Several numerical methods could be employed to approximate $\boldsymbol{\delta}$ but here, spectral methods, Chebyshev polynomials of the first type in the radial direction and Fourier series in the azimuthal direction, with a collocation approach are used. The dense, nonsymmetric matrix containing the term a_2 is inverted and multiplied to the matrix containing the terms a_0 and a_1. The resultant matrix is reduced to Hessenburg form and all the eigenvalues are calculated. The eigenfuction for the least stable eigenvalue is then calculated. There are more details on the numerical methods in Chapter 2.

The routine used for this problem returns all of the eigenvalues and associated eigenfunctions. Spurious eigenvalues are generated as an artifact of the numerical procedure and these are rejected based on their size and their associated eigenfunction, which should be a smooth function satisfying the conditions on both boundaries. The disturbance associated with the least stable eigenvalue is of interest because it is the most likely to become unstable and grow exponentially, and in real world flows it would be this eigenmode which would interact with the base flow nonlinearly downstream.

3.2.4 Stability results for circular pipe flow

Garg & Rouleau investigated linear spatial stability in their 1972 paper[15] and the model discussed in this thesis will be validated against that data. First, it is important to note that in the results produced here the eigenmode associated with the $n = 1$ Fourier mode is always the least stable. This phenomenon was noted by Garg & Rouleau and they made the link with

$n = 1$ being the only mode for which V and W are non-zero at $r = 0$. This means that the $n = 1$ mode is non-zero at the point where the base flow is fastest and where there is a turning point in the gradient of the streamwise velocity. The plot of the eigenvalues can be seen in Figure 3.2.

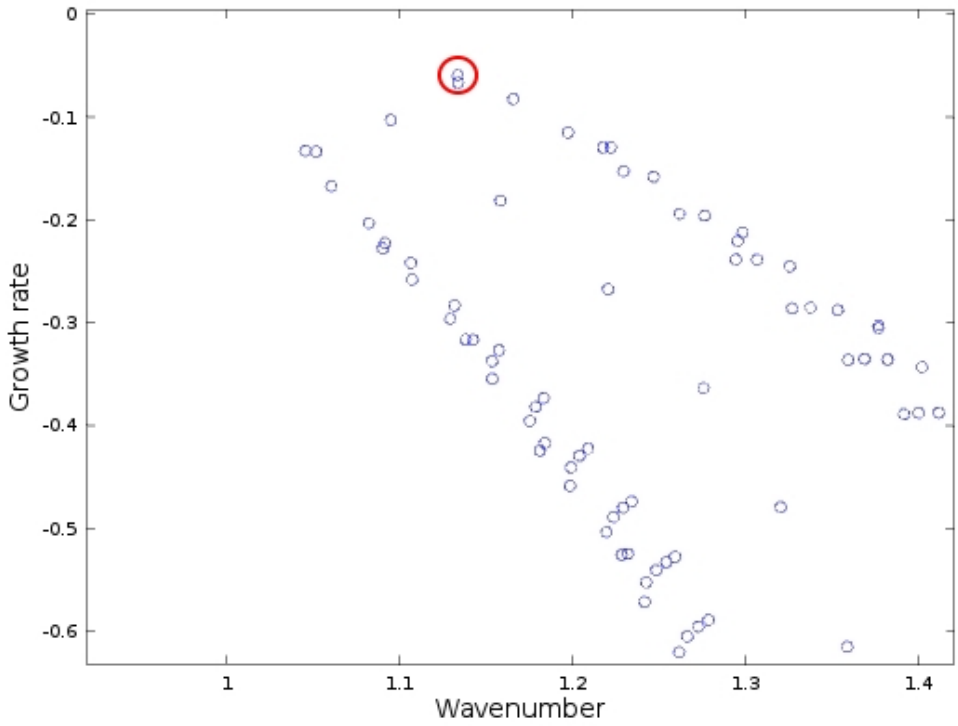


Figure 3.2: The eigenvalue solutions of circular pipe flow when $\omega = 1$ and $R = 2000$. The least stable eigenvalue, circled in red, is the $n = 1$ eigenmode.

Figure 1 from Garg & Rouleau's paper[15] is recreated in Figure 3.3 in this thesis, and the data and the plots show good agreement. Garg & Rouleau pointed out that for a fixed frequency wave but increasing Reynolds number the least stable eigenvalue becomes less stable and has a larger wavelength. It is also noteworthy that the growth rates and wavenumbers appear to be asymptoting towards a constant at large Reynolds number, confirming that there is a large Reynolds number asymptotic solution.

Garg & Rouleau's[15] Figure 4 shows the disturbance profiles for the $n = 1$ Fourier mode, and these plots have also been recreated, without normalization, in Figure 3.4 here. From the boundary conditions at the centre of the

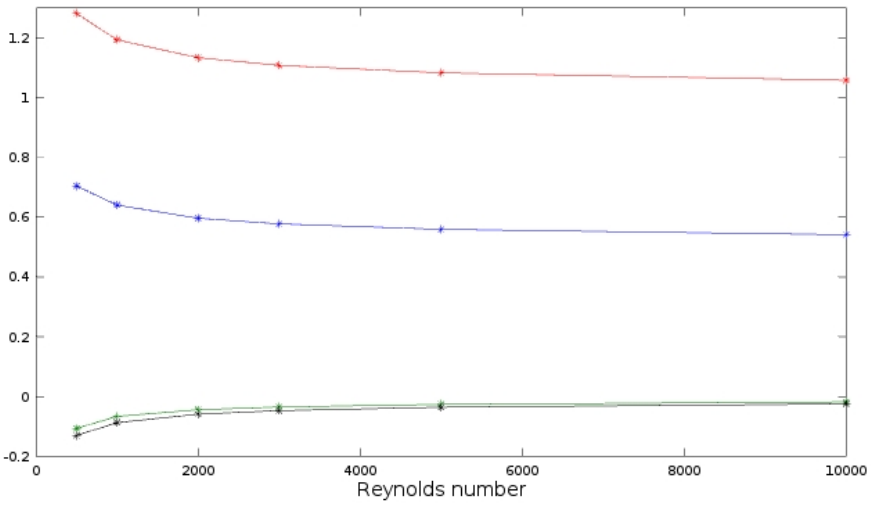


Figure 3.3: Variation of growth rate and wavenumber for the least stable eigenvalue, mode $n = 1$, for circular pipe flow. Wavenumber (blue) and growth rate (green) when $\omega = 0.5$. Wavenumber (red) and growth rate (black) when $\omega = 1.0$.

pipe, detailed in Numerical Methods subsection 2.3, it is known that the speed of the radial and azimuthal velocities is non-zero at the centre of the pipe, $r = 0$, and that the real part of the radial velocity would be equal to the imaginary part of the azimuthal velocity, while the imaginary part of the radial velocity is equal to negative of the real part of the azimuthal velocity. The entire disturbance velocity field tends to zero at $r = 1$, however the pressure perturbation is not zero on the wall.

Garg & Rouleau[15] noted several other stability features of non-axisymmetric disturbances, including the asymptotic nature of the wavenumber and growth rate at large Reynolds numbers and the 'nearly' constant phase velocity, which are demonstrated in Figure 3.3. These characteristics are particularly important because they hold true when suction is applied to the circular pipe flow.

These non-axisymmetric disturbances can be plotted in two dimensions for a clearer understanding of their profile. As the Reynolds number, R, and frequency, ω, are increased the disturbances change shape, as is demonstrated by Figure 3.5. The orientation of the disturbance profile is arbitrary in the azimuthal direction as there is no boundary condition fixing any variable in

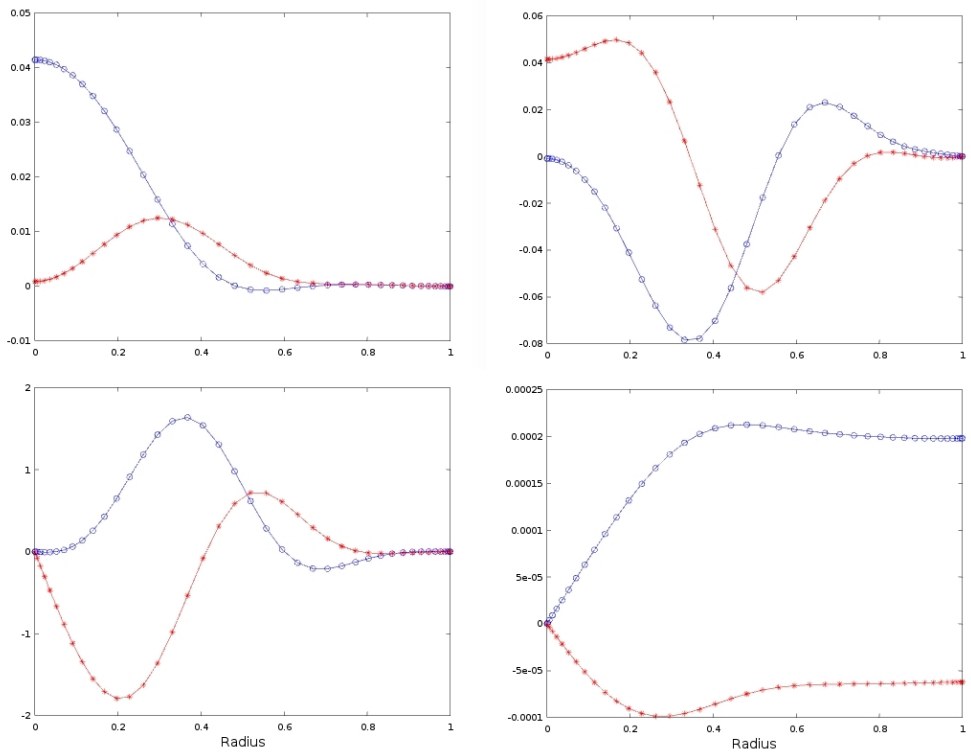
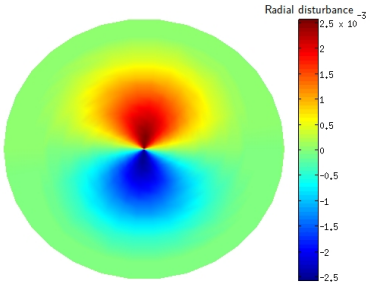


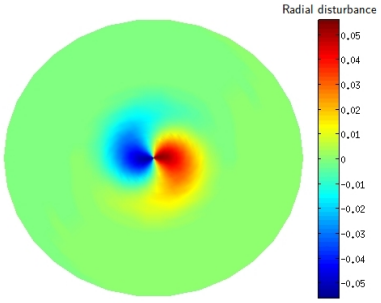
Figure 3.4: Circular pipe flow least stable mode $n = 1$ eigenfunctions plotted against the radius. (V top left, W top right, U bottom left, P bottom right - real part (blue circles), imaginary part (red stars)). $R = 5000$, $\omega = 0.1$.

the azimuthal direction. The first major noticeable difference is the localisation of most of the velocity disturbance energy towards the centre of the pipe when $\omega = 0.1$. Although there is no critical layer in the flow, as the growth rate is always negative, there is a change in sign of the real part of the nonlinear term associated with $(\alpha u - \omega)$ in the Navier-Stokes equations (3.11)-(3.13), as the spatial parameter, α, and the temporal parameter, ω, are both always positive. The area where the sign of this term is positive is where the streamwise base flow is the fastest and there is a turning point in terms of the change in the speed.

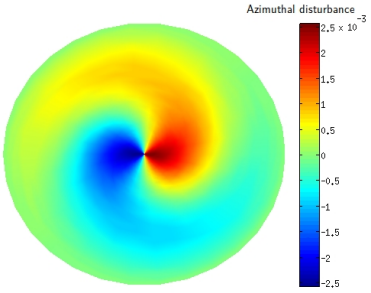
The change of the disturbance profile is not just a localisation however, and the actual shape of the perturbations are modified at different frequencies and Reynolds numbers. The radial and azimuthal disturbance components can be combined to produce a streamline plot in the plane, as described by



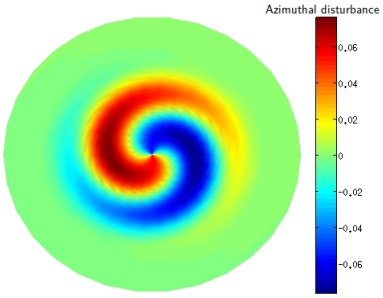
(a) Radial disturbance.



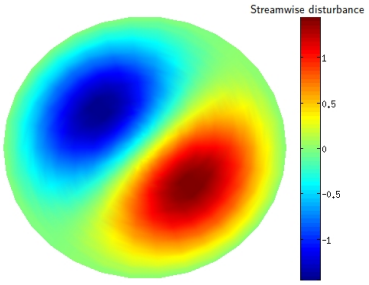
(b) Radial disturbance.



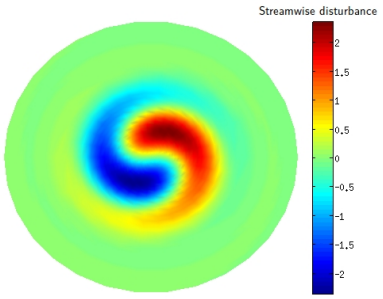
(c) Azimuthal disturbance.



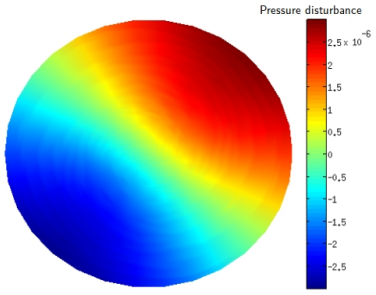
(d) Azimuthal disturbance.



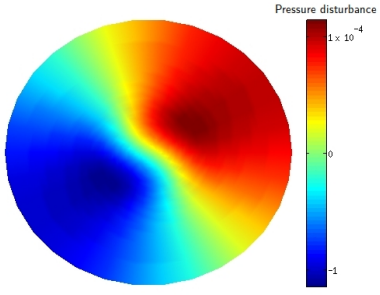
(e) Streamwise disturbance.



(f) Streamwise disturbance.



(g) Pressure disturbance.



(h) Pressure disturbance.

Figure 3.5: Disturbance profiles for Hagen-Poiseuille flow. Plots on the left when $\omega = 0.001$ and $R = 10000$, on the right $\omega = 0.1$ and $R = 20000$.

the arrows in Figure 3.6. The streamwise disturbance is fixed by the radial-azimuthal streamlines, and the streamwise perturbation is positive when the streamlines are moving clockwise and negative when the streamlines are moving counter-clockwise.

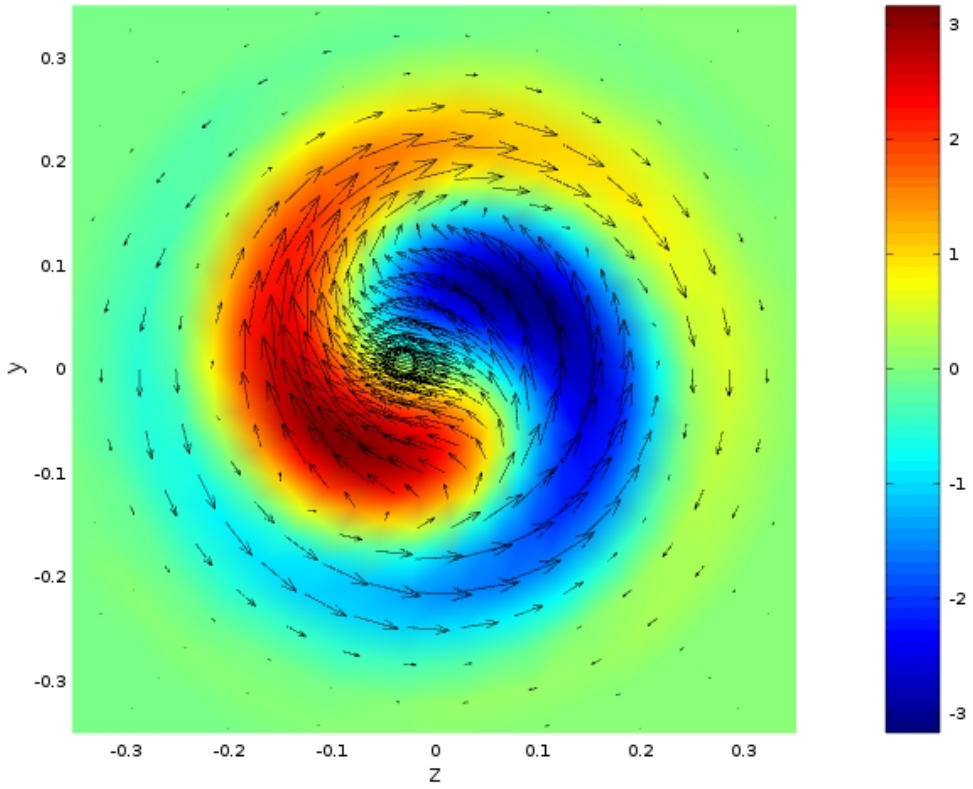


Figure 3.6: The velocity disturbance, the streamwise component (colour scale) and the streamlines of the radial and azimuthal components (arrows), when $\omega = 1.$ and $R = 20000$. The plot is focused in the area 0.35 radius lengths from the centre of the pipe.

3.2.5 Conclusions

The objective of this section was to validate the spatial stability numerical model for flows best described in cylindrical geometry. By comparing the results produced here to those of Garg & Rouleau[15] the model was validated. It was shown that even non-axisymmetric disturbances that are allowed to

develop downstream are linearly stable. The least stable mode in all cases was found to be the $n = 1$ eigenmode, and this is related to its property of having non-zero V and W disturbance velocity components at the centre of the pipe. This section revealed more insights into the shape of the disturbances and the relationship to the streamwise velocity of the base flow. The foundations have been laid now to introduce suction to the problem and move to non-parallel flow.

3.3 Pipe flow with suction at the boundaries

3.3.1 Introduction

The previous section didn't yield any unstable wave solutions and for that reason they can't help to explain the transition to turbulence through primary mode growth. In order to find unstable waves something must be changed in the formulation of the problem. One such change is to introduce a small amount of suction and injection at the pipe wall boundary. Through suction it is possible to distort the mean flow and this should lead to spatially exponentially growing waves.

In real world situations a fluid flow would never be absolutely parallel and even the most rigorous experiments will have an element of non-parallelism. Faisst & Eckhardt[12] built on the ideas of self-sustained processes and considered a stimulated, initial vortex and streak flow that has a neutral periodic travelling wave solution. The authors identified a configuration where this system was self-sustained and this showed that for a non-parallel flow there are circumstances where nonlinear equilibrium solutions exist for Reynolds as low as 1250. Wedin & Kerswell[57] also found a family of wave solutions through this numerical method and later Ozcakir[37] managed to reconcile these solutions with the large Reynolds number theory of vortex-wave interactions.

Ozcakir's[37] starting point differed to those of the authors before. Ozcakir began with changing the pipe wall boundary conditions from zero to non-zero periodic suction and injection on the wall. This condition introduces non-parallel effects to the flow and can be thought of as a porous wall. The idea of suction on boundaries in pipes goes back to Bansal[1]. Ozcakir sought neutral equilibrium solutions for what is described here as 'π-periodic' suction, where the suction behaviour is repeated every π radians. That investigation is extended to focus on finding the neutral curve for a range of Reynolds numbers for 2π-periodic suction in this thesis. This case is special because the maximum velocity of the base flow is moved from the centre of the pipe, which is common in real world problems.

In this section the problem of flow stability in an infinitely long pipe modified by suction and injection on the pipe wall boundaries is investigated. This suction and injection is in a completely radial direction and the total rate of suction and injection is equal, resulting in a zero change in flux of the fluid through the pipe. It will be shown that the nonlinear base flow is unstable under certain conditions, resulting in a neutral curve dependent on Reynolds number, R, and frequency, ω. The effect of increasing the suction will be analysed and it will be shown that the respective neutral curves for each suction coefficient collapse on to one curve. The flow at large R will be investigated and the significance of the phase velocity will be described. A nonlinear study into this flow will follow and it will be shown that there is a ultimate equilibrium state in the supercritical region where the amplitude of the disturbance is finite but still small.

3.3.2 Formulation

As in the preceding section, the mathematical analysis will be conducted in a cylindrical coordinate system. There are no-slip boundary conditions on the pipe wall for the axial and azimuthal components of the base flow, but the radial component is non-zero on the wall. The boundary condition is periodic but will generate no change in the flux in the cross-section of the pipe. There will be suction, where the radial velocity is positive at the pipe wall, and injection, where the radial velocity is negative. The assumptions that the base flow terms are steady and independent of x remain, and this is possible if the streamwise velocity is of order Reynolds number larger than the other base flow components. To be consistent with the previous section the streamwise flow is still driven by a constant pressure gradient of $\frac{\partial p}{\partial x} = -\frac{4}{R}$. However, unlike in the pipe flow without suction problem, now the radial and swirl components are non-zero. The base flow problem is now three-dimensional and nonlinear.

At large values of R an analytical solution to the Navier-Stokes equations is possible with radial and azimuthal rolls in the flow of size $\mathcal{O}(R^{-1})$ and streamwise streaks of $\mathcal{O}(1)$. Problems with the same scaling can be traced

back to the work of Taylor[49] who did work on small gap Taylor vortices, and are now known to be important in the equilibrium solutions of vortex-wave interactions. The flow field has the following form:

$$\begin{aligned}\mathbf{u} = &(u(r,\theta) + \epsilon(U(r,\theta,z)E(x,t) + c.c.),\\ &\frac{v(r,\theta)}{R} + \epsilon(V(r,\theta,z)E(x,t) + c.c.),\\ &\frac{w(r,\theta)}{R} + \epsilon(W(r,\theta,z)E(x,t) + c.c.)),\end{aligned} \tag{3.20}$$

$$p = -\frac{4x}{R} + \epsilon(P(y,z)E(x,t) + c.c.), \tag{3.21}$$

$$\text{with} \quad E = e^{i(\alpha x - \omega t)}. \tag{3.22}$$

The terms (u, v, w) constitute the base flow, the terms (U, V, W) define the flow disturbance profiles, p is the total pressure with P the pressure disturbance and ϵ is a small constant. The form of the wave disturbance isn't required to change from the previous section, (3.9). The disturbance shapes are dependent on the radial and azimuthal directions and they are allowed to grow or decay in space. This type of disturbance is the Tollmien-Schlicting wave and is known to be one of the most likely small perturbations to drive the development of full transition. Upon substitution of (3.20) and (3.21) into (3.4) and (3.5) the result is decoupled 'roll' and 'streak' problems for the base flow terms and a disturbance-level problem, and these equations can be found in the following subsection, (3.23-3.25), (3.31).

The numerical schemes used in this section are similar to those used in the section on pipe flow with solid wall boundaries. The general detail of the numerical methods can be found in Chapter 2 and the specific computational strategies are commented on in the following sections. The next subsection is concerned with the non-parallel, 'roll' base flow in the pipe, and then the axial flow is considered, and the formulation is completed with the set-up of the linear spatial stability problem.

3.3.3 Two-dimensional swirl flow in a pipe with suction

The two-dimensional swirl flow, or the so-called roll problem, is formed from the nonlinear radial and azimuthal momentum equations and the continuity equation. From substituting the base flow terms into the Navier-Stokes equations the result is:

$$v\frac{\partial v}{\partial r} + \frac{w}{r}\frac{\partial v}{\partial \theta} - \frac{w^2}{r} = \left[\frac{1}{r}\frac{\partial}{\partial r}\left(r\frac{\partial v}{\partial r}\right) + \frac{1}{r^2}\frac{\partial^2 v}{\partial \theta^2} - \frac{v}{r^2} - \frac{2}{r^2}\frac{\partial w}{\partial \theta}\right], \tag{3.23}$$

$$v\frac{\partial w}{\partial r} + \frac{w}{r}\frac{\partial w}{\partial \theta} + \frac{wv}{r} = \left[\frac{1}{r}\frac{\partial}{\partial r}\left(r\frac{\partial w}{\partial r}\right) + \frac{1}{r^2}\frac{\partial^2 w}{\partial \theta^2} - \frac{w}{r^2} + \frac{2}{r^2}\frac{\partial v}{\partial \theta}\right], \tag{3.24}$$

$$\frac{\partial}{\partial r}(rv) + \frac{\partial w}{\partial \theta} = 0. \tag{3.25}$$

It can be seen that the streamwise base flow component, u, doesn't appear in these equations and therefore the axial problem is decoupled and can be solved separately. These equations are solved in the radial-azimuthal plane at a fixed x. Equation (3.25) yields a streamfunction solution, $\phi(r, \theta)$, for v and w, leaving a single nonlinear fourth order equation

$$\frac{\partial^4\phi}{\partial r^4}+\frac{2}{r}\frac{\partial^3\phi}{\partial r^3}+\frac{1}{r^2}\left(2\frac{\partial^4\phi}{\partial r^2\partial\theta^2}-\frac{\partial^2\phi}{\partial r^2}\right)+\frac{1}{r^3}\left(\frac{\partial\phi}{\partial r}-2\frac{\partial^3\phi}{\partial r\partial\theta^2}\right)$$
$$+\frac{1}{r^4}\left(\frac{\partial^4\phi}{\partial\theta^4}+4\frac{\partial^2\phi}{\partial\theta^2}\right)=\frac{2}{r^4}\frac{\partial\phi}{\partial\theta}\frac{\partial^2\phi}{\partial\theta^2}+\frac{1}{r^3}\left[\frac{\partial\phi}{\partial r}\frac{\partial\phi}{\partial\theta}+\frac{\partial\phi}{\partial r}\frac{\partial^3\phi}{\partial\theta^3}-\frac{\partial^3\phi}{\partial\theta^2\partial r}\frac{\partial\phi}{\partial\theta}\right]$$
$$+\frac{1}{r^2}\left[\frac{\partial\phi}{\partial r}\frac{\partial^2\phi}{\partial\theta\partial r}-\frac{\partial^2\phi}{\partial r^2}\frac{\partial\phi}{\partial\theta}\right]-\frac{1}{r}\left[\frac{\partial\phi}{\partial\theta}\frac{\partial^3\phi}{\partial r^3}-\frac{\partial\phi}{\partial r}\frac{\partial^3\phi}{\partial\theta\partial r^2}\right], \tag{3.26}$$

where

$$v=-\frac{1}{r}\frac{\partial\phi}{\partial\theta},\ w=\frac{\partial\phi}{\partial r}. \tag{3.27}$$

Boundary conditions

The type of suction investigated in this paper acts radially at the pipe wall and for this reason it is chosen to be the same order of magnitude as the radial flow, $\mathcal{O}(R^{-1})$. A consideration for this type of boundary condition is the flux across the pipe. For simplicity, the suction here is chosen such that it is periodic and the flux remains constant. That is, there is positive suction and negative suction, or injection, on the wall. Specifically, the boundary conditions at the pipe wall are,

$$v(1,\theta)=\lambda\cos\left(m\theta\right),\ w(1,\theta)=0, \tag{3.28}$$

where m is a chosen mode of the suction and λ is the suction (and injection) coefficient that is varied in this investigation. In the streamfunction notation, which is needed for the numerical calculation, the boundary conditions become

$$-\frac{\partial\phi(1,\theta)}{\partial\theta} = \lambda\cos(m\theta) \Rightarrow \phi(1,\theta) = -\frac{\lambda}{m}\sin(m\theta),$$
$$\frac{\partial\phi(1,\theta)}{\partial r} = 0. \tag{3.29}$$

Two conditions are needed at both the pipe wall and the centre of the pipe for the streamfunction as the problem is fourth order in this variable. At the centre of the pipe the boundary conditions are more complicated because of the coordinate singularity. Once again the work of Batchelor & Gill[2] on uni-directional flows that was described in the Numerical methods Chapter in subsection 2.3 can be followed. As $r \to 0$ the continuity equation tends to the following form:

$$v(0,\theta) + \frac{\partial w(0,\theta)}{\partial\theta} = 0. \tag{3.30}$$

If we think of this in terms of the streamfunction it is clear that to make mathematical sense $\frac{\partial\phi}{\partial\theta}$ must be zero at $r = 0$. If the streamfunction is expressed in terms of Fourier components, $\phi(0,\theta) = \sum_{n=-\infty}^{\infty}\phi_n(0)e^{in\theta}$, in the azimuthal direction the form of the velocity isn't limited. Consider the Fourier mode $n = 0$ in isolation. For this Fourier mode alone, ϕ_n is non-zero and this enables ϕ to be non-zero at the origin. For all other n, $\phi_n = 0$. This can be thought about as ϕ_n acting like r near the centre of the pipe. If we continue to assume $\phi_n \sim r$ near the centre of the pipe, then, by taking the derivative of the expression of the streamfunction in Fourier modes, $\frac{\partial\phi}{\partial r} \sim e^{in\theta}$. For the Fourier mode $n = 1$, $v + iw = 0$, and Batchelor & Gill note that v and w act sinusoidally as $r \to 0$. The condition $w = \frac{\partial\phi}{\partial r} = i\sin\theta$ is consistent with the formulation of ϕ and corresponds to a 2π periodic function. For all other Fourier modes n, $\frac{\partial\phi}{\partial r} = 0$.

Numerical method for the two-dimensional swirl flow

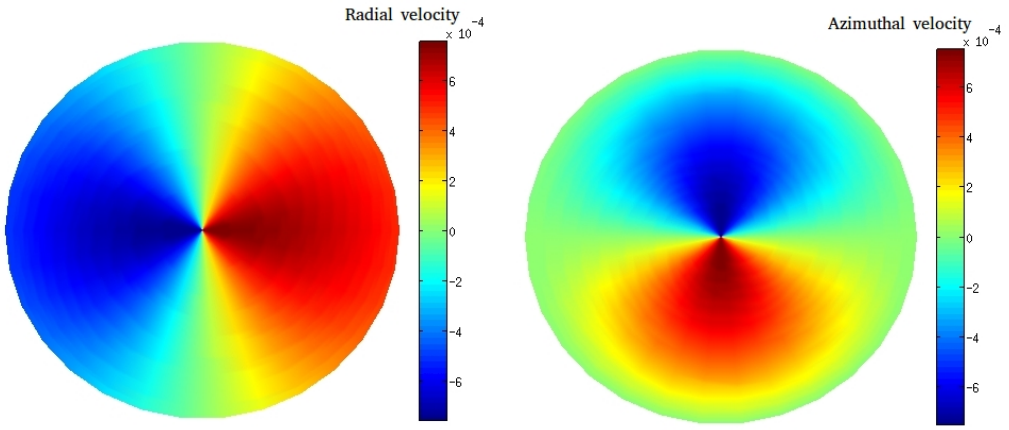
As before, spectral methods, Chebyshev polynomials of the first type in the radial direction and Fourier series in the azimuthal direction, with a colloca-

tion approach are used to solve this problem.

The roll flow problem is not straight forward to solve because it is nonlinear. This issue can be resolved by finding the solution to a linear approximation initially and using this solution to estimate the nonlinear terms. Iterating on this process will find solutions to the nonlinear problem to a desired accuracy. In this thesis the criteria is that the change in the maximal value of the radial velocity changes by less than 10^{-6} from it's previous iteration. In lower resolution numerical grids it is possible for the solutions not to converge but this was not an issue at the resolution used in this research.The initial linear system solved for this problem, to give initial guesses for the radial and azimuthal velocities, is the Stokes flow approximation to the equations. The Stokes flow solution is a reasonable first guess of the solution because the radial and azimuthal velocities are small in comparison to the axial velocity, and the length scales in the (r, θ) plane are typically much smaller than the streamwise length scale in pipe flow problems.

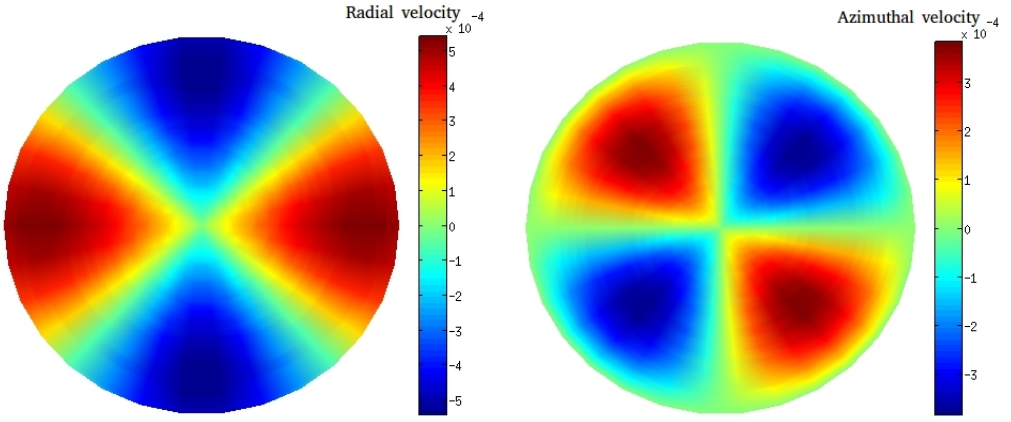
Figure 3.7 depicts the base radial and azimuthal velocity for 2π-periodic ($m = 1$) suction. With the suction-injection boundary condition enforced in this section, the radial flow is injected fastest at the $\theta = \pi$ position and sucked out fastest at the $\theta = 0$ position, where $\theta = 0$ is the radii on the horizontal to the right of the centre of the pipe. At the $\theta = \pi/2$ and $\theta = 3\pi/2$ positions the radial velocity on the wall is zero. The azimuthal velocity is zero on the wall and is fastest along the $\theta = \pi/2$ and $\theta = 3\pi/2$ radii. The magnitude of the velocity is determined by the Reynolds number and the suction coefficient. At the centre of the pipe the velocity is bounded but quicker than in the rest of the pipe.

Figures 3.8 and 3.9 plot the base radial and azimuthal velocities for π-periodic ($m = 2$) and $3\pi/2$-periodic ($m = 3$) suctions respectively. Although the functionality has been built to conduct the stability analysis on these higher suction mode base flows they have not been investigated in this thesis.



(a) Radial velocity. **(b)** Azimuthal velocity.

Figure 3.7: Circular pipe flow $R = 10000$ with 2π-periodic and $\lambda = 5$ suction. $(v(1,\theta) = 5cos(\theta))$.



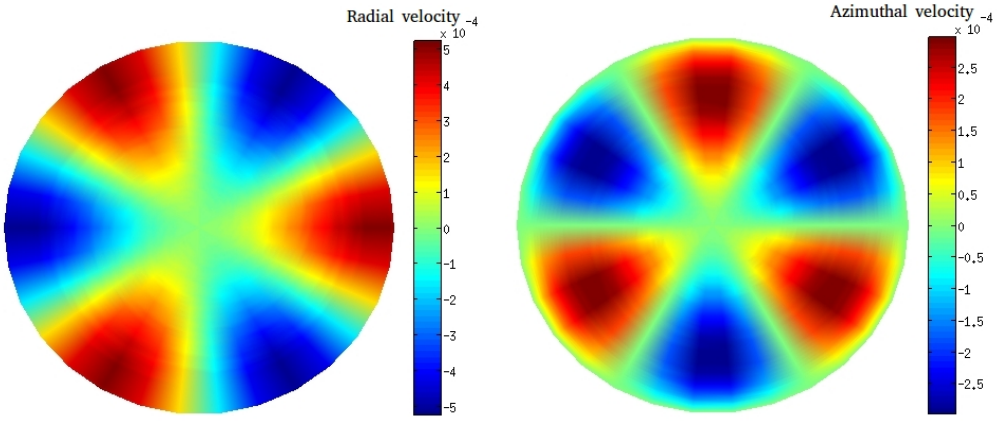
(a) Radial velocity. **(b)** Azimuthal velocity.

Figure 3.8: Circular pipe flow $R = 10000$ with 2π-periodic and $\lambda = 5$ suction. $(v(1,\theta) = 5cos(2\theta))$.

3.3.4 Axial flow in a pipe with suction

Turning attention to the streak problem, the governing streamwise momentum equation from the Navier-Stokes equations, with flow as described by (3.20), is

$$v\frac{\partial u}{\partial r} + \frac{w}{r}\frac{\partial u}{\partial \theta} = 4 + \left[\frac{1}{r}\frac{\partial}{\partial r}\left(r\frac{\partial u}{\partial r}\right) + \frac{1}{r^2}\frac{\partial^2 u}{\partial \theta^2}\right]. \tag{3.31}$$



(a) Radial velocity. **(b)** Azimuthal velocity.

Figure 3.9: Circular pipe flow $R = 10000$ with $3\pi/2$-periodic and $\lambda = 5$ suction. $(v(1,\theta) = 5cos(3\theta))$.

The Reynolds number does not appear in the equation by virtue of the way radial and azimuthal velocities and the pressure are scaled. The appearance of the constant 4 term in equation (3.31) is from the definition of the pressure derivative, $\frac{\partial p}{\partial x} = -\frac{4}{R}$. This is the same pressure term as used in the previous section and has the significance that when the suction coefficient, λ, is zero the flow returns back to Hagen-Poiseuille flow with a maximum non-dimensional velocity of 1.

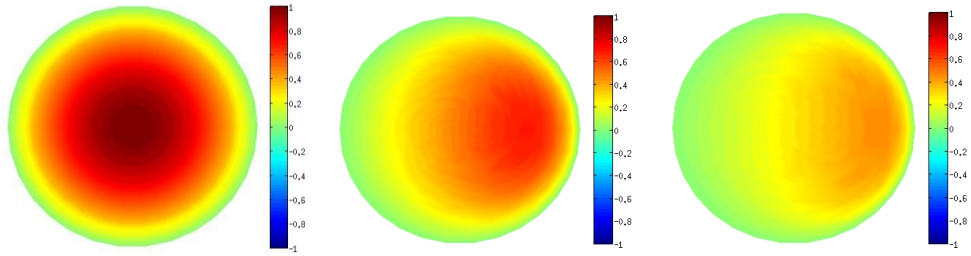
The boundary condition at the pipe wall is simply $u(1,\theta) = 0$ while at the centre of the pipe $u_n(0) = 0$ for all Fourier modes $n \neq 0$ and $\frac{du_0(0)}{dr} = 0$, as detailed in the Numerical methods subsection 2.3.

Numerical method and results for the axial flow

The streak equation is effectively a linear problem numerically because the radial and swirl flow components are known from the solution of the roll problem. Again, this boundary value problem is discretized and solved as linear system of equations using spectral methods.

As the suction (and injection) coefficient λ is increased the maximum of the streamwise velocity is pushed in the direction of the radial flow, and the maximum of the base flow is reduced. In the plots of Figure 3.10 the

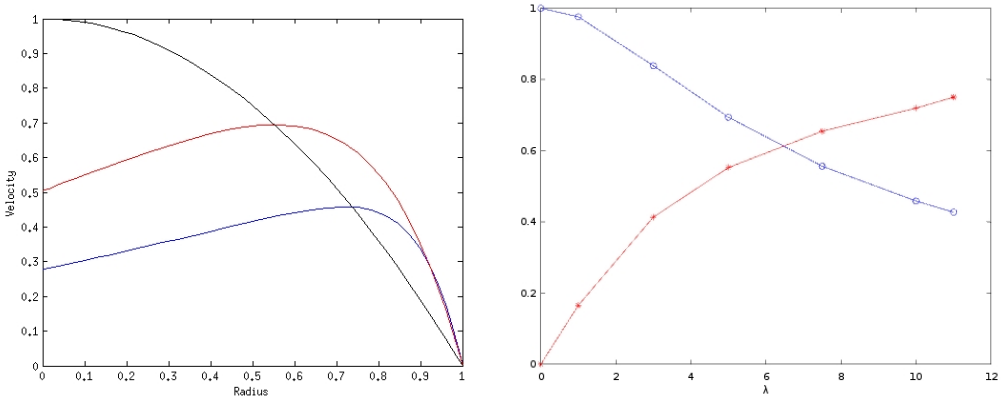
suction type is once again 2π-periodic but λ ranges between zero and 10. By making the pressure gradient in x, $\frac{\partial p}{\partial x}$, Reynolds number dependent, the radial position of the maximum of the streamwise flow is only dependent on the suction coefficient, and not the Reynolds number.



(a) $\lambda = 0$. **(b)** $\lambda = 5$. **(c)** $\lambda = 10$.

Figure 3.10: The streamwise velocity in circular pipe flow with 2π-periodic suction. $v(1, \theta) = \lambda cos(\theta)$ on the pipe wall. (Same scales).

Not only is the maximum of the streamwise velocity displaced from the centre of the pipe as λ increases but the magnitude of the maximum is diminished, as depicted in Figure 3.11. As the suction coefficient increases above $\lambda = 10$ the basic flow problem becomes more difficult to solve computationally, requiring many more grid points to converge to a solution. This issue arises from the increasingly large streamwise velocity gradients in the streak problem around the $\theta = 0$ radius near the wall.

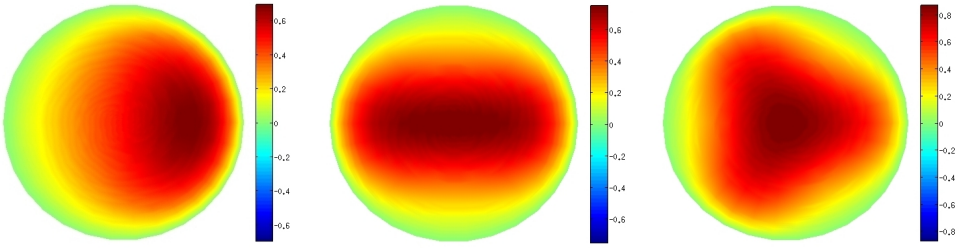


(a) Streamwise velocity profile at $\theta = 0$ for $\lambda = 0$ (black), 5 (red), 10 (blue).

(b) Streamwise velocity maximum (blue) and distance of maximum from centre (red).

Figure 3.11: The streamwise velocity in circular pipe flow at $\theta = 0$ with varying λ.

The formulation of this problem allows for different modes of suction to be investigated separately. Figure 3.12 compares the different profiles of the streamwise base velocity, u. The stability properties of these base flow modes are not investigated here however.



(a) $m = 1$. **(b)** $m = 2$. **(c)** $m = 3$.

Figure 3.12: The streamwise velocity in circular pipe flow with varying suction periodicity. $R = 10000$, $\lambda = 5$. Where $v(1, \theta) = \lambda cos(m\theta)$ is the non-zero boundary condition on the pipe wall.

3.3.5 Linear spatial stability of pipe flow with suction

A similar strategy to the spatial stability analysis of the pipe flow without suction will be used here. The small disturbance field, (U, V, W, P), is considered as a wave-like, non-axisymmetric velocity disturbance and there is a corresponding pressure perturbation. The form of the small perturbations is the same as before, with disturbance profiles $\boldsymbol{\delta}$ independent of x,

$$\boldsymbol{\delta}(r, \theta) = (U(r, \theta), V(r, \theta), W(r, \theta), P(r, \theta)) \tag{3.32}$$

These match the form of the 'normal modes' from traditional linear hydrodynamic stability theory. This method ensures that the Tollmien-Schlicting waves, which are most dominant in fully developed pipe flow, are captured. The partitioned disturbances account separately for the wave-like nature of the disturbance, $E = e^{i(\alpha x - \omega t)}$, and the profile of the disturbances, $\boldsymbol{\delta}$.

Once again, the disturbances are small enough such that the products will be infinitesimal and can be neglected, resulting in a linearised problem. It

is known that in the real world and experiments pipe flow transitions to turbulence under certain conditions but linear theory on pipe flow without suction fails to predict this. However, it is believed that in the case of pipe flow with suction exponentially growing perturbations can be found by linear stability theory and this can provide the starting point for nonlinear analysis which can reveal more about turbulence. The linear disturbance equations are shown in equations (3.33-3.36).

$$\begin{aligned} &i\alpha uU - i\omega U + V\frac{\partial u}{\partial r} + \frac{W}{r}\frac{\partial u}{\partial \theta} + \frac{1}{R}\left[v\frac{\partial U}{\partial r} + \frac{w}{r}\frac{\partial U}{\partial \theta}\right] \\ &= -\alpha i P + \frac{1}{R}\left[\frac{1}{r}\frac{\partial U}{\partial r} + \frac{\partial^2 U}{\partial r^2} + \frac{1}{r^2}\frac{\partial^2 U}{\partial \theta^2} - \alpha^2 U\right], \end{aligned} \tag{3.33}$$

$$\begin{aligned} &i\alpha uV - i\omega V + \frac{1}{R}\left[V\frac{\partial v}{\partial r} + v\frac{\partial V}{\partial r} - \frac{2wW}{r} + \frac{w}{r}\frac{\partial V}{\partial \theta} + \frac{W}{r}\frac{\partial v}{\partial \theta}\right] \\ &= -\frac{\partial P}{\partial r} + \frac{1}{R}\left[\frac{1}{r}\frac{\partial V}{\partial r} + \frac{\partial^2 V}{\partial r^2} + \frac{1}{r^2}\frac{\partial^2 V}{\partial \theta^2} - \frac{V}{r^2} - \frac{2}{r^2}\frac{\partial W}{\partial \theta} - \alpha^2 V\right], \end{aligned} \tag{3.34}$$

$$\begin{aligned} &i\alpha uW - i\omega W + \frac{1}{R}\left[V\frac{\partial w}{\partial r} + v\frac{\partial W}{\partial r} + \frac{wV}{r} + \frac{vW}{r} + \frac{w}{r}\frac{\partial W}{\partial \theta} + \frac{W}{r}\frac{\partial w}{\partial \theta}\right] \\ &= -\frac{1}{r}\frac{\partial P}{\partial \theta} + \frac{1}{R}\left[\frac{1}{r}\frac{\partial W}{\partial r} + \frac{\partial^2 W}{\partial r^2} + \frac{1}{r^2}\frac{\partial^2 W}{\partial \theta^2} - \frac{W}{r^2} + \frac{2}{r^2}\frac{\partial V}{\partial \theta} - \alpha^2 W\right], \end{aligned} \tag{3.35}$$

$$i\alpha U + \frac{1}{r}V + \frac{\partial V}{\partial r} + \frac{1}{r}\frac{\partial W}{\partial \theta} = 0. \tag{3.36}$$

The addition of the suction, and consequently, radial and azimuthal velocity components, to the base flow does not affect the boundary conditions of the disturbance problem. Exactly the same conditions apply here as in the previous section and these are the same as in the Numerical methods Chapter

in subsection 2.3.

Numerical method for the linear stability analysis

The problem described by the set of four disturbance equations (3.33-3.36) and boundary conditions in subsection 2.3 is essentially an eigenvalue problem for α. The basic flow terms, u, v, w, are known but the perturbation velocity, U, V, W, and pressure, P, are unknown. In order to solve this system for the spatial eigenvalue, α, and the corresponding eigenfuction, $\boldsymbol{\delta} = (U, V, W, P)$, the equations are rearranged into a generalised eigenvalue problem similar to (3.15),

$$L\boldsymbol{\delta} = \left(\begin{bmatrix} a_0 & a_1 \\ 0 & I \end{bmatrix} + \alpha \begin{bmatrix} 0 & a_2 \\ -I & 0 \end{bmatrix} \right) \begin{pmatrix} \boldsymbol{\delta} \\ \alpha\boldsymbol{\delta} \end{pmatrix} = \begin{pmatrix} 0 \end{pmatrix}, \tag{3.37}$$

where

$$a_0 = \begin{bmatrix} M & \frac{\partial u}{\partial r} & \frac{1}{r}\frac{\partial u}{\partial \theta} & 0 \\ 0 & \frac{1}{R}\left[\frac{\partial v}{\partial r} + \frac{1}{r^2}\right] + M & \frac{1}{R}\left[\frac{1}{r}\frac{\partial v}{\partial \theta} - \frac{2w}{r} + \frac{2}{r^2}\frac{\partial}{\partial \theta}\right] & \frac{\partial}{\partial r} \\ 0 & \frac{1}{R}\left[\frac{\partial w}{\partial r} + \frac{w}{r} - \frac{2}{r^2}\frac{\partial}{\partial \theta}\right] & \frac{1}{R}\left[\frac{v}{r} + \frac{1}{r}\frac{\partial w}{\partial \theta} + \frac{1}{r^2}\right] + M & \frac{1}{r}\frac{\partial}{\partial \theta} \\ 0 & \frac{1}{r} + \frac{\partial}{\partial r} & \frac{1}{r}\frac{\partial}{\partial \theta} & 0 \end{bmatrix}, \tag{3.38}$$

$$a_1 = \begin{bmatrix} iu & 0 & 0 & i \\ 0 & iu & 0 & 0 \\ 0 & 0 & iu & 0 \\ i & 0 & 0 & 0 \end{bmatrix}, \tag{3.39}$$

$$a_2 = \begin{bmatrix} \frac{1}{R} & 0 & 0 & 0 \\ 0 & \frac{1}{R} & 0 & 0 \\ 0 & 0 & \frac{1}{R} & 0 \\ 0 & 0 & 0 & 0 \end{bmatrix}, \tag{3.40}$$

$$M = -\omega i - \frac{1}{R}\left[-v\frac{\partial}{\partial r} - \frac{w}{r}\frac{\partial}{\partial \theta} + \frac{1}{r}\frac{\partial}{\partial r} + \frac{\partial^2}{\partial r^2} + \frac{1}{r^2}\frac{\partial^2}{\partial \theta^2}\right], \tag{3.41}$$

and L is a matrix operator. The same spectral scheme is used here as in the previous section to form the basis functions of the unknown terms. Similar to before, the disturbance associated with the least stable eigenvalue is of interest because it is the most likely to become increasingly unstable and cause transition downstream. The frequency, ω, is chosen to be real and the growth or decay of the disturbance in space is entirely captured in the spatial eigenvalue.

3.3.6 Linear stability results for 2π-periodic suction

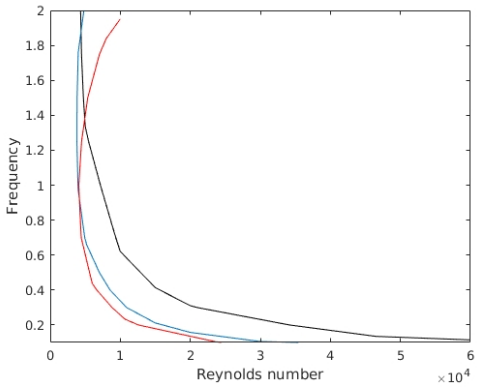
With the base flow subject to suction and injection on the pipe wall it can be shown that the least stable eigenvalues become unstable under certain conditions. In this disturbance-level analysis only the 2π-periodic, $m = 1$, suction will be considered.

Neutral curves

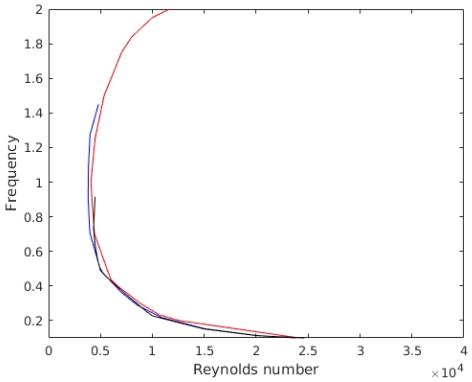
As there are now unstable disturbances it is sensible to plot the neutral curve of the least stable eigenvalue in the Reynolds number-frequency plane. Each suction coefficient λ generates a different neutral curve and this curve moves to smaller Reynolds numbers and frequencies as the suction is increased, as can be seen in Figure 3.13a.

Figure 3.13a suggests that there is a critical Reynolds of around 4000, that is, a smallest Reynolds for all suction coefficients for which the least stable eigenvalue becomes unstable. This value falls within the range of critical Reynolds numbers observed in experiments. Davey & Drazin[7] state that the critical number for Poiseuille flow in a pipe can be from $R = 2000$ up to $R = 40000$ in carefully configured experiments.

It is unsurprising that the influence of varied suction does not change the critical Reynolds number as the two are unrelated in the formulation. The



(a) Neutral curve plots for λ=5 (black), λ=7.5 (blue), λ=10 (red).



(b) Collapsed neutral curve plots for λ=5 ($\frac{\omega}{2.73}$, black), λ=7.5 ($\frac{\omega}{1.38}$, blue), λ=10 (red).

Figure 3.13: Neutral curve plots for pipe flow with suction at varying suction coefficients.

suction is taken at the same order of magnitude as the roll velocity terms, v and w. The profile of the swirl velocity components, v and w, in the radial-azimuthal plane is unchanged by the suction parameter λ. As described earleir, the result of the $\mathcal{O}(R^{-1})$ scaling of the 'roll' flow, is that this problem is decoupled from the axial velocity problem and the Reynolds number does not appear in the streamwise momentum equation. In the disturbance problem the base flow swirl components, and therefore the effects of varied suction, are contained in the convection terms of the Navier-Stokes equations and are balanced independently of R by the diffusion terms. However, the relative scale between the wave frequency and the swirl flow components is not independent of the Reynolds number, resulting in the neutral curves having similar shapes scaled by frequency.

Figure 3.13b shows that the curves collapse on to one another when the frequency is linearly scaled appropriately. From the scaling relationship described in the collapsed plot the neutral curves for any suction parameter should be predictable. Using a colour plot, as in Figure 3.14, the growth rate over the whole spectrum of Reynolds numbers and frequencies can be considered. These plots show that there is a frequency for a given combination of suction and Reynolds number that results in the most unstable eigenvalue with the highest growth rate. For frequencies below a certain critical value,

dependent on the suction coefficient and Reynolds number, the growth rate is increasing as frequency is increased but above this critical value the growth rate is decaying.

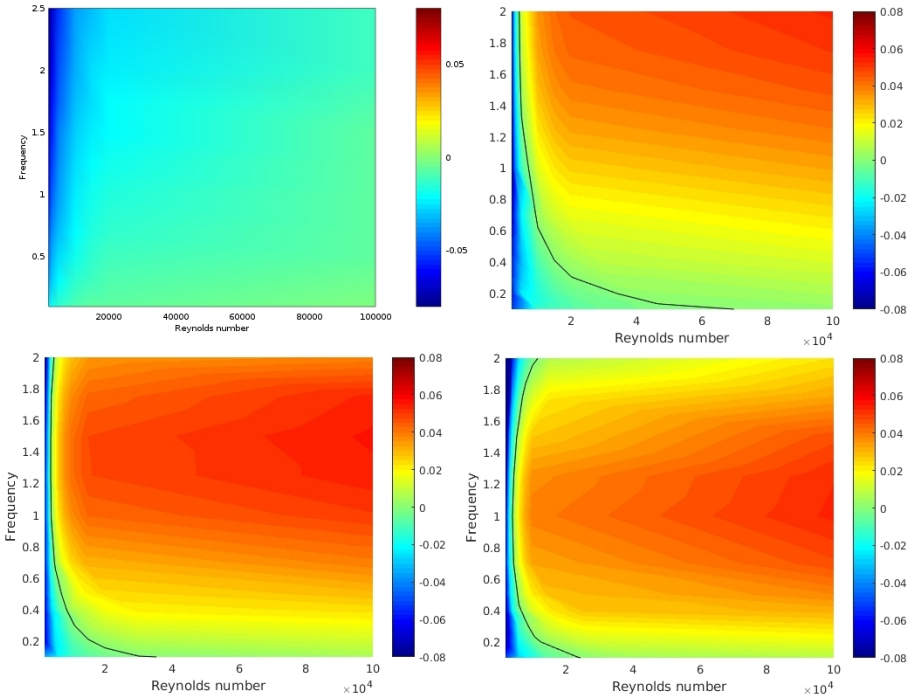


Figure 3.14: Colour plot for growth rates and neutral curves (same scales). a) λ=0, b) λ=5, c) λ=7.5, d) λ=10.

For a fixed frequency increasing the Reynolds number results in an increasing growth rate, asymptoting to a constant. In Hagen-Poiseuille the growth rate also asymptotes to a constant but the value is always negative. The relationships between the growth rates and frequency, and growth rates and Reynolds number are depicted in Figure 3.15.

Disturbance profiles and constant phase velocity

Turning attention to the disturbance profiles, it is noticeable that the main activity is concentrated around the area where $\alpha_r u = \omega$, where subscript r denotes the real part. This relationship comes from the term in the Navier-Stokes equations for Tollmien-Schlichting waves relating the wavenumber and

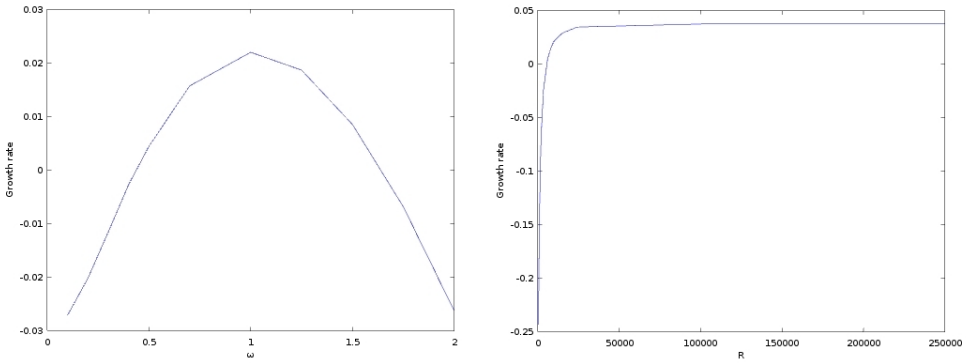


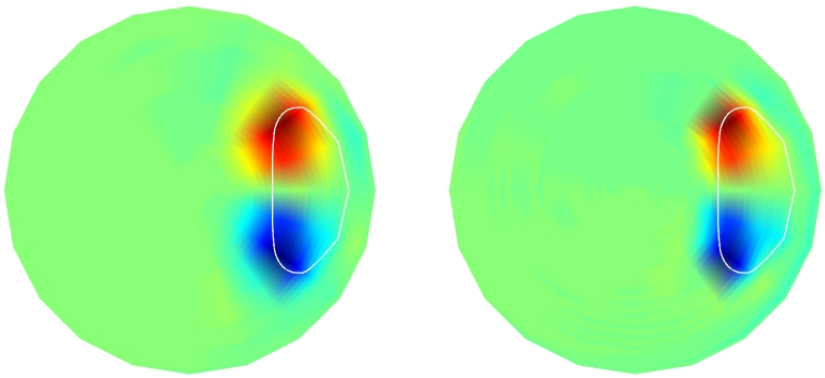
Figure 3.15: Growth rate plotted against a) frequencies at $R = 6000$, b) Reynolds number at $\omega = 0.5$. $\lambda = 10$.

wave frequency. Figure 3.16 plots the streamwise disturbance profile in the (r, θ) plane for a fixed suction and fixed frequency but increasing Reynolds numbers. At greater Reynolds numbers the influence of the diffusion terms in the Navier-Stokes equations are diminished and in Figure 3.16 it is evident that the disturbance peaks seem to localise as the Reynolds number increases, which is also true in Hagen-Poiseuille flow.

When the disturbance profiles for fixed suction and fixed Reynolds numbers but varying frequency are analysed it would be reasonable to assume that the boundary where $\alpha_r u = \omega$, would change, however the sequence of plots for increasing frequency in Figure 3.17 appear to describe a similar pattern to Figure 3.16.

Phase velocity, defined as $\left(\frac{\omega}{\alpha_r}\right)$ with subscript r denoting the real part, is very nearly constant across the spectrum of Reynolds numbers and frequencies. The almost linear relationship between frequency and wavenumber on the neutral curve for $\lambda = 5$ is plotted in Figure 3.18. A similar plot can be made for the neutral curves for every λ. The proportionality of the wave frequency and the wavenumber means that phase velocity equals group velocity and the wave will travel undistorted at this velocity.

The phase velocity of the most unstable eigenvalue decreases as suction is increased, in other words, for the same frequencies wavelengths are longer. When suction is increased the magnitude of the streamwise base flow is re-



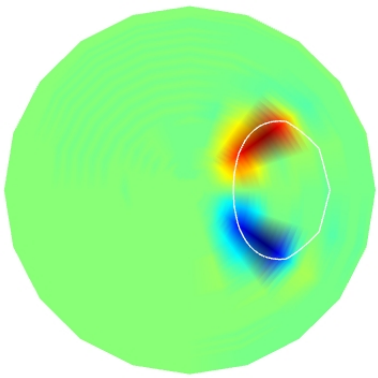
(a) Streamwise disturbance, $R = 2000$.

(b) Streamwise disturbance, $R = 10000$.

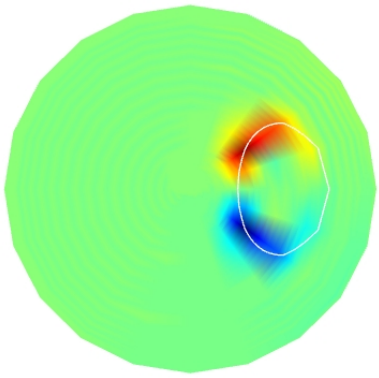
(c) Streamwise disturbance, $R = 25000$.

(d) Streamwise disturbance, $R = 100000$.

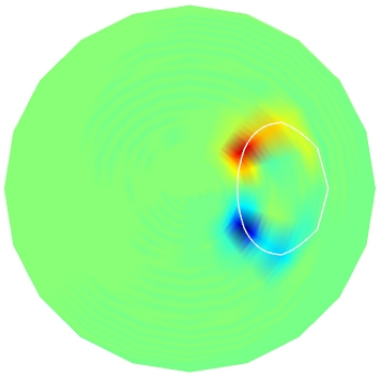
Figure 3.16: Comparison of streamwise disturbance profiles in pipe flow with 2π-periodic suction when $\omega = 0.4$, $\lambda = 10$. White line indicates where $\alpha_r u = \omega$.



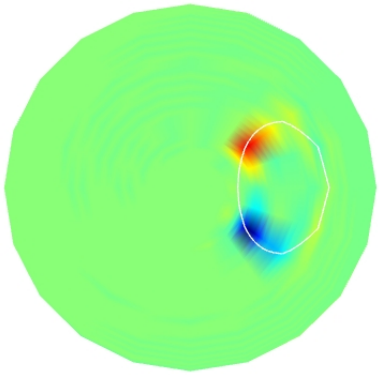
(a) Streamwise disturbance, $\omega = 0.2$.



(b) Streamwise disturbance, $\omega = 0.7$.



(c) Streamwise disturbance, $\omega = 1.5$.



(d) Streamwise disturbance, $\omega = 2.5$.

Figure 3.17: Comparison of streamwise disturbance profiles in pipe flow with 2π-periodic suction when $R = 20000$, $\lambda = 10$. White line indicates where $\alpha_r u = \omega$.

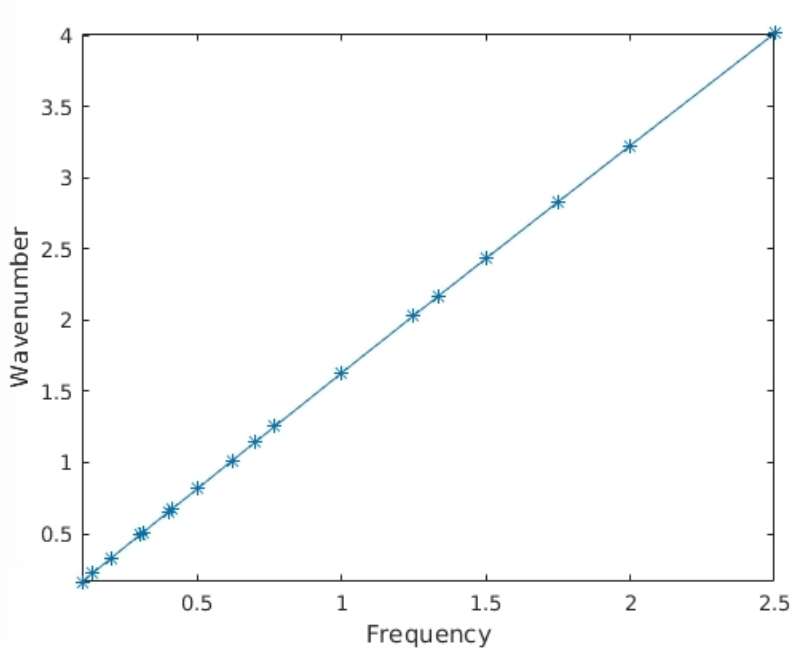


Figure 3.18: Frequency against wavenumber on the neutral curve for pipe flow with 2π-periodic suction and $\lambda = 5$.

duced and Figure 3.19 reveals that the phase velocity is directly proportional to the maximum of the streamwise base flow velocity. Therefore, the phase velocity can be calculated from the streamwise base flow velocity directly when the wave growth rate is neutral. Further, for any given frequency the wavenumber is approximately known.

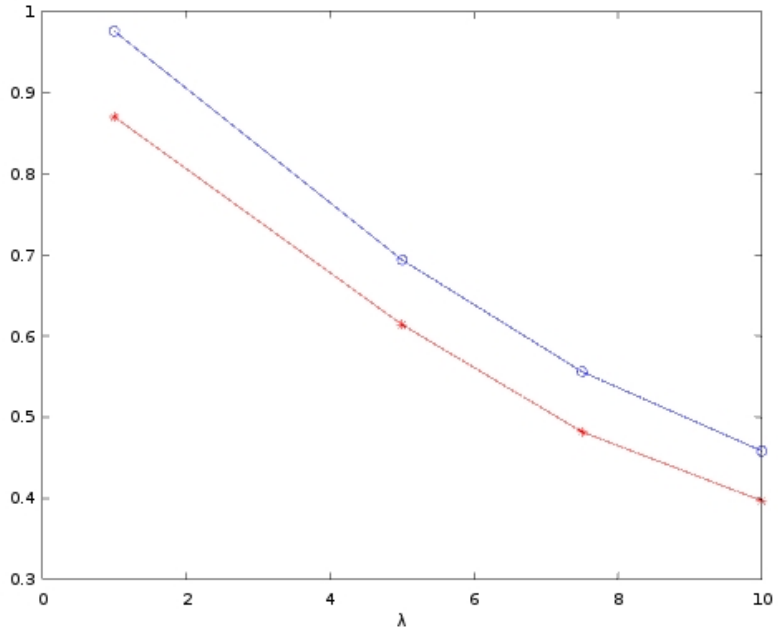


Figure 3.19: Streamwise velocity maximum (blue circles) and phase velocity (red dots) against suction coefficient λ for pipe flow with 2π-periodic suction.

3.3.7 Weakly nonlinear spatial stability

In order to understand more about the spatial stability properties of this viscous, incompressible flow through a pipe with suction on the pipe wall, and model something more similar to experiments, a weakly nonlinear study is conducted in this section. By doing a nonlinear analysis it is hoped it can be shown that the disturbance reaches some sort of ultimate equilibrium, rectifying the limitation in the linear stability theory that a disturbance will always grow or decay exponentially in space depending on whether the Reynolds number is greater than some critical value or not. The effect the nonlinear terms have on the growth or decay of the disturbance will be described and numerical calculations will establish that there are only valid solutions for weakly nonlinear theory in the supercritical region for pipe flow with suction.

The broad idea of weakly nonlinear analysis is to consider the problem close to the neutral stability conditions and explore the expansions of several variables. The disturbance found from linear stability analysis is now expanded

in terms of amplitudes and harmonics,

$$\boldsymbol{\delta} = \boldsymbol{\delta_1} e^{i(\alpha x - \omega t)} + \overline{\boldsymbol{\delta_1}} e^{-i(\overline{\alpha} x - \omega t)} + \epsilon \boldsymbol{\delta_0} + \epsilon \boldsymbol{\delta_2} e^{2i(\alpha x - \omega t)} + \epsilon \overline{\boldsymbol{\delta_2}} e^{-2i(\overline{\alpha} x - \omega t)} + \text{higher harmonics}, \tag{3.42}$$

where $\boldsymbol{\delta_j} = (U_j(r,\theta), V_j(r,\theta), W_j(r,\theta), P_j(r,\theta))$, for $j = 0, 1, 2$, are the shape functions for the zeroth, first and second harmonics. The notation and configuration of the last section is continued here and ϵ is a small scalar. The first harmonic is then expanded into the leading order term, which is the solution to the linear disturbance problem, and a correction term, $\boldsymbol{\delta_1} = \boldsymbol{\delta_{10}} + \epsilon^2 \boldsymbol{\delta_{11}}$. $\boldsymbol{\delta_{10}}$ is now reformulated such that $\boldsymbol{\delta_{10}} = A\boldsymbol{\phi_{10}}$, where A is an amplitude term. In the spatial analysis conducted here it makes sense to consider A as some function of the streamwise coordinate, $A = A(X)$, where $X = \epsilon^2 x$ is a short streamwise length scale, following the work of Stuart[46] and Watson[56]. This short length scale ensures that the streamwise derivative of the amplitude appears initially at $\mathcal{O}(\epsilon^3)$ where it can be addressed.

By solving the disturbance problem in a sequence, starting with the problem for the greatest amplitude, what remains is a solvability condition on the amplitude A. This condition is a differential equation and the solution reveals that in certain circumstances the amplitude can reach equilibrium in space.

Formulation

The full formulation of this problem occupies several pages and can be found in Appendix A. The equations which recover the linear stability of the last section are (A.1-A.4), and the solution to these is $\boldsymbol{\phi_{10}}$. The zeroth and the second harmonics are $\mathcal{O}(\epsilon^2)$ and the equations to these problems are (A.11-A.14) and (A.15-A.18) respectively. With the solutions $\boldsymbol{\phi_0}$ and $\boldsymbol{\phi_2}$ from those problems it is possible to tackle the first harmonic correction term problem. This problem is similar to (A.1-A.4) but the right hand side of the equations is a nonlinear differential problem. For a solution to be possible and consistent mathematically the solvability condition (A.24) must

be satisfied. The solvability condition is reproduced below,

$$\int \int \hat{\mathbf{\Phi}} \cdot \boldsymbol{h} r \partial r \partial \theta = 0. \tag{3.43}$$

$\hat{\mathbf{\Phi}}$ is the adjoint function of the matrix operator L, equation (3.37), and $\boldsymbol{h}$ is the nonlinear terms described in (A.19-A.22). $\boldsymbol{h}$ can be rearranged and written in the form $\boldsymbol{h} = \boldsymbol{h_1}\frac{\partial A}{\partial X} + \boldsymbol{h_2} R_1 A + \boldsymbol{h_3} A|A|^2$, where $\boldsymbol{h_1}, \boldsymbol{h_2}$ and $\boldsymbol{h_3}$ are known vectors. The integral condition, equation (3.43), can now be described by the differential equation for the amplitude in equation (3.44).

$$\frac{\partial A}{\partial X} = \beta_1 R_1 A + \beta_2 A|A|^2. \tag{3.44}$$

Where the constants β_1, β_2 are defined below.

$$\beta_1 = -\frac{\int \int \hat{\mathbf{\Phi}} \cdot \boldsymbol{h_2} r \partial r \partial \theta}{\int \int \hat{\mathbf{\Phi}} \cdot \boldsymbol{h_1} r \partial r \partial \theta} \tag{3.45}$$

$$\beta_2 = -\frac{\int \int \hat{\mathbf{\Phi}} \cdot \boldsymbol{h_3} r \partial r \partial \theta}{\int \int \hat{\mathbf{\Phi}} \cdot \boldsymbol{h_1} r \partial r \partial \theta} \tag{3.46}$$

This manipulation is possible in all but the unlikely case where denominator in equations (3.45) and (3.46) is zero, and this possibility is not considered here.

Theoretical investigation into amplitude changes in space

Stuart[46] finds a similar equation to (3.44). Following his paper, consider this equation multiplied by the conjugate of A and the conjugate equation multiplied by A,

$$\overline{A}\frac{\partial A}{\partial X} = \beta_1 R_1 \overline{A} A + \beta_2 \overline{A} A |A|^2. \tag{3.47}$$

$$A\frac{\partial \overline{A}}{\partial X} = \overline{\beta_1} R_1 A \overline{A} + \overline{\beta_2} A \overline{A} |A|^2. \tag{3.48}$$

Then by summing both equations the result is

$$\overline{A}\frac{\partial A}{\partial X} + A\frac{\partial \overline{A}}{\partial X} = \beta_1 R_1 \overline{A} A + \beta_2 \overline{A} A |A|^2 + \overline{\beta_1} R_1 A \overline{A} + \overline{\beta_2} A \overline{A} |A|^2, \tag{3.49}$$

and this can be rewritten in the more concise form,

$$\frac{\partial |A|^2}{\partial X} = 2\beta_{1r} R_1 |A|^2 + 2\beta_{2r} |A|^4, \tag{3.50}$$

where β_{1r}, β_{2r} are the real parts of the respective complex constants β_1, β_2. It follows that a solution to problem (3.50) is

$$|A|^2 = \frac{\beta_{1r} R_1 C exp(2\beta_{1r} R_1 X)}{1 - \beta_{2r} C exp(2\beta_{1r} R_1 X)}, \tag{3.51}$$

where C is an arbitrary real constant. $|A|^2$ must be positive and there are two possibilities for R_1: it is negative, and this is called the subcritical case, where the Reynolds number is less than the linear stability critical value, or it is positive, being the supercritical case. β_{1r} and β_{2r} are still yet to be determined but given that $|A|^2$ must be positive the values which β_{1r} and β_{2r} can take are restricted. Figure 3.20 demonstrates what happens when X tends to negative infinity or infinity in the valid cases. Cases where the amplitude tends to infinity are considered invalid here as they are contrary to the assumption the amplitudes are small in this investigation. The case $\beta_{1r} R_1 = 0$ is the trivial solution because this results in $|A|^2 = 0$.

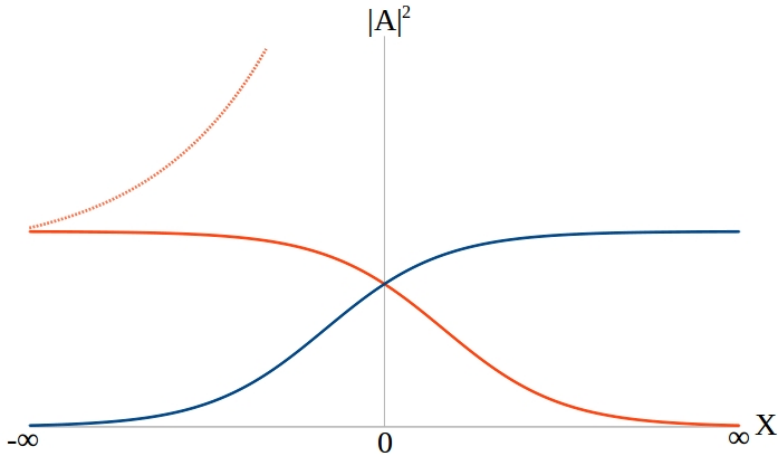


Figure 3.20: Sketches for the behaviour of $|A|^2$. Blue is the case $\beta_{1r}R_1 > 0$, $\beta_{2r} < 0$, and the two variations of red are for the cases $\beta_{1r}R_1 < 0$, $\beta_{2r} > 0$. (When C is chosen to be positive.)

The flow itself is independent of the streamwise variable but the amplitude of the perturbations is not. In an infinitely long pipe, such as the one considered here, there are three cases towards the origin of the disturbance, where X tends to negative infinity. In the case where $\beta_{1r}R_1 > 0$ and $\beta_{2r} < 0$, the blue line in Figure 3.20, the perturbation will be infinitesimal upstream, however this disturbance will slowly grow until the square of the absolute value of the amplitude approaches an equilibrium far downstream. The cases shown in red in Figure 3.20 are when $\beta_{1r}R_1 < 0$ and $\beta_{2r} > 0$. The light red line shows that if $|A|^2$ is greater than $|\beta_{1r}R_1|/|\beta_{2r}|$ initially then the amplitude grows to infinity and the mathematical structure in this investigation does not support this solution, and therefore this equilibrium is unstable. If $|A|^2$ is less than $|\beta_{1r}R_1|/|\beta_{2r}|$, the case in dark red, the amplitude will eventually decay to zero downstream.

To understand the nature of A take equation (3.44) multiplied by $\overline{A}^{-1}$ and the conjugate of equation (3.44) multiplied by $-A\overline{A}^{-2}$, and then add the resultant equations:

$$\frac{\partial}{\partial X}\left(\frac{A}{\overline{A}}\right) = 2i\beta_{1i}R_1\frac{A}{\overline{A}} + 2i\beta_{2i}A^2, \tag{3.52}$$

where β_{1i}, β_{2i} are the imaginary parts of the respective complex constants. This equation can be manipulated further to get a solution for A in known terms. By multiplying by $\overline{A}A^{-1}$ and taking the integral over the axial spectrum the result is

$$ln\left(\frac{A}{\overline{A}}\right) = 2i\int_{-\infty}^{\infty} \beta_{1i}R_1 + \beta_{2i}|A|^2\partial X. \tag{3.53}$$

Then by taking the exponential multiplied by $|A|^2$ the equation becomes,

$$A^2 = |A|^2 exp\left(2i\int_{-\infty}^{\infty} \beta_{1i}R_1 + \beta_{2i}|A|^2\partial X\right). \tag{3.54}$$

Finally, the square root gives the equation for A.

$$A = |A| exp\left(i\int_{-\infty}^{\infty} \beta_{1i}R_1 + \beta_{2i}|A|^2\partial X\right). \tag{3.55}$$

From the definition of $|A|^2$ in equation (3.51), the integral in equation (3.55) can be evaluated,

$$\begin{aligned}\int |A|^2\partial X &= \int \frac{\beta_{1r}R_1 C exp(2\beta_{1r}R_1 X)}{1-\beta_{2r}C exp(2\beta_{1r}R_1 X)}\partial X \\ &= -\frac{1}{2\beta_{2r}} ln\left(|1-\beta_{2r}C exp(2\beta_{1r}R_1(X-X_0))|\right),\end{aligned} \tag{3.56}$$

where X_0 is a arbitrary real constant. Then A can be written,

$$A = |A| exp\left(i\beta_{1i} R_1 (X - X_0) - \frac{i\beta_{2i}}{2\beta_{2r}} ln|1 - \beta_{2r} C exp(2\beta_{1r} R_1 (X - X_0))| \right), \tag{3.57}$$

where $|A|$ is known and defined in equation (3.58),

$$|A| = (\beta_{1r} R_1 C)^{1/2} exp(\beta_{1r} R_1 X) \left(1 - \beta_{2r} C exp(2\beta_{1r} R_1 X)\right)^{-1/2}. \tag{3.58}$$

Given this definition of the amplitude and the restrictions on β_{1r},β_{1r} and R_1 described before, the nature of A can be described. Consider the case where $\beta_{1r} R_1 > 0$, $\beta_{2r} < 0$, the blue curve in Figure 3.20. As $X \to -\infty$,

$$A \to (\beta_{1r} R_1 C)^{1/2} exp(\beta_{1r} R_1 X + i\gamma), \tag{3.59}$$

where γ is a number dependent on X_0, β_{1i} and R_1. In the limit where $X \to \infty$,

$$A \to \left(\frac{\beta_{1r} R_1}{-\beta_{2r}} \right)^{1/2} exp\left(i\beta_{1i} R_1 \left(1 - \frac{\beta_{2i}}{\beta_{2r}} \right) (X - X_k) \right), \tag{3.60}$$

where X_k is an arbitrary shift related to the arbitrary number X_0. The equations (3.59) and (3.60) show that if A is non-oscillatory at $X \to -\infty$, a fluctuation develops in the amplitude as X progresses and there is a limiting form. As A is known in the limits, now the limiting form of the first harmonic disturbance can be described in more clarity. Recall the definitions from the start of this section, $X = \epsilon^2 x$ and $R - R_c = \epsilon^2 R_1$, and

$$\boldsymbol{\delta_1} e^{i(\alpha_c x - \omega t)} = A\boldsymbol{\phi_1} e^{i(\alpha_c x - \omega t)} = A(\boldsymbol{\phi}_{10} + \epsilon^2 \boldsymbol{\phi_{11}}) e^{i(\alpha_c x - \omega t)}. \tag{3.61}$$

Then, the leading order, limiting form of the first harmonic disturbance, which is also the leading order term of the disturbance as a whole as described in (3.42), is

$$(\beta_{1r} R_1 C)^{1/2} exp(i\gamma)\phi_{10} exp(i\left(\alpha_c x - i\beta_{1r}(R - R_c)x - \omega t\right)) \\ as \;\; X \to -\infty, \tag{3.62}$$

$$\left(\frac{\beta_{1r} R_1}{-\beta_{2r}}\right)^{1/2} \phi_{10} exp\left(i\left(\left[\alpha_c + \beta_{1i}(R - R_c)\left(1 - \frac{\beta_{2i}}{\beta_{2r}}\right)\right](x - x_k) - \omega t\right)\right) \\ as \;\; X \to \infty, \tag{3.63}$$

where $X_k = \epsilon^2 x_k$. Equation (3.62) reveals that, when $X \to -\infty$ the disturbance has an amplitude factor of $(\beta_{1r} R_1 C)^{1/2} exp(i\gamma)$, however this is arbitrary except for being small to satisfy the limitations of this weakly nonlinear analysis. In this case, R must be chosen such that $\beta_{1r}(R - R_c) > 0$. This means that the wave growth rate is positive, and therefore this is the supercritical case. In Stuart's paper[46], the growth rate is used directly in the formulation rather than $\beta_{1r} R_1$. In the ultimate equilibrium state in space, equation (3.63), the growth rate has disappeared as expected but there is a change in the wavenumber of $\beta_{1i}(R - R_c)\left(1 - \frac{\beta_{2i}}{\beta_{2r}}\right)$, with an arbitrary shift of x_k in the wave.

In the case where $\beta_{1r} R_1 < 0$ and $\beta_{2r} > 0$, the solutions are very similar. The leading order, limiting form of the first harmonic disturbance is as follows

$$\left(\frac{\beta_{1r}R_1}{-\beta_{2r}}\right)^{1/2}\phi_{10}exp\left(i\left(\left[\alpha_c+\beta_{1i}(R-R_c)\left(1-\frac{\beta_{2i}}{\beta_{2r}}\right)\right](x-x_k)-\omega t\right)\right)$$
$$as\ \ X\to-\infty, \tag{3.64}$$

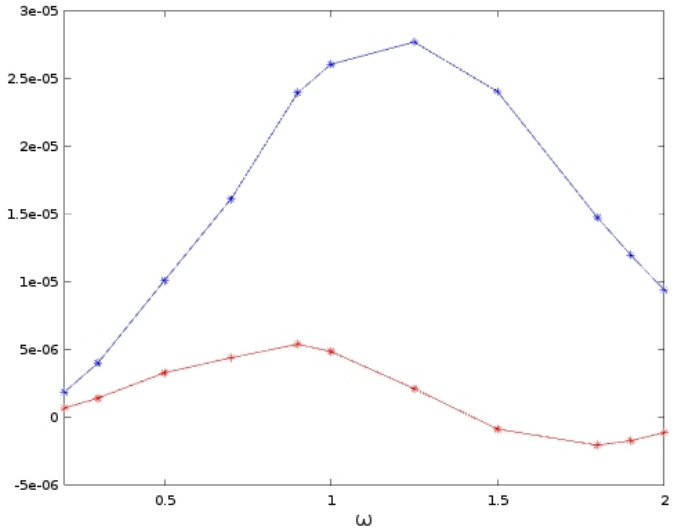
$$(\beta_{1r}R_1C)^{1/2}exp(i\gamma)\phi_{10}exp(i\left(\alpha_c x-i\beta_{1r}(R-R_c)x-\omega t\right))$$
$$as\ \ X\to-\infty. \tag{3.65}$$

The significant difference here to the first case, other than that the limits are reversed, is that here $\beta_{1r}(R-R_c)<0$. This time this is the subcritical case and the growth rate is negative until the disturbance amplitude decays to zero.

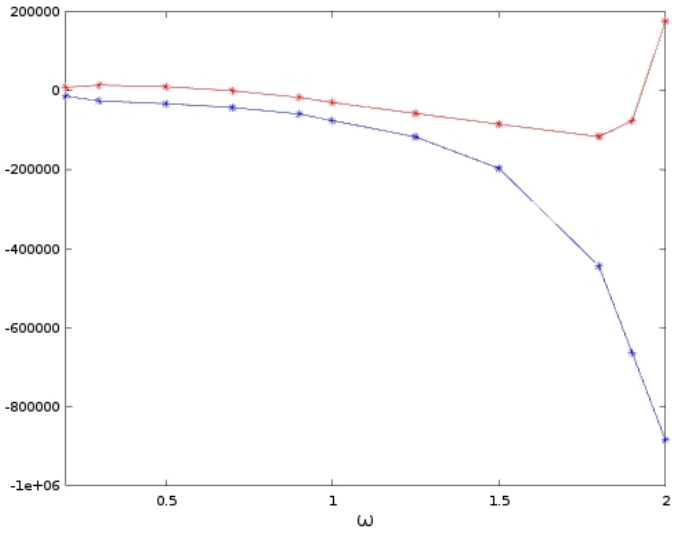
Numerical investigation into weakly nonlinear stability

It is worth remembering at this point that this numerical investigation of weakly nonlinear theory is specifically concerned with pipe flow with suction boundaries. This flow has been shown in the previous sections to be linearly unstable under certain conditions and here it will be demonstrated that weakly nonlinear theory can reveal more insight into the ultimate equilibrium state of this flow.

As with the other numerical problems encountered in this thesis a spectral approach is used to find solutions. The linear systems of equations for the zeroth (A.11-A.14) and second harmonic (A.15-A.18) can be solved directly. Finding the adjoint operator is also a matter of solving a linear system of equations. To approximate the critical Reynolds number linear interpolation was used and the process was iterated until the absolute value of the growth rate was found to be less than 10^{-4}. From these solutions the terms β_1 and β_2 are calculated by numerical integration using Simpson's rule. The solutions for supercritical and subcritical Reynolds number over a range of frequencies are plotted in figures 3.21 and 3.22.



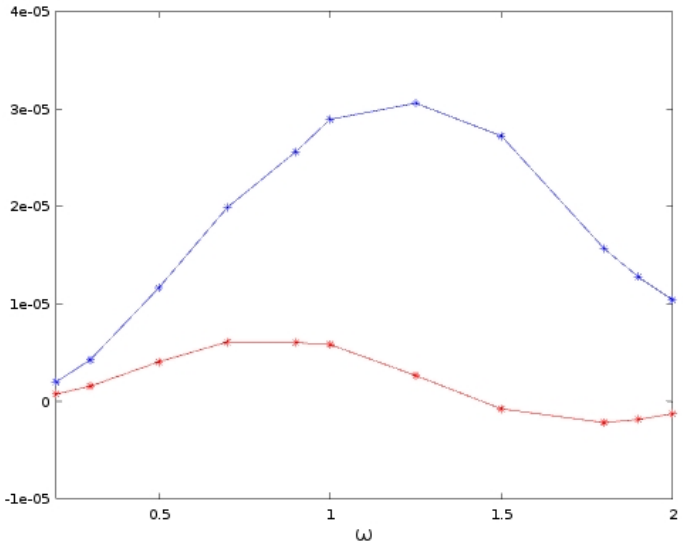
(a) β_1 real part (blue line) and imaginary part (red line) against ω.



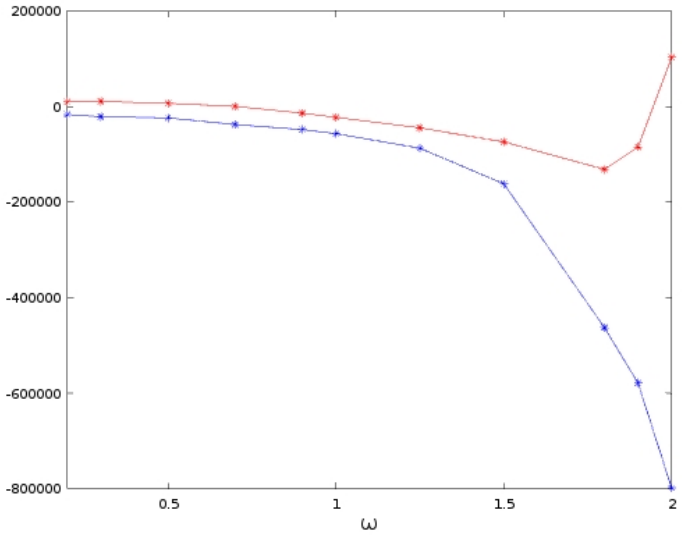
(b) β_2 real part (blue line) and imaginary part (red line) against ω.

Figure 3.21: Weakly nonlinear stability of pipe flow with suction. Supercritical case, $R > R_c$.

It is the real parts of β_1 and β_2, the blue lines in figures 3.21 and 3.22, which are important in determining the validity of the solutions. The imaginary parts modify the wavenumber and are of lesser importance at this stage.



(a) β_1 real part (blue line) and imaginary part (red line) against ω.



(b) β_2 real part (blue line) and imaginary part (red line) against ω.

Figure 3.22: Weakly nonlinear stability of pipe flow with suction. Subcritical case, $R < R_c$.

With the weakly nonlinear theory presented here, solutions for the terms β_1 and β_2 can exist that result in $|A|^2 < 0$ and these are invalid. For valid solutions, either $\beta_{1r}R_1 > 0$ and $\beta_{2r} < 0$ must be true or $\beta_{1r}R_1 < 0$ and $\beta_{2r} > 0$. Figures 3.21 and 3.22 display very similar trends and attributes:

$\beta_{1r} > 0$ for all frequencies, while $\beta_{2r} < 0$ for all frequencies. This means that only one of these sets of solutions is valid and it is the supercritical case, where $R_1 > 0$, which is valid. Therefore it is equation (3.63) which describes the ultimate equilibrium of this disturbance.

Stuart's investigation[46] into the temporal stability of Poiseuille flow yields an equation similar to equation (3.44). Instead of the $\beta_{1r}R_1$ term that appears here, Stuart has the temporal growth rate from the linear problem. This is the result of having a simple two-dimensional base flow. In this investigation, with a three-dimensional base flow, the nonlinear growth rate is $\beta_{1r}(R - R_c)$ and it is notable that this value is always greater than the linear growth rate. The difference in the growth rates is a function of the frequency and this relationship is shown in Figure 3.23.

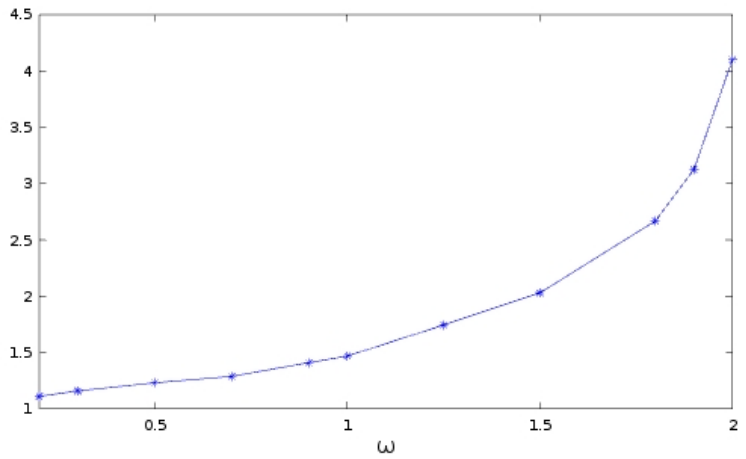


Figure 3.23: The ratio of $\beta_{1r}(R - R_c)$ to the growth rate from linear theory, over a range of disturbance frequencies, ω.

The effect on the wavenumber isn't so clear. The values β_{1i} and β_{2i} change sign and magnitude depending on the frequency. This intricate calculation will not reveal more about the stability properties of the flow and therefore is not explored further here. One final remark on the results for β_1 and β_2 is regarding the difference in scale. The relative sizes can be anticipated from equation (3.44), where the terms A and $A|A|^2$ have the coefficients $\beta_1 R_1$ and β_2 respectively. From this equation it is possible to say that $\beta_1(R - R_c)/\epsilon^2 \sim \beta_2$, where ϵ is small. The solutions for β_1 and β_2 substantiate this relationship.

3.3.8 Conclusions

In the first section of this chapter a spatial stability model was validated against the well-known results for parallel Hagen-Poiseuille flow. The flow is shown to be linearly stable, that is stable to all linear disturbances including ones that are non-axisymmetric. The next section investigated Hagen-Poiseuille flow when suction and injection is applied at the pipe walls. These boundary conditions force the flow to become non-parallel.

It was shown that as the 2π-periodic suction on the pipe wall is increased the maximum of the streamwise base flow component is dragged from the centre of the pipe towards the boundary where the flow is exiting the pipe. The maximum of the axial flow component is also reduced as suction is increased. This non-parallel flow is shown to be unstable to infinitesimal disturbances under certain conditions and the neutral curve for various suction coefficients was plotted. The neutral curves are linearly scaled in frequency and collapse on to one another, revealing that there is actually only one neutral curve. This also results in a minimum Reynolds number of around 4000. This number coincides with previously published material on similar flows but it is a new result for Hagen-Poiseuille flow with suction.

The stability model solutions also show that the disturbance profiles are only significantly greater than zero close to the point where the streamwise velocity, u, multiplied by the wavenumber, α_r, equals the wave frequency, ω. This is a reasonable result given that this is close to where the streamwise velocity is at its greatest and it's where the velocity gradient changes sign. There also appears to be several linear relationships. These include the relationship between frequency and wavenumber and the relationship between the maximum of the streamwise base flow and the phase velocity of the travelling wave.

The weakly nonlinear analysis of Hagen-Poiseuille flow with suction showed that there exists an equilibrium amplitude for small disturbances in the supercritical region. This result is similar to those found for other flows and indicates that in a supercritical flow disturbance level structures can be maintained. In the subcritical region disturbances decay to zero and the flow

returns to its laminar state.

The formulation of these problems was based on a large Reynolds number assumption and it was shown that there are asymptotic limits for the growth rate and wavenumber. These results provide new insights into pipe flow and suggest that the transition seen in pipe flow experiments that has so long avoided detection in theory could be related to the parallel flow assumption. Other than revealing new results this chapter also sets the foundation for the next chapter which moves from pipes to channels but many other similarities between the investigations exist.

4

Parallel wall channel flows

The main objective of this chapter is to develop a new mathematical model for finding Couette flow solutions with spanwise variation that are at equilibrium in time. The type of flow that will be studied is driven by a sinuous wave disturbance and there are several types of equilibria: lower and upper branch solutions, travelling and non-travelling waves, and periodic waves. Previous studies have suceeded in describing these solutions but all of these investigations have been limited in some way. Purely numerical methods neglect the known asymptotics of the problem while analytical solutions haven't been able to capture multiple equilibria. The paper by Hall & Sherwin[22] will be referred to several times during this chapter and that study showed it was possible to find lower branch solutions with the vortex-wave interaction equations. The nature of the numerical method for that paper meant that only the lower branch solution could be found but with the method developed here it's possible all solutions can be found.

Whereas in the previous chapter the basis was a cylindrical coordinate system the majority of this chapter will be set in a Cartesian coordinate system. The exception to this is the first problem on flow between concentric cylinders. The study of this configuration was originally undertaken by Taylor[49] as he

attempted to move on from the pipe flow studies that had preceded. At the time of Taylor's research it had been shown experimentally that flows moving at a greater velocity than some critical value contained growing unstable disturbances but nobody had been successful in explaining this phenomenon mathematically. Taylor found it was easier to design an experiment for a flow between two concentric cylinders than in a parallel wall channel and he managed to show mathematically that this flow would be unstable under certain conditions.

Although the study of a flow between concentric cylinders is in a cylindrical coordinate system in the asymptotic limit where the distance between the cylinders is tending to zero the configuration is approximately between parallel walls. This problem provides a good bridge between the cylindrical configurations of the previous chapter and the Cartesian coordinate system of this chapter. The majority of studies on this type of flow are concerned with temporal stability rather than spatial stability which was considered in the first half of this thesis. Before more sophisticated temporal stability problems are considered it seems reasonable to validate a numerical method for temporal analysis against the results for concentric cylinder flow.

Following the investigation into flow between concentric cylinders the focus turns to Couette flow with periodic spanwise variation. This study will concentrate on the vortical disturbances that interact with this flow. These interactions have been studied intensively in recent history and ultimately they now are understood to be common structures in transitioning and turbulent flow. Vortex-wave interaction theory, developed by Hall & Smith[23, 24, 25, 26], describes the interaction between nonlinear longitudinal vortices and Tollmien-Schlichting waves that had been observed in experiments. These interactions can be in equilibrium in time and therefore persist as structures in the flow. The highly nonlinear interactions are believed to be relevant in the process of transition to turbulence.

In vortex-wave interaction theory the wave is sufficiently large to drive the vortices which in turn sustain the wave. This mechanism has also been known as a 'self-sustained process'. This is an analytic solution of the Navier-Stokes equations and without the interaction between the wave and the vortices the

problem reduces to simple Couette flow. The theory is described in detail in the following sections and a special case, where the unsteady flow has a wave with a fixed shape, is studied in this thesis. Equilibrium solutions that are time invariant are sought and found with the new method developed in this thesis, and these are shown to be consistent with previous literature.

4.1 Flow between concentric cylinders and Taylor vortices

4.1.1 Introduction and formulation

In this section the flow between two concentric cylinders is considered. Taylor's classic research[49] into the temporal stability of channel flows produced several results that can be used as a reference for the numerical methods developed in this thesis. Central to the stability of this flow is the nondimensional Taylor number, the ratio of centrifugal forces to viscous forces, and when this quantity is greater than some critical value the flow perturbations grow rapidly. The Taylor number, T, is defined as,

$$T = 2\Omega^2 R_1 d^3/\nu^2. \tag{4.1}$$

In this thesis the critical Taylor number, T_c, will be found, the results at large time will be produced and the streamlines of the disturbances will be confirmed. Flows with a Taylor number greater than T_c are called supercritical and it will be shown that when the model is linearised the disturbances grow exponentially, while when nonlinear terms are included in the formulation the Taylor vortices reach an equilibrium amplitude. The exact stabilising effect of including the nonlinear terms will also be quantified.

Taylor considered a number of configurations in his theoretical and experimental research. The configuration with the radii of the cylinders large compared to the gap between the cylinders has been investigated several times since Taylor's publication and it is the configuration being studied here. The other main characteristics of this concentric cylinders setup is that the axial length of the cylinders is assumed to be infinite and the smaller, inner cylinder rotates at a constant angular velocity but the outer one is held static. The perturbations to the basic flow, which are taken to be small, are expected to be toroidal vortices aligned periodically along the axis of the cylinders. These disturbances are known as Taylor vortices. It is assumed that the disturbances are azimuthally invariant.

Taylor[49] was the first to demonstrate theoretically and experimentally that a flow in this configuration would become unstable if the velocity of the cylinder is large enough, where instability is defined as a rapidly growing disturbance velocity in the flow. The condition can be described by the nondimensionalised Taylor number, T, and the critical Taylor number is where the amplitude of the perturbed velocity neither grows nor decays but is at an equilibrium. The well known critical Taylor number, T_c, depends on how the Navier-Stokes equations are nondimensionalised but the commonly reported number is $T_c = 3389.9$.

In Taylor's linear theory the growth or decay of infinitesimal disturbances will continue exponentially in time but his experiments revealed that in a supercritical flow a finite equilibrium is reached. It is the nonlinear terms that determine this behaviour and this goes beyond the infinitesimal perturbations of Taylor's theory. In order to study the nonlinear growth and large time equilibrium states, Davey[5] considered asymptotic expansions of the perturbations and later Hall[18] investigated expansions of the Taylor number and velocity field. The particular problem under investigation here is in the limit where the distance between the cylinders is small and numerical methods are required to solve the nonlinear problem.

In this thesis, for this problem, the method of collocation pseudo-spectral methods is used once again. The perturbed velocity in the radial direction is approximated by Chebyshev functions, while in the axial coordinate the disturbances are taken to be periodic along the infinite cylinders and an expansion by Fourier series is appropriate here. The problem becomes a linearised system of equations and it can be solved with boundary conditions. The solution is normalised such that the maximum of the radial perturbed velocity component is 1. The solution is marched forward in time and through this mechanism the solution is found at each subsequent time position.

The solution to the linearised problem at the initial time position also provides the starting point for the nonlinear solution where the nonlinear terms are calculated from the known solution. After the new solutions have been calculated the process is repeated and this is iterated on until the perturbed velocity solutions no longer change, and then the solution is marched forward

in time.

In the results section of the linear case the plot of the Taylor number against axial wavenumber when the system is in equilibrium will be produced. This will confirm that the minimum critical Taylor number of $T = 3389.9$ occurs when the axial wavenumber $\lambda = 3.1266$. The shapes of the disturbances are shown to be cellular periodic vortices, as Taylor first noticed, and the exponentially decaying and growing amplitudes of the perturbed velocity components in the subcritical, where $T < T_c$, and supercritical, where $T > T_c$ cases will be plotted up to large time.

With the linear model validated the solutions of the nonlinear problem will establish that the nonlinear terms slightly stabilise the flow, something found by Davey[5] and Hall[18]. The vortical shapes of the disturbances will be shown to persist in the nonlinear case and the supercritical equilibrium states are explored.

Although the problem is approximated by two parallel walls at the small d length scale, where d is the distance between the concentric cylinders, the precedent for this problem is to work in cylindrical coordinates (r, θ, z). Once again r is the radius from the centre of the cylinders, θ is the azimuthal position and z is the axial coordinate. In this study the formulation by Hall[18] is followed. New, nondimensionalised variables $\zeta = (r - R_1)/d$, $\phi = z/d$ and $\tau = \omega t$ are introduced, where R_1 is the radius of the inner cylinder and ω is the wave disturbance frequency parameter. As the ratio of the distance d between the cylinders to R_1 is small any term with d/R_1 as a coefficient can be neglected.

The flow under consideration is incompressible with density ρ and kinematic viscosity ν. The $\mathcal{O}(1)$ base flow is simply unidirectional, forced by the rotation of the inner cylinder. Corresponding to the coordinate system, the base flow is $(0, \Omega R_1 V, 0)$, where Ω is the angular velocity of the inner cylinder and $V = 1 - \zeta$. The perturbed flow has the form $(u(\zeta, \phi, \tau), \Omega R_1 V + v(\zeta, \phi, \tau), w(\zeta, \phi, \tau))$, where u, v and w are small compared to the base flow and invariant in the azimuthal direction. Hall[18] rescales the perturbed velocity components and the frequency parameter to

$$u = -(\nu/2d)u^* \;\; v = (\Omega R_1/2)v^* \;\; w = -(\nu/2d)w^*; \;\; \omega = \nu\omega/d^2. \tag{4.2}$$

By combining the radial and axial momentum equations and eliminating pressure from the system the resultant equations are

$$\left(L - \omega\frac{\partial}{\partial\tau}\right) Lu^* = TV\frac{\partial^2 v^*}{\partial\phi^2} - \frac{1}{2}\frac{\partial^2 Q_1}{\partial\phi^2} + \frac{1}{2}\frac{\partial^2 Q_2}{\partial\zeta\partial\phi}, \tag{4.3}$$

$$\left(L - \omega\frac{\partial}{\partial\tau}\right) v^* = -u^*\frac{\partial V}{\partial\zeta} - \frac{1}{2}Q_3, \tag{4.4}$$

$$\frac{\partial u^*}{\partial\zeta} + \frac{\partial w^*}{\partial\phi} = 0, \tag{4.5}$$

where $L = \frac{\partial^2}{\partial\zeta^2} + \frac{\partial^2}{\partial\phi^2}$ and Q_1, Q_2, Q_3 are the nonlinear terms,

$$Q_1 = u^*\frac{\partial u^*}{\partial\zeta} + w^*\frac{\partial u^*}{\partial\phi} - \frac{1}{2}Tv^{*^2}, \tag{4.6}$$

$$Q_2 = u^*\frac{\partial w^*}{\partial\zeta} + w^*\frac{\partial w^*}{\partial\phi}, \tag{4.7}$$

$$Q_3 = u^*\frac{\partial v^*}{\partial\zeta} + w^*\frac{\partial v^*}{\partial\phi}, \tag{4.8}$$

T is the Taylor number as defined in 4.1 and the boundary conditions are $(u^*, v^*, w^*) = 0$ at $\zeta = 0, 1$.

Now that the problem for concentric cylinders has been described mathematically it remains to solve these equations numerically and validate these results against previous studies. The final part of this section draws the

conclusions from this chapter and structures the path to move forward into three-dimensional channel flow.

4.1.2 Numerical methods

In the first case under investigation, the linearised problem, Q_1, Q_2 and Q_3 are omitted. At a given time position, n, the system can be represented in the following matrix form,

$$\begin{pmatrix} \left(L - \omega\frac{1}{\Delta_\tau}\right) L & -TV\frac{\partial^2}{\partial\phi^2} & 0 \\ \frac{\partial V}{\partial\zeta} & \left(L - \omega\frac{1}{\Delta_\tau}\right) & 0 \\ \frac{\partial}{\partial\zeta} & 0 & \frac{\partial}{\partial\phi} \end{pmatrix} \begin{pmatrix} u_n^* \\ v_n^* \\ w_n^* \end{pmatrix} = \begin{pmatrix} -\omega\frac{Lu_{n-1}^*}{\Delta_\tau} \\ -\omega\frac{v_{n-1}^*}{\Delta_\tau} \\ 0 \end{pmatrix}, \tag{4.9}$$

where Δ_τ is the step size in time and u_{n-1}^* and v_{n-1}^* are the known solutions from the previous time position. The solution here can be found with a linear solver routine and can be continually stepped forward in time with a first order finite difference scheme.

The problem at $\tau = 0$ requires an initial condition. The nature of the scheme means that an almost arbitrary function can be chosen for this condition but it makes sense to chose a function which satisfies the periodicity properties and boundary conditions at the cylinder walls. In previous work the axial period is set such that the axial velocity is zero at the edges and centre of the period. The initial condition used in the investigation here replicates this position.

In the nonlinear case the nonlinear terms are introduced on the right hand side of the system,

$$\begin{pmatrix} \left(L - \omega\frac{1}{\Delta_\tau}\right) L & -TV\frac{\partial^2}{\partial\phi^2} & 0 \\ \frac{\partial V}{\partial\zeta} & \left(L - \omega\frac{1}{\Delta_\tau}\right) & 0 \\ \frac{\partial}{\partial\zeta} & 0 & \frac{\partial}{\partial\phi} \end{pmatrix} \begin{pmatrix} u_n^* \\ v_n^* \\ w_n^* \end{pmatrix} = \begin{pmatrix} -\omega\frac{Lu_{n-1}^*}{\Delta_\tau} - \frac{1}{2}\frac{\partial^2 Q_1}{\partial\phi^2} + \frac{1}{2}\frac{\partial^2 Q_2}{\partial\zeta\partial\phi} \\ -\omega\frac{v_{n-1}^*}{\Delta_\tau} - \frac{1}{2}Q_3 \\ 0 \end{pmatrix}$$

(4.10)

The effect of these additional terms is a nonlinear forcing. The left hand side of the problem is still a linear set of equations but the solution is used to update the nonlinear terms. The system is solved again and the new solution is compared to the previous one. This process is iterated until there is change of less than 10^{-5} in the maximum of the radial disturbance velocity, v_n^*. At $\tau = 0$ the linear problem solution is used to give the initial guess for the nonlinear terms.

4.1.3 Linear stability results

Hall[18], and other authors, found that the critical value for the Taylor number at which the perturbed flow becomes unstable depends on the choice of the axial wavenumber, λ. For the concentric cylinders problem, when the inner one rotates and the outer one remains static, and there is a small gap between the cylinders, the minimum critical value has been reported as $T = 3389.9$ by several researchers and this occurs when $\lambda = 3.1266$. Figure 4.1 describes the critical Taylor number curve calculated for this thesis. Interpolation was used to find the critical number and the value found here agrees with previous literature. It makes sense to work with the wavenumber that associated with the minimum critical value as has been done in the past. The following plots and analysis are all with $\lambda = 3.1266$.

Taylor[49] produced plots of the radial disturbance velocity in his Figure 4 and Figure 6. Unfortunately, these plots show the cases when the outer cylinder is non-stationary and are not exactly comparable to the configuration in this study. Davey's[5] section 7.2 is concerned with the small gap, d, problem and he reported the values for the radial disturbance in his Table B. As it happens, Davey's radial disturbance shape between the inner and outer cylinder is almost exactly the same as Taylor's Figure 4. In Figure 4.2 here the same shape is produced again. This curve is the same shape at all points in the azimuthal period but is scaled by the value of θ, where θ is the azimuthal position. This axial conformity gives the Taylor vortices a periodic

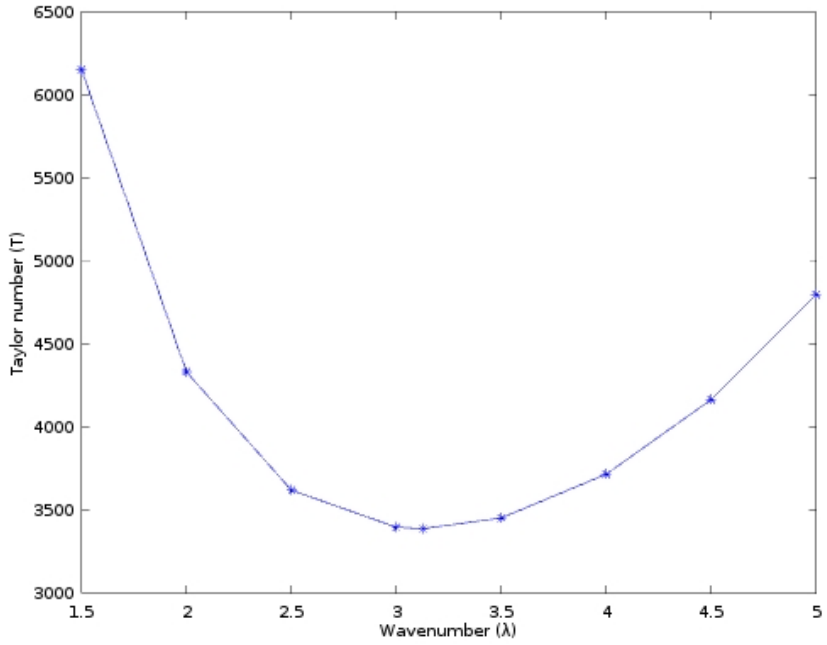


Figure 4.1: Critical Taylor number against wavenumber from the linear equations.

and regular shape.

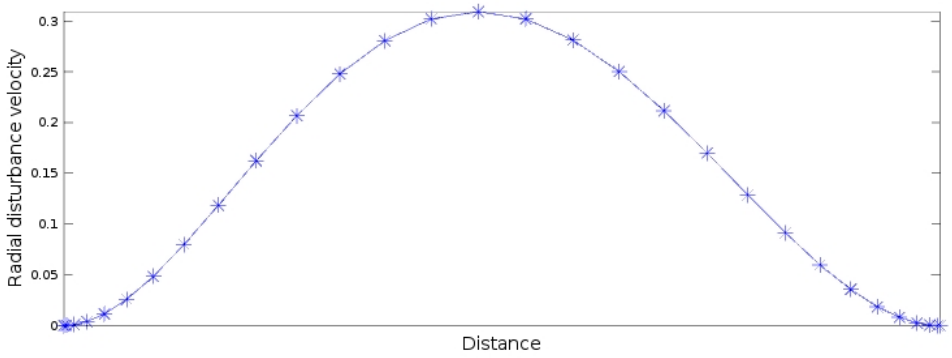


Figure 4.2: Radial disturbance velocity taken at π in the azimuthal direction.

Taylor also plotted the so-called Taylor vortices for the cases when the outer cylinder is rotating in the same direction as the inner cylinder and when the outer cylinder is rotating in the opposite direction. These can be found in his Figure 5 and Figure 7. As the shape of the radial disturbance calculated here is similar to that of Figure 4 from Taylor's work it is expected, and true,

that the Taylor vortices calculated here should be consistent with Figure 5 of Taylor. Figure 4.3 confirms the appearance of toroidal vortices and resemble Taylor's hand drawn diagrams for cases when the outer cylinder is also rotating.

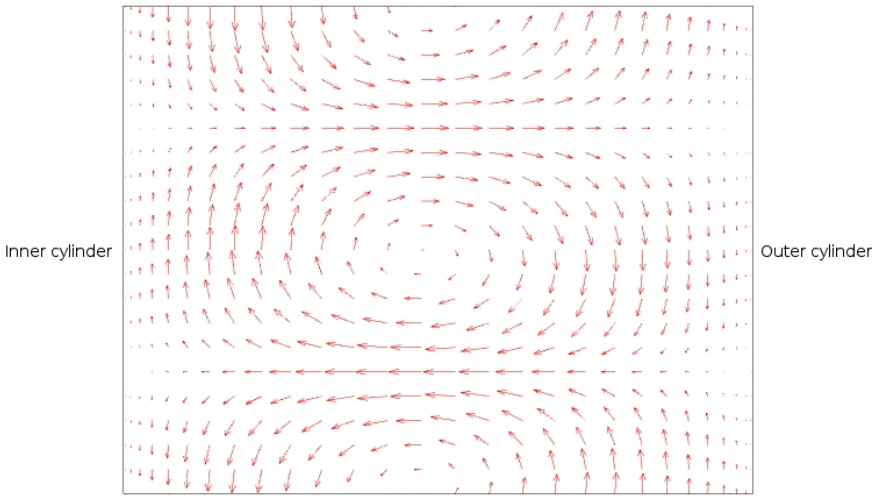


Figure 4.3: Vector field plot of axially periodic Taylor vortices.

Linearised theory suggests that the perturbation velocity will grow exponentially with time in the supercritical region of T and decrease exponentially in the subcritical region. Figure 4.4 confirms that the model developed here captures this phenomena. This large time linearised outcome does not reflect the reality shown in several experiments however. The experiments conducted by Taylor, and others later, revealed that in supercritical region the disturbances reach a finite equilibrium amplitude. This effect can be attributed to the nonlinear terms and in the next section the differences at large time are described.

4.1.4 Nonlinear stability results

Including the nonlinear terms in the formulation is known to have a significant effect on the equilibrium properties of flow between concentric cylinders, however the change in the shape of the Taylor Vortices is minute.

As mentioned in the previous section, when the Taylor number is greater

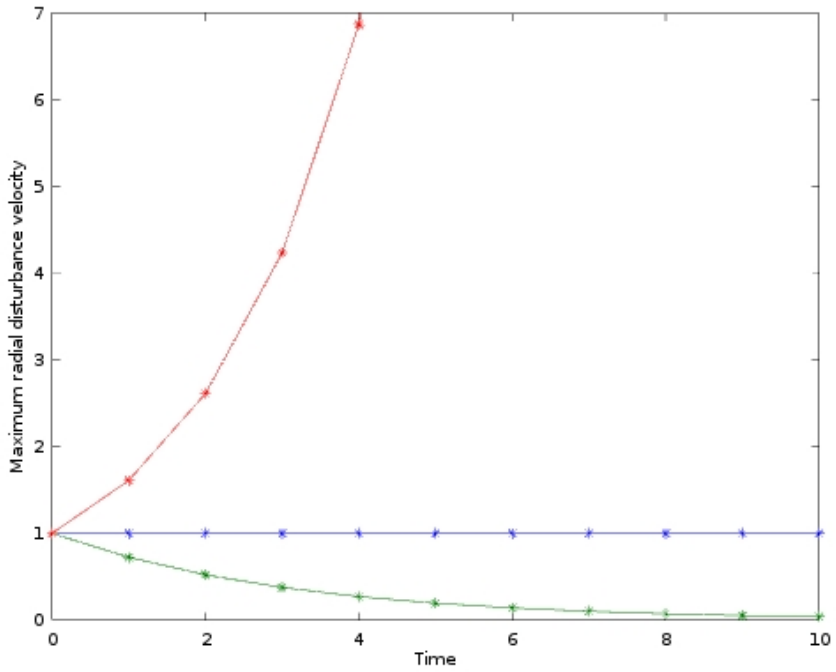


Figure 4.4: Maximum radial disturbance velocity against time for flow between concentric cylinders. (Linear stability analysis.) Blue: $T = 3389.9$; Green: $T = 3289.9$; Red: $T = 3489.9$.

than the critical value the amplification of the disturbance velocities isn't infinite, rather the disturbance attains a finite value. Davey noted that in the subcritical region the disturbance velocities still decay to zero and these properties are plotted in Figure 4.5.

The equilibrium amplitude of the supercritical flow is reported to be proportional to $(T - T_c)^{1/2}$ and that relationship is shown in Table 4.1, where the critical Taylor number, T_c, increases slightly to $T_c = 3395.7$ in the nonlinear solution. Hall and Davey both noted that for certain cases of modulation and frequency the critical Taylor number could be increased or, in other terms, the flow could be stabilised. The other pattern worth noting is that the further from the critical value the Taylor number is the quicker it attains its equilibrium amplitude. Table 4.1 contains the values of equilibrium amplitudes and the time it took to achieve 99% of this value for the same supercritical Taylor numbers as described in Figure 4.5.

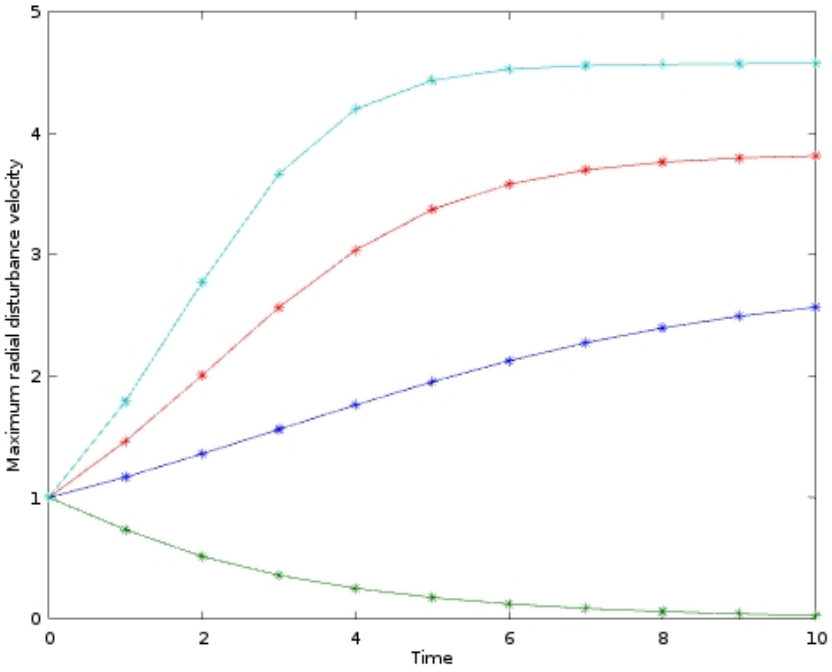


Figure 4.5: Maximum radial disturbance velocity against time for flow between concentric cylinders. (Nonlinear stability analysis.) Green: $T = 3289.9$; Blue: $T = 3440.0$; Red: $T = 3489.9$; Cyan: $T = 3540.0$.

4.1.5 Conclusions

In this section the classic stability problem of flow between concentric cylinders studied by Taylor[49] has been resolved. Specifically, the configuration is Couette flow driven by a rotating inner cylinder turning with constant angular momentum and a static outer cylinder with no-slip boundary conditions. The distance between the cylinders is small and the cylinders are infinitely long, and, therefore, the channel can be approximated as having flat walls.

Taylor[49] showed that linear theory predicts that this type of flow can be unstable when the Taylor number is greater than some critical value but he could not reconcile his experimental findings that for a supercritical Taylor number the disturbance velocity attains an equilibrium value at large time. The linear results of Taylor, including the critical Taylor number, were successfully reproduced here. The nonlinear problem was also tackled in this

T	$(T - T_c)^{1/2}$	Equilibrium radial velocity	Time (seconds)
3440.0	6.66	2.75	18.00
3489.9	9.71	3.84	10.50
3540.0	12.01	4.61	7.25

Table 4.1: Nonlinear amplitude effects. A comparison of Taylor number, equilibrium radial velocity and time taken to reach 99% of equilibrium velocity value.

section and an iterative scheme at each time step was sufficient to show that the nonlinear effects resulted in a disturbance flow field which reaches a steady state at large time.

The validation and consistency of the temporal stability model developed here provides a bridge from the cylindrical spatial stability problems of the first chapter to the vortex-wave interaction problems which follow in this chapter. In the next section the theory of vortex-wave interactions is fleshed-out and a special case of the problem is solved for the first time. Much of the work covered so far in this thesis is used in solving this final set of problems.

4.2 Three dimensional vortex-wave interaction equilibria

4.2.1 Introduction

Having solved the problem of flow between concentric cylinders it is now possible to extend the theory and numerical methods to tackle the main problem of this thesis, the stability of spanwise-varying Couette flow in time. The study will be approached from the theory of vortex-wave interactions that were described by Hall & Sherwin[22]. The work presented here deviates from the numerical approach of Hall & Sherwin, allowing additional equilibrium solutions to be investigated.

The vortex-wave interaction equations are a large Reynolds number asymptotic derivation of the Navier-Stokes equations and the flow is broken down into components of different scales. For shear flows the solution of the vortex-wave interaction equations are coherent structures that have also been found through numerical computation and in experiments.

A full description of the vortex-wave interaction equations is presented in the following subsections but it is worthwhile reviewing the history of the theory here. Papers published by Hall & Smith[23, 24, 25, 26] presented a formal asymptotic framework for what is now called vortex-wave interaction theory. The framework is fully nonlinear, in that the mean flow is entirely changed from its unperturbed profile, and can be applied to both small amplitude inviscid Rayleigh waves and Tollmien-Schlichting waves, which interact with longitudinal vortices. These papers are concerned with boundary-layer flow with a large Reynolds number assumed throughout and in some cases a triple-deck approach is used. When these waves have a neutral temporal growth rate the system is in equilibrium in time. These waves are of the utmost interest because their interactions can be observed and followed in time.

Around the same as these papers were published Nagata[34] extended the work of Taylor[49] that was studied in the previous section. Nagata took a numerical approach and considered Couette flow between two co-rotating cylinders with a small gap but without curvature. As noted before, for a long time experiments showed that this flow becomes unstable above a critical Taylor

number but Nagata discovered finite-amplitude solutions with a steady three-dimensional form. The numerical approach in this investigation follows the three-dimensional solution branches which bifurcate from the Taylor vortex flow.

A similar result was published by Waleffe[52], who focused on a sinusoidal shear flow. This paper proposed that the lower branch on the neutral stability has self-sustaining states. The Reynolds number is taken to be finite and the production of the wave is generated by the linear instability of the streamwise velocity, the 'streak'. The author noticed that the process was remarkably insensitive to the boundary conditions. Waleffe[53] built on this research and investigated coherent states that are unstable travelling waves in Poiseuille flows. These states have a similar configuration to the solutions found in Nagata's approach with wavy, slow streaks and streamwise vortices. Waleffe pointed out that these are similar to the asymmetric coherent structures found in turbulent flows near the wall but they exist without the fragmented spatial and temporal relationships. For this reason they are called exact coherent structures. The method used in this investigation was to calculate by homotopy the solution of the no-slip boundary condition problem for the free-slip boundary conditions.

Several other papers, including those by Faisst & Eckhardt[12] and Waleffe[54], developed the theory of self-sustained processes with finite-R solutions. Another significant paper in the development of the ideas underpinning the research into shear flows with longitudinal vortices was by Wedin & Kerswell[57]. The subject of the study was once again three-dimensional travelling wave solutions this time in flow through a pipe driven by pressure. The now well-established configuration of longitudinal rolls and streaks are the main characteristics of the flow and there exist streamwise-dependent waves. The travelling waves are a class of solutions where there are several variations with different number of rotational symmetries about the pipe axis. The approach used in Wedin & Kerswell is described as constructive continuation from the key physical mechanisms observed in all wall-bounded shear flows.

The research was continued by Wang[55] who considered a artificially stimulated Couette flow with neutral, stationary Rayleigh waves and confirmed

numerically the relative scaling of the self-sustained processes for plane Couette flow and the importance of the linear stability of the streak. The paper determined that lower branch solutions have an exact coherent structure of $\mathcal{O}(1)$ streaks and $\mathcal{O}(R^{-1})$ rolls at large Reynolds numbers, and that the wave develops a critical layer where higher harmonics are infinitesimal. These lower branch solutions are claimed to be edge states, where initial disturbances will either eventually become turbulent or return to laminar.

Another alternative theory developed with the goal of furthering the understanding behind the dynamics of the streamwise roll and streak structure is stochastic structural stability theory. The paper by Farrell & Ioannou[13] described the method of analysis as using the streamwise-averaged flow with perturbation dynamics generated by a stochastic turbulence model. The authors claim this autonomous and deterministic nonlinear dynamical systems model can approximate the turbulent state of the flow. The analysis by Farrell & Ioannou revealed the same interaction between the longitudinal rolls, the streak and the turbulent perturbations that had been remarked upon by other authors, and that these disturbances are systematically organized and that the Reynolds stresses they produce coherently force the vortex rolls.

Farrell & Ioannou[13] show that in the time-independent problem the perturbation Reynolds stresses can maintain the rolls and streak in equilibrium. The authors further claim that when the forcing from the perturbations is sufficiently high the equilibrium of the system is broken but that the flow transitions to a time-dependent state. The state persists when the forcing is removed and in that sense is self-sustaining.

The follow-up paper to Farrell & Ioannou[13] by Thomas et al.[51] developed a restricted nonlinear model for plane Couette flow. This system is derived from the Navier-Stokes equations and should result in better approximations to the maintenance of self-sustaining turbulence than the stochastic turbulence model which is a second order statistical approximation of the longitudinal vortex flow. The approach in the paper by Thomas et al. shows good comparison the direct numerical simulations and once again reveals the self-sustaining nature of these structures in the flow.

Other than travelling waves, time periodic solutions also exist. Kawahara & Kida[31] discovered two three-dimensional time periodic structures in Couette flow. Through the method of direct numerical simulation the authors found a solution with strong structural variation in space and time. This variation involves the formation, breakdown and regeneration of streamwsie vortices and slow streaks. The other solution involves a 'gentle' variation, where there is a spanwise standing-wave motion of low-velocity streaks. The two solutions are unstable and a turbulent state can be found close to the strong variation solution for the most part. The velocity fluctuations and mean profile of plane Couette turbulence correspond closely to this strong solution however the turbulent state can achieve the gentle periodic state before eventually exhibiting strong turbulence activity and returning to the strong solution.

The papers mentioned above describe numerical solutions at finite Reynolds number. Many, or even most, interesting flows occur at high Reynolds and in the asymptotic limit the Navier-Stokes equations can be addressed as a series of scales. Hall & Sherwin[22] considered the analytic solution of the Navier-Stokes equations for Couette flow where the longitudinal 'streak' is $\mathcal{O}(1)$ and there is a $\mathcal{O}(1/R)$ 'roll'. This base flow is taken to be moving on the slow time scale $T = t/R$ and a wave, acting on the faster timescale t, is superimposed on the vortex system. This wave interacts with the base flow at the critical layer, $y = f(z)$, where the wavespeed is real and equal to the streak velocity. In vortex-wave interaction theory the roll modifies the streak, the streak has a wave-like linear stability solution, and the nonlinear Reynolds stresses of the wave velocity force the roll.

The paper by Blackburn, Hall & Sherwin[3] extended the work of Hall & Sherwin[22] to a range of spanwise wavenumbers and reveals that for small wavelengths the disturbances are localized to the centre of the flow. As these states feel no influence from the walls they are relevant to arbitrary shear flows. This paper also introduced the hybrid computational approach for calculating the forcing terms in the roll equations directly from the wave. For finite amplitude waves the averaged Reynolds stresses balance the dissipation in the rolls.

The solutions in Blackburn, Hall & Sherwin[3] are considered 'lower branch'

equilibria. For the same parameters there are another set of solutions, the 'upper branch', which appear when the wave has a greater amplitude. Hall & Sherwin[22] noted that the hybrid computational approach for the forcing may be able to capture the upper branch and Blackburn, Hall & Sherwin[3] suggested the upper branch equilibrium solutions are organizing centres about which the flow slowly cycles during the approach to turbulence. Deguchi & Hall[9] resolved the upper branch states with the same method as they did for the lower branch. The authors found that the upper branch solution is of vortex-wave type, with the usual scalings, but have a multivalued critical layer in the spanwise direction. Therefore the upper branch is also a steady solution and, in the case of a sinusoidal wave disturbance, subject to the same symmetries as the lower branch.

Deguchi & Hall[9] extended the canonical vortex-wave interaction theory by revealing solutions were also possible in an infinite region. Exact coherent structures were found in unbounded flows and a second type of structure, corresponding to free stream coherent structures in boundary layer flows, were described for an asymptotic suction boundary layer. This paper showed that these canonical problems can be embedded in general shear flows and are pervasive in applicability.

Hall & Sherwin[22], Deguchi & Hall[9] and several other papers showed that even though the vortex-wave interaction equations have been determined with the condition that the Reynolds number is large the solutions are consistent with other results for relatively small Reynolds numbers. Therefore, the self-sustained lower branch solutions found by the numerical investigations of Waleffe[52,53], Wedin & Kerswell[57] and Wang[55], amongst others, are finite Reynolds number solutions of the vortex-wave interaction equations. It is expected to be possible to reconcile all of these numerical solutions with the large Reynolds number asymptotics of vortex-wave interaction theory.

Vortex-wave interaction equilibrium solutions in Couette flow

The analysis conducted in this thesis closely follows the work of Hall & Sherwin[22] and Blackburn, Hall & Sherwin[3]. The flow under investigation is

through a channel bounded on the lower and upper surface by parallel plates and these are nondimensionalised to heights of ± 1, whilst the longitudinal and spanwise dimensions are infinite. The rigid channel walls are moving in opposite directions at equal speeds and the flow is periodic in the longitudinal and spanwise directions. The inviscid Tollmien-Schlichting waves which are known to play a crucial part in the highly nonlinear transition to turbulence are studied in this flow. In this investigation temporally neutral waves are sought and the longitudinal wavennumber, α, and the Reynolds number, R, are fixed. The size of the wave is determined by the time dependent amplitude ρ and this variable is modified to drive the system to a neutral solution.

The papers by Hall & Sherwin[22] and Blackburn, Hall & Sherwin[3] took different approaches to viscosity, the critical layer and the forcing from the wave to vortex rolls. Hall & Sherwin explored the inviscid form of the wave problem, tackling the discontinuity at the critical layer asymptotically with jump conditions. However, for their numerical solutions Hall & Sherwin consider a viscous wave and take the wave's streamwise velocity and pressure to generate forcing terms for the roll problem. Blackburn, Hall & Sherwin[3] calculate the forcing directly from the wave's Reynolds stresses and they call this the hybrid computational approach. Neither paper addressed the upper branch states that have been identified by the research into the self-sustained processes. Deguchi & Hall[9] developed a direct numerical simulations model which showed that even the upper branch solutions deformed to vortex-wave interaction states in the large Reynolds number limit in the steady case.

To find the stationary waves with zero frequency a number of symmetries in the flow need to be fixed to ensure that the critical layer is pinned in position. Hall & Sherwin[22] laid out a strategy for implementing the symmetries in their paper, beginning with an artificial forcing which has these symmetries embedded. To find the steady state for the vortex system the roll is iterated on until it no longer changes and then the steady streak problem is solved. The wave that is generated on the streak is forced to zero growth by modifying its amplitude.

The approach in this thesis is markedly different. There is no prior as-

sumption that the system will reach an equilibrium state. The full unsteady problem is solved at each time position in the spanwise-wall normal plane but at one point in the longitudinal direction. When a solution is found at a time t it is marched forward by a small increment, $t + \Delta_t$, with a backward Euler method. The steps taken in this approach are: solve the nonlinear roll problem with the wave forcing, calculate the streak and solve the linear temporal eigenvalue problem for the wave on the streak. At each time position these steps are repeated with the time dependent amplitude adjusted until the wave frequency is neutral. Despite the number of differences between the approaches of these previous papers and the method used here the results show close agreement.

This chapter begins with the formulation of the base Couette flow. The next section covers the theory behind the vortex-wave interaction equations and reveals the asymptotic scalings of Hall & Sherwin[22]. The special case of the vortex-wave interaction equations which is studied in this thesis is then described. This is followed by the numerical method, the results and the validation of the work. Finally the section, chapter and thesis are concluded.

4.2.2 Couette flow formulation

The formulation of Hall & Sherwin[22] is closely followed here and once again the starting point is the nondimensionalised incompressible Navier-Stokes equations. The general form for the momentum and continuity equations are as follows,

$$\frac{\partial \mathbf{u}}{\partial t} + \mathbf{u}\cdot\nabla\mathbf{u} = -\nabla p + \frac{1}{R}\nabla^2\mathbf{u}, \tag{4.11}$$

$$\nabla\cdot\mathbf{u} = 0, \tag{4.12}$$

where $\mathbf{u}$ is the velocity scaled on the maximum velocity of the dimensional Couette flow, p is the nondimensionalised pressure, t is the time variable and the Cartesian coordinate system (x, y, z) is scaled on the characteristic half

height of the channel such that $-1 \leq y \leq 1$. R is the Reynolds number based on this nondimensionalisation. The boundary conditions on the parallel plates forming the channel are the no-slip conditions and the plates are moving in opposite directions such that

$$\mathbf{u} = (1, 0, 0) \quad at \quad y = 1, \tag{4.13}$$

$$\mathbf{u} = (-1, 0, 0) \quad at \quad y = -1. \tag{4.14}$$

It is known that the vortex system, comprising of an $\mathcal{O}(R^{-1})$ roll and an $\mathcal{O}(1)$ streak, is an analytical solution of the Navier-Stokes equations. In the absence of any perturbation the flow can be written as

$$\mathbf{u} = \left(u(y, z, T), \frac{1}{R} v(y, z, T), \frac{1}{R} w(y, z, T) \right), \tag{4.15}$$

$$p = \frac{p(y, z, T)}{R^2}, \tag{4.16}$$

where $T = t/R$ is a slow time variable employed to balance convection and the viscous diffusion terms. For this flow the equations (4.11) and (4.12) become

$$Lu = \nabla^2 u, \tag{4.17}$$

$$Lv = -\frac{\partial p}{\partial y} + \nabla^2 v, \tag{4.18}$$

$$Lw = -\frac{\partial p}{\partial z} + \nabla^2 w, \tag{4.19}$$

$$\frac{\partial v}{\partial y} + \frac{\partial w}{\partial z} = 0, \tag{4.20}$$

where $L = \frac{\partial}{\partial T} + v\frac{\partial}{\partial y} + w\frac{\partial}{\partial z}$ and $\nabla = \frac{\partial^2}{\partial y^2} + \frac{\partial^2}{\partial z^2}$. It is worth noting at this point that the u-momentum equation for the streak has decoupled from the rolls, so that the roll system (4.18)-(4.20) can be solved separately to the streak problem. This enables the problem to be solved in a step-wise fashion, with the roll equations solution being used in the streak equation. This outcome is a result of the asymptotic scales and it captures something important about the flow that otherwise might be missed. It is the rolls which drive the streak but at this point the equations do not account for how the rolls are forced. Without any forcing, the solution to this version of the Navier-Stokes equations will result in basic Couette flow, $u = y$ with $v, w, p = 0$. If curvature is present and scaled appropriately it is possible to recover the nonlinear equations (4.3)-(4.5) for Taylor vortices in the small gap limit that were derived and solved in the previous section.

4.2.3 Vortex-wave interaction equations

Hall & Sherwin[22] brought together several ideas from theory, numerical research and experiment and incorporated them in their so-called vortex-wave interaction equations. For a deeper background to this part of the thesis, and completeness regarding the theory underpinning the problems described later, Hall & Sherwin's paper will be summarised here.

The formulation of the vortex-wave interaction equations starts with setting the Reynolds number R as asymptotically large. The resultant problem is inviscid in nature and only applicable to flows that can be approximated as such. The streak and the roll solutions of equations (4.17)-(4.20) from the previous section will be used to demonstrate the vortex-wave interaction problem here and these solutions are taken to be steady. It is worthwhile pointing out that other roll-streak base flows, such Poiseuille flow, could be used in place of Couette flow.

Now consider a small wave superimposed on to the vortex flow. This wave will have the property of being periodic in the longitudinal direction, x, with the wavenumber α. This wave develops on a RT timescale, which is faster than that of the base flow, and the wave's instantaneous frequency is defined as $\Omega = \alpha Rc(T)$. A critical layer, $y = f(z)$, is formed when the wavespeed c is real and equal to the streak velocity u. First, consider the area distant to the critical layer,

$$\begin{aligned}\mathbf{u} = (u + ... + \delta R^{-1/3}(\rho(T)U(y,z,T)E + c.c.) + ...,\\ \frac{1}{R}v + ... + \delta R^{-1/3}(\rho(T)V(y,z,T)E + c.c.) + ...,\\ \frac{1}{R}w + ... + \delta R^{-1/3}(\rho(T)W(y,z,T)E + c.c.) + ...), \qquad (4.21)\end{aligned}$$

$$p(y,z) = \frac{p(y,z,T)}{R^2} + ... + \delta R^{-1/3}(\rho(T)P(y,z,T)E + c.c.) + ... \qquad (4.22)$$

In this flow field '*c.c.*' denotes the complex conjugate. The wave velocity components (U, V, W) have the same length scales as the vortex base flow, and they are taken to be of the same order of magnitude. The size of the wave will be $\mathcal{O}(1)$ inside the critical layer but away from this layer the wave is size $\delta R^{-1/3}$ with δ to be fully described later. ρ can be described as the wave amplitude and it is another variable slowly varying in time. The pressure is addressed slightly differently, and its size is determined by the relationship, $u\frac{\partial U}{\partial x} \sim \frac{\partial P}{\partial x}$. Finally, the term E is the wave-like part and is defined below.

$$E = e^{i\alpha\left(x - R\int^T c(T)dT\right)} \qquad (4.23)$$

When the full flow field (4.22) is inserted into the Navier-Stokes equations (4.11) and continuity equation (4.12) the order R^{-1} and R^{-2} equations recover the Couette flow problem of the last section (4.3-4.5). Now consider the terms proportional to ρE and of order $\delta R^{-1/3}$, the wave terms, and assume this wave is inviscid. When R is asymptotically large the Navier-Stokes

equations are,

$$i\alpha\,(u-c)\,U + V\frac{\partial u}{\partial y} + W\frac{\partial u}{\partial z} = -i\alpha P, \tag{4.24}$$

$$i\alpha\,(u-c)\,V = -\frac{\partial P}{\partial y}, \tag{4.25}$$

$$i\alpha\,(u-c)\,W = -\frac{\partial P}{\partial z}, \tag{4.26}$$

$$i\alpha U + \frac{\partial V}{\partial y} + \frac{\partial W}{\partial z} = 0. \tag{4.27}$$

Following Hall & Sherwin's[22] theoretical study, which followed the approach of Hall & Horseman[21], the next step in defining the vortex-wave interaction equations is to eliminate U, V and W from the Navier-Stokes wave problem (4.24-4.27). This is possible because the wave is inviscid and the result is a generalization of Rayleigh's equation for the pressure term in two dimensions (4.28).

$$\frac{\partial^2 P}{\partial y^2} + \frac{\partial^2 P}{\partial z^2} - \alpha^2 P - \frac{2}{u-c}\frac{\partial P}{\partial y}\frac{\partial u}{\partial y} - \frac{2}{u-c}\frac{\partial P}{\partial z}\frac{\partial u}{\partial z} = 0. \tag{4.28}$$

This one equation governs the linear stability of a unidirectional flow depending on a single variable. It is an eigenvalue problem for the complex wavespeed $c(T)$ on the streak $u(y,z,T)$ and for a given real wavenumber α. The boundary conditions are modal and described in detail in Hall & Horseman[21].

In this vortex-wave configuration the equilibrium solutions to the wave eigenvalue problem are of interest because they are the ones that can sustain the vortex system. Therefore, $c(T)$ must be real, that is the wave should have zero temporal growth. Several modes will occur simultaneously but the mode that has been identified as commonly the least stable one is the wavy sinuous mode. As the least stable it is this mode that is most likely to interact with the base flow and sustain the vortices which would otherwise decay to zero velocity.

Interaction at the critical layer

As discussed before, the wave problem, (4.24)-(4.27) or (4.28), will have a critical layer, $y = f(z, T)$, at $u = c$. From the formulation above this layer has mathematical singularities, however this is caused by the inviscid assumption and Hall & Sherwin[22] argue that viscosity would 'smooth' out these singularities. For this argument to be consistent with the formulation, U, V and W must be like $(y - f)^{-1}$ at the critical layer, while P remains regular and $\mathcal{O}(1)$.

Now attention can be turned to the interaction between the wave and the vortex at the critical layer. For this Hall & Sherwin[22] switch to a local coordinate system in their theoretical study. The authors define the local coordinate system (x, n, s) with n measuring the distance normal to the critical layer and s the tangential distance at any position x. At a fixed x the wave solution is a time periodic motion arranged around the critical layer. The Reynolds stresses vary in s but have a stationary influence which forces the base flow rolls. These rolls then sustain the streak and the wave is maintained. This process is known as the vortex-wave interaction.

To show this mathematically the critical layer variable $N = R^{1/3}n$ is defined, and the leading order velocity and pressure terms become

$$\rho\delta(\mathcal{U}(N,s,T),R^{-1/3}\mathcal{V}(N,s,T),\mathcal{W}(N,s,T))E+c.c, \tag{4.29}$$

$$\rho\delta R^{-1/3}\mathcal{P}(N,s,T)E+c.c.... \tag{4.30}$$

The δ size term is still yet to be determined and it is used to match the wave size outside of the critical layer to the roll solution and therefore forcing the wave to drive the roll. The spanwise flow velocity field (v,w) now needs to be considered in the normal and tangential directions. Taking $\nu_i^s(N,s,T)$ as the flow component in the s direction, then the s-momentum equation has the following leading order approximation:

$$\frac{1}{R^2}R^{2/3}\frac{\partial^2\nu_i^s}{\partial N^2}=\delta^2\rho^2\left(-i\alpha\mathcal{U}\overline{\mathcal{W}}+\mathcal{V}\overline{\mathcal{W}}_N+\mathcal{W}\overline{\mathcal{W}}_s\right)+c.c+..., \tag{4.31}$$

where a line above a term denotes the complex conjugate. However, in the configuration here the integration of equation (4.31) in the normal direction shows that the normal derivative of the roll velocity in the tangential direction has a jump. This is because the Reynolds stresses are localised to an internal layer rather than a boundary. The roll velocity terms will be adapted to enable the jump.

Turning attention to the normal momentum equation,

$$\frac{1}{R^2}R^{1/3}\frac{\partial\mathcal{P}^s}{\partial N}=-\delta^2\rho^2\Lambda_0(s,T)\mathcal{W}\overline{\mathcal{W}}_s+c.c+... \tag{4.32}$$

Here $\mathcal{P}^s$ is the roll pressure resolved in the tangential direction and $\Lambda_0(s,T)$ is curvature term related to the curvature of the critical layer. Similarly to the integration of equation (4.31), integrating equation (4.32) also results in a jump, this time in the pressure. It is notable that the direction of the jump in the pressure is conditional on the sign of the curvature of the critical layer. Using the continuity equation of the wave and the fact that $\mathcal{W}$ is equal

to zero as N tends to positive or negative infinity, the integrated equations (4.31), (4.32) in the normal direction are as follows,

$$\left[\frac{\partial v_o^s(n,s,T)}{\partial n}\right]_-^+ = 2\delta^2\rho^2 R^{5/3}\int_{-\infty}^{\infty}\frac{\partial}{\partial s}|\mathcal{W}(N,s,T)|^2 dN, \tag{4.33}$$

$$[p]_-^+ = -2\Lambda_0\delta^2\rho^2 R^{5/3}\int_{-\infty}^{\infty}|\mathcal{W}(N,s,T)|^2 dN. \tag{4.34}$$

The roll velocity term $v_o^s(n,s,T)$ is the variation of v^s from the critical layer, and it is equal to $\mathbf{e_s}\cdot[0,v(x,y,T),w(x,y,T)]$, where e_s is a unit vector tangential to the critical layer. As described earlier, the wave terms U,V,W are $\mathcal{O}(1)$ and for the roll to accommodate the jump conditions across the critical layer the choice of $\delta = R^{-5/6}$ is appropriate. The result of this scaling is that for Couette flow the streak is $\mathcal{O}(1)$, the rolls are $\mathcal{O}(R^{-1})$ and the wave has a size of $\mathcal{O}(R^{-5/6})$ in the critical layer. The numerical investigation of Wang[55], which used a different norm to Hall & Sherwin[22], found that the wave scales like $\mathcal{O}(R^{-9/10})$, and therefore is in close agreement.

In summary, the roll velocity is found from equations (4.18) and (4.19) and the streak (4.17) can be found using the roll. The entire flow field has no-slip boundary conditions but at the critical layer, $y = f(z)$, the jump conditions must be satisfied by the pressure, p, and the normal derivative of the vortex roll velocity resolved in the tangential direction. The base flow components u,v,w are continuous at the critical layer and periodic in the spanwise direction. The jump conditions can be simplified by using the relationship between $\mathcal{W}(n,s,T)$ and the pressure eigenfunction $P(y,z,T)$ that comes from the momentum equation in the tangential direction for the wave in the critical layer,

$$\frac{\partial^2\mathcal{W}}{\partial N^2} - i\alpha\mu(s,T)N\mathcal{W} = \frac{\partial\mathcal{P}}{\partial s}. \tag{4.35}$$

Notably, the jump conditions are dependent on the pressure eigenfunction which is found from equation (4.28), which closes the vortex-wave system. The Rayleigh equation is actually nonlinear because of the dependency between P and u. Hall & Sherwin[22] approached solving the vortex-wave interaction equations by assuming that all quantities are known at the instant T. The system is then marched forward in time ensuring that $c(T)$ remains real by varying the amplitude function $\rho(T)$, which determines the size of the rolls.

In fact, these scalings hold true for channels of any cross section and the only modification needs to be a different boundary shape where the condition is non-slip. This chapter of the thesis is concerned with Couette flow, as was the paper of Hall & Sherwin[22], but the configuration could be used to find results for the circular pipe Poiseuille flow that was studied in the previous chapter. The centrality of vortex-wave interaction theory to viscous flows promises increased knowledge of turbulence and the possibility of controlling transition.

4.2.4 Special case of the vortex-wave interaction equations

The vortex-wave interaction equations presented by Hall & Sherwin[22] in their theoretical section are difficult to solve numerically. Several varitions on the equations have been suggested and solved, and a new proposal is made here. Consider a similar system to the one described above but where the wave is not fully time dependent. As before the wave components are split into an amplitude, a shape function and a wave-like part, but now just the amplitude and the wave-like part are time-dependent. The combined vortex and wave flow field has the following form:

$$\mathbf{u} = (u + \rho(T)(U(y,z)E(x,T) + c.c.), \tag{4.36}$$

$$\frac{1}{R}v + \rho(T)(V(y,z)E(x,T) + c.c.), \tag{4.37}$$

$$\frac{1}{R}w + \rho(T)(W(y,z)E(x,T) + c.c.)), \tag{4.38}$$

where '*c.c.*' is the complex conjugate and $E = e^{i\alpha\left(x - R\int^T c(T)\partial T\right)}$. Once again, the wave velocity components (U, V, W) are defined on the same length scales as the vortex velocity and they are assumed to have similar magnitudes. This wave is still assumed to be periodic in the longitudinal direction with a wavenumber α and acting on the fast timescale RT compared to the vortex.

When this flow is substituted into the Navier-Stokes equations, (4.11) and (4.12), the system will no longer be fully time-dependent. The vortex problem will still be time-dependent as before but the wave is only partially time-dependent as the shape of the wave velocity components (U, V, W) are not dependent on time. This simplification or approximation is still sufficient to capture the characteristics of the vortex-wave interaction problem, where the wave does not change shape or changes very slowly. The solutions sought in this thesis are equilibrium solutions and the wave shape should be maintained throughout time, however the size of the wave and the periodicity are allowed to vary in time.

Another deviation from equations (4.24)-(4.27) in the last subsection is the treatment of viscosity and the critical layer. Hall & Horseman[21] and Hall & Sherwin[22] used the asymptotically large Reynolds number R to justify the removal of the viscous terms in the Navier-Stokes equations. By treating the wave as inviscid the result was the pressure term generalization of Rayleigh's equation in two dimensions. In this configuration the system needs special treatment at the critical layer to handle the jumps in velocity and pressure and two wave amplitude coefficients exist to enable this. There is the wave amplitude term ρ, dependent on time, and the δ term that depends on proximity to the critical layer. In this thesis R is still taken to be large but the viscous terms are retained, and without the jump conditions there is no need for the δ coefficient. When comparing results with Hall & Sherwin it will be required that the definition of the terms δ and ρ are taken into account.

When the combined flow (4.38) is substituted into the Navier-Stokes equations (4.11) and (4.12) the terms independent of E recover the equations (4.17)-(4.20), while the terms proportional to ρE form the resultant wave system,

$$i\alpha\left(u-c\right)U+V\frac{\partial u}{\partial y}+W\frac{\partial u}{\partial z}=-i\alpha P+\frac{1}{R}\left[\frac{\partial^2 U}{\partial y^2}+\frac{\partial^2 U}{\partial z^2}-\alpha^2 U\right], \quad (4.39)$$

$$i\alpha\left(u-c\right)V=-\frac{\partial P}{\partial y}+\frac{1}{R}\left[\frac{\partial^2 V}{\partial y^2}+\frac{\partial^2 V}{\partial z^2}-\alpha^2 V\right], \quad (4.40)$$

$$i\alpha\left(u-c\right)W=-\frac{\partial P}{\partial z}+\frac{1}{R}\left[\frac{\partial^2 W}{\partial y^2}+\frac{\partial^2 W}{\partial z^2}-\alpha^2 W\right], \quad (4.41)$$

$$i\alpha U+\frac{\partial V}{\partial y}+\frac{\partial W}{\partial z}=0. \quad (4.42)$$

The boundary conditions (4.14) hold true throughout, meaning that in the wave problem the conditions are $U, V, W = 0$ at $y = \pm 1$. In previous studies the inviscid wave system could be reduced to the pressure version of Rayleigh's equation. That is not possible here and, although the system can be reduced in dimension, ultimately a multivariate generalised eigenvalue problem for the temporal eigenvalue is the result. As this system is linear a normalisation condition is required. Hall & Sherwin[22], and others since, used the following normalisation and it is also used here to ensure comparability,

$$\sqrt{\frac{\int |P|^2 dA}{A}}=1, \quad (4.43)$$

where P is the wave pressure and A is the area of one spanwise period between the channel plates. In this study, as in previous ones, equilibrium solutions are sought. These occur when the $Im(c) = 0$ and mean that there is neither temporal growth nor decay in the wave system. If there was growth or decay

the impact through the vortex-wave interactions would be exponential in the vortex system.

Earlier authors showed that in the high Reynolds number limit the wave is localised around the critical layer and the retention of the viscous terms ensures the correct asymptotic structure of the wave solution. As discussed before, the vortex system in the form of (4.17)-(4.20), which is not subject to any forcing, will deteriorate to basic Couette flow with $v, w = 0$. However, from former studies it is known that an appropriate forcing in the roll equations in (4.17)-(4.20) can be enough to generate a self-sustained process,

$$Lu = \nabla^2 u, \tag{4.44}$$

$$Lv = -\frac{\partial p}{\partial y} + \nabla^2 v + F_1, \tag{4.45}$$

$$Lw = -\frac{\partial p}{\partial z} + \nabla^2 w + F_2, \tag{4.46}$$

$$\frac{\partial v}{\partial y} + \frac{\partial w}{\partial z} = 0, \tag{4.47}$$

where F_1 and F_2 are the forcing terms. Papers by Farrell & Ioannou[13] and Thomas et al.[51] developed upon the ideas that the forcing comes from the Reynolds stresses of the wave. The models used in these papers have a streamwise-averaged flow and Farrell & Ioannou perturb this flow with a disturbance that is stochastic in nature. Thomas et al. use a perturbation which they call a restricted nonlinear model. Both of these papers show close agreement to direct numerical simulations and the approach can be adapted for an asymptotic investigation. Blackburn, Hall & Sherwin's[3] variation on

this method involves taking the vortex forcing terms F_1, F_2 as proportional to the nonlinear zero-harmonic Reynolds stresses of the wave velocity field and they call this the hybrid computational approach,

$$F_1 = \rho^2 \left(i\alpha \overline{U} V - i\alpha U \overline{V} + \overline{V} \frac{\partial V}{\partial y} + V \frac{\partial \overline{V}}{\partial y} + \overline{W} \frac{\partial V}{\partial z} + W \frac{\partial \overline{V}}{\partial z} \right), \tag{4.48}$$

$$F_2 = \rho^2 \left(i\alpha \overline{U} W - i\alpha U \overline{W} + \overline{V} \frac{\partial W}{\partial y} + V \frac{\partial \overline{W}}{\partial y} + \overline{W} \frac{\partial W}{\partial z} + W \frac{\partial \overline{W}}{\partial z} \right), \tag{4.49}$$

where the superscript bar denotes the complex conjugate. The scaling is such that the equivalent nonlinear terms from the x-momentum equation of the wave system do not interact with the streak flow problem, while the non-zero harmonics act on different time and spatial scales to the vortex system and were reported by Wang[55] to decay faster and become insignificant at large Reynolds numbers.

Up to this point the spanwise wavelength Λ and wavenumber γ of the wave have not been introduced. In Hall & Sherwin[22] the study was focused on $\gamma = 2$, while Blackburn, Hall & Sherwin[3] studied several wavelengths and the large wavelength limit. For the neutral, stationary solution, $c = 0$, the behaviour does not change significantly for higher wavelengths but the numerical difficulty is increased. This thesis will keep the focus on the $\gamma = 2$ problem, to ensure comparability with previous studies, and the wavelength will be important in defining the symmetries in the flow.

The full system of equations (4.39)-(4.42) and (4.44)-(4.47) describe the vortex-wave interactions that must be solved numerically. A detailed explanation of the numerical methods used to find results for this flow configuration can be found in the numerical methods section of this chapter. In the next section the theoretical approach for finding neutral, stationary solutions is outlined.

4.2.5 The sinuous instability mode

The paper by Swearingen & Blackwelder[48] studied the vortex flow that is the theme of this chapter. Through experiments the authors identified that the sinuous instability mode is the most common and dominant in the flat-plate boundary layer flow. The vortices become tilted in this configuration and the slow velocity at the wall is drawn up in between the vortices, and this demonstrated in the Figures 1.3 and 1.4. Hall & Sherwin[22] acknowledged that this sinuous layer mode is the most dangerous and is present in channel flows as well. In the experiments of Swearingen & Blackwelder the instabilities are launched by a Görtler vortices generator but in the theoretical investigations an alternative approach must be adopted.

Neutral, stationary waves where $c = 0$ were the subject of Hall & Sherwin[22]. The investigation noted that, as other authors had suggested, other solutions are possible where $c \neq 0$ and that these would propagate left and right. To ensure the temporal eigenvalue had a zero real part the authors imposed symmetry conditions on the flow and a specific, initial artificial forcing. They found that for each α and γ there's a stationary solution with a ρ that drives the temporal growth rate to zero.

The first symmetry employed in Hall & Sherwin[22] is the symmetry of the vortex velocity about the midpoint of the spanwise period. The authors enforced this by numerically solving the problem in the half period domain with appropriate boundary conditions at the midpoint. A further symmetry, rotational this time, is forced upon the streak at a quarter period length. The authors state that this ensures that the wave solution and, consequently, the forcing, 'pin' the critical layer and hence fix the frequency at zero. For numerical solutions to have a stationary wave the enforcement of the symmetries has been shown to be necessary.

This effort in keeping the wave stationary would be pointless if the initial roll solution did not have these symmetries. Before a wave solution has been calculated an artificial body forcing replaces the previous definitions of F_1 and F_2. The idea behind the artificial forcing comes from Waleffe[54] and takes the following form:

$$F_1 = C\gamma cos(\pi y)cos(\gamma z), \tag{4.50}$$

$$F_2 = C\pi sin(\pi y)sin(\gamma z), \tag{4.51}$$

where C is a constant analogous to the ρ^2 amplitude in the regular forcing. In this study the same initial, artificial forcing terms are used. As is common, the solution at the zero time position is calculated with steady equations. The symmetries are enforced slightly differently to Hall & Sherwin[22], with the odd and even separation of the Fourier series utilised.

4.2.6 Numerics of the vortex-wave interaction equations

The numerics of the vortex-wave interaction equations are normally considered as an iterative step-wise procedure. Hall & Sherwin[22] sought the lower branch equilibrium identified by Wang[55] through the solutions of the vortex-wave interaction equations for Couette flow. Wang used a numerical procedure to solve the full Navier-Stokes but the asymptotic theory of vortex-wave interaction requires more consideration. Hall & Sherwin begin by fixing the spanwise and the streamwise wavenumbers of the wave system. The scaling that is used in this paper allows for the Reynolds number to be dropped from the equation. This differs from the method of Wang, where a finite Reynolds number must be specified.

The iterative scheme that Hall & Sherwin[22] employed isn't completely time dependent. In the roll system the time derivatives are retained and the solution is marched forward until it is at equilibrium. Then the streak problem is solved in the steady state and finally the wave amplitude is modified until the wave growth rate is neutral. This approach is vindicated by being unable to capture the time dependent equilibrium solution which was shown to be unstable by Waleffe[54].

One of the significant difficulties with this scheme is having enough resolution around the critical layer, where the wave velocity gradients are greatest. Hall & Sherwin[22] use a spectral/hp element discretisation scheme that was developed in the earlier publication by Karniadakis & Sherwin[30]. This method allows for smaller, more detailed subdomains to be placed strategically in the domain.

The hybrid system described by Blackburn, Hall & Sherwin[3] a finite Reynolds number must defined that is sufficiently large, however it is shown that the results converge for increasing Reynolds number. In the subsequent paper by Deguchi & Hall[9] the authors use a Galerkin spectral approach with the solutions approximated in the normal direction by Chebyshev polynomials and Fourier series in the other two directions. Deguchi & Hall begin their computations with the solutions of Nagata[34] and use Newton's method to seek equilibrium solutions.

Isoni's[27] numerical approach differs again and reverts back to using the jumps in stresses across the critical layer. After calculating the roll and streak solutions, and solving the wave eigenvalue problem, a new critical layer is defined and extracted by Newton's method from the solutions. The jump conditions are then recalculated and used for the nonlinear interaction between the wave and the roll in the next iteration of the system. The approach requires an adjustable mesh to retain the resolution in the desired area and this is achieved with a spectral/hp element method.

Numerical methods for the special case

The approach used in this thesis uses elements from several previous investigations. The general framework of the numerical approach is to solve the base flow and disturbance problem at time t in the y, z plane at a fixed longitudinal position x. The solution is then marched forward in time using a backward Euler method. At each t the roll, streak and wave problems must be solved and the solutions are iterated on until the wave has zero growth before they are marched forward in time.

Beginning with the roll problem, the solution to the three equations (4.45)-(4.47) can be found more quickly if the problem is reduced in dimension by combining equations (4.45) and (4.46) and eliminating p. Taking the derivative in the normal direction leads to the requirement of an additional boundary condition, which is derived from the continuity equation in this case and taken as $\frac{\partial v}{\partial y} = 0$ at $y = 1$. As before, the the functions v and w are expanded at collocation points in terms of Chebyshev functions in the normal direction and Fourier series in the spanwise direction.

It is known from Hall & Sherwin[22] that the stationary wave requires symmetries and the first of these is about the midpoint in the period. The Fourier series can be reduced to just the cosine terms for a symmetric function about the midpoint, while an antisymmetric function is approximated by just the sine terms. Following the insight from Hall & Sherwin v is known to be an even function and w is an odd function in z. This reduces the size of the problem again because now the system should only be solved in the half period to avoid the pseudo-spectral matrix from being singular. This method of enforcing this symmetry is different to that of Hall & Sherwin but the effect is the same. There is no need to impose specific boundary conditions on the spanwise ends of the half period because of the periodicity of the Fourier series.

Hall & Sherwin[22] didn't solve the full unsteady vortex problem as is being done here. The authors point out that their steady state solution is only valid when the wave frequency, c_i, is zero. In this thesis the time derivatives are retained and it is shown that by modifying ρ the wave frequency can be driven to zero at each time position. The time derivatives are calculated by a simple backward Euler method.

The forcing comes from the wave solution as outlined in the previous section in (4.48) and (4.49). Of course, as derivatives have been taken so that the dimensionality of the problem is reduced, the derivatives of the forcing terms must also be taken. At the inital time position the body forcing is artificial, as described in (4.50) and (4.50). This artificial forcing is turned off and replaced the by correct form of the forcing terms after the first time step.

The roll equations are nonlinear and these terms need to be addressed numerically. The nonlinear terms could be calculated from the solution at the previous time position and added to the forcing terms or, as is the case here, the terms are treated in an iteratively implicit manner. This means that only one part of the nonlinear term is unknown, let these be subscripted n at the nth iteration, and the other part is known from the previous iteration, $n-1$. Equation (4.52) describes the combined momentum equation and the nonlinear numerical scheme,

$$\begin{aligned}
&\frac{\partial^2 v_n}{\partial T \partial z} + \frac{\partial^3 v_n}{\partial y^2 \partial z} + \frac{\partial^3 v_n}{\partial z^3} - \left(\frac{\partial^2 w_n}{\partial T \partial y} + \frac{\partial^3 w_n}{\partial y^3} + \frac{\partial^3 w_n}{\partial y \partial z^2} \right) \\
&- \left(\frac{\partial v_{n-1}}{\partial y}\frac{\partial v_n}{\partial z} + v_{n-1}\frac{\partial^2 v_n}{\partial y \partial z} + \frac{\partial v_{n-1}}{\partial z}\frac{\partial w_n}{\partial z} + w_{n-1}\frac{\partial^2 v_n}{\partial z^2} \right) \\
&+ \frac{\partial v_{n-1}}{\partial y}\frac{\partial w_n}{\partial y} + v_{n-1}\frac{\partial^2 w_n}{\partial y^2} + \frac{\partial w_{n-1}}{\partial y}\frac{\partial w_n}{\partial z} + w_{n-1}\frac{\partial^2 w_n}{\partial y \partial z} = \frac{\partial F_1}{\partial z} - \frac{\partial F_2}{\partial y}. \quad (4.52)
\end{aligned}$$

When $n = 1$, the first iteration, the approximation to the $n-1$ terms comes from the solution at the previous time position. When the new solution is found the process is iterated on until the change in the maximum value of w is less than 0.1%. At the initial time position the steady equations are used. Using this type of iterative scheme for the nonlinear terms can impact the symmetries on the roll solution even when the forcing has all the correct symmetries. At the converged solution for v and w the symmetries are reinforced with the quarter period symmetry of Hall & Sherwin[22]. This rotational symmetry, at the quarter period point, can not be imposed as succinctly as the odd and even function symmetries. In the half period the v and w functions are neither odd nor even at all heights in the channel and the quarter basis, double parity properties of the Fourier series can not be used. This symmetry is achieved by averaging the first quarter and the rotated second quarter as described in equations (4.53) and (4.54),

$$v_{symm}(y,z) = (v(y,z) - v(-y,\pi/2 - z))/2$$
$$for \ -1 \leq y \leq 1, \ 0 \leq z \leq \pi/2, \tag{4.53}$$

$$w_{symm}(y,z) = (w(y,z) - w(-y,\pi/2 - z))/2$$
$$for \ -1 \leq y \leq 1, \ 0 \leq z \leq \pi/2. \tag{4.54}$$

The final result is a nonlinear roll flow from the unsteady, viscous Navier-Stokes equations with quarter rotational symmetry. v and w can now be substituted directly into the x-momentum equation for u.

The x-momentum equation, or streak problem, with v and w already found becomes a linear problem. The method for solving the problem is addressed with spectral techniques again, and once more an insight into the shape of the solution is known from Hall & Sherwin[22]. u is an even function and therefore only the cosine terms are used in the spanwise Fourier expansion. The quarter symmetries of the roll solution produce a streak with quarter rotational symmetries and thereby fix the critical layer, driving stationary waves.

4.2.7 Solving the wave problem and correcting the wave amplitude

As discussed before the wave system is an eigenvalue problem. The equations (4.39)-(4.42) are for the four variables U, V, W and P. As this is the most computationally intensive part of the method it makes sense to reduce the dimensionality of the problem. U can be eliminated from the equations by substituting the rearranged continuity equation into the streamwise momentum equation.

$$-(u-c)\left(\frac{\partial V}{\partial y}+\frac{\partial W}{\partial z}\right)+V\frac{\partial u}{\partial y}+W\frac{\partial u}{\partial z}=-i\alpha P$$
$$+\frac{1}{R}\left[\frac{i}{\alpha}\left(\frac{\partial^3 V}{\partial y^3}+\frac{\partial^3 W}{\partial y^2\partial z}\right)+\frac{i}{\alpha}\left(\frac{\partial^3 V}{\partial y\partial z^2}+\frac{\partial^3 W}{\partial z^3}\right)-i\alpha\left(\frac{\partial V}{\partial y}+\frac{\partial W}{\partial z}\right)\right]. \tag{4.55}$$

The division by α here is permissible as the longitudinal wavenumber will always be chosen to be greater than zero. Equation (4.55) can be simplified further by eliminating c with substitutions from the wall normal and spanwise momentum equations.

$$2V\frac{\partial u}{\partial y}+2W\frac{\partial u}{\partial z}=-i\alpha P+\frac{i}{\alpha}\frac{\partial^2 P}{\partial y^2}+\frac{i}{\alpha}\frac{\partial^2 P}{\partial z^2}. \tag{4.56}$$

The additional boundary condition for the third order derivative in the wall normal direction comes from the wave continuity problem and is taken as $\frac{\partial V}{\partial y}=0$ at $y=1$. The streamwise disturbance momentum U can be recovered from the solutions for V and W and the continuity equation (4.42). The method for solving the eigenvalue problem is dependent on the size of the problem and different strategies are presented in subsection (2.5). At the stage where the eigenfunctions have been found the normalisation condition (4.43) must be applied. The integration is performed by Simpson's rule and all the velocity disturbance functions are normalised by the factor.

A crucial part of the process at each time position is modifying wave amplitude ρ so that the wave growth rate is driven to zero. At a new time position the first approximation to ρ is based on the relative size of the forcing terms compared the size of the forcing terms at the previous time step. The first solution is unlikely to have a growth rate very close to zero and the change in ρ for the next iteration is proportional to the initial growth rate. After the second iteration there are two solutions for two different amplitudes and for the subsequent iterations the new ρ is determined by linear interpolation

using the growth rate. The wave amplitude is modified until the growth rate is less than 10^{-5}. This typically takes about five iterations but it can be less or more.

4.2.8 Results

The results presented here are for a spanwise wavenumber $\gamma = 2$ and a Reynolds number $R = 10000$. $\gamma = 2$ was used in several previous papers and those results will provide a comparison for the investigation presented here. $R = 10000$ is big enough to be considered asymptotically large, as demonstrated in Table 1 in Blackburn, Hall & Sherwin[3].

The stimulated Couette flow with longitudinal vortices, that was also the focus of so much other recent work, has been generated here and is shown in Figure 4.6. In each of the three plots the colour scale represents the speed of the flow in the streamwise direction. The arrows plotted on top of the streak describe the rolls which are on a smaller scale to the streamwise flow. The three plots are for different values of the wavenumber, α, and are the large time, steady, lower branch equilibrium solutions.

It can be seen that as the wavenumber, α, is increased the rolls become more angled to the horizontal, decreasing the speed of the streak in the centre of the period and increasing the speed at the ends of the period. This is due to the location of the critical layer which is steeper at the equilibrium point for greater α. Similar plots to these have been produced several times before and Figure 1.4 from the beginning of this thesis, which was taken from Blackburn, Hall & Sherwin[3], shows close likeness. Figure 4.6 has been designed to be comparable to the plots in Figure 3 of Deguchi & Hall[9], and Figure 4.7 simply plots the critical layer $y = f(z)$, where the streak velocity $u = 0$ and therefore is equal to the wavespeed c.

The amplitude ρ of the forcing that drives the lower branch equilibrium solution and the wall drag of these states can be found in Hall & Sherwin[22], Deguchi & Hall[9] and Isoni[27]. Hall & Sherwin[22] produced a full curve of results for α against ρ when the growth rate is zero in their Figure 5 and

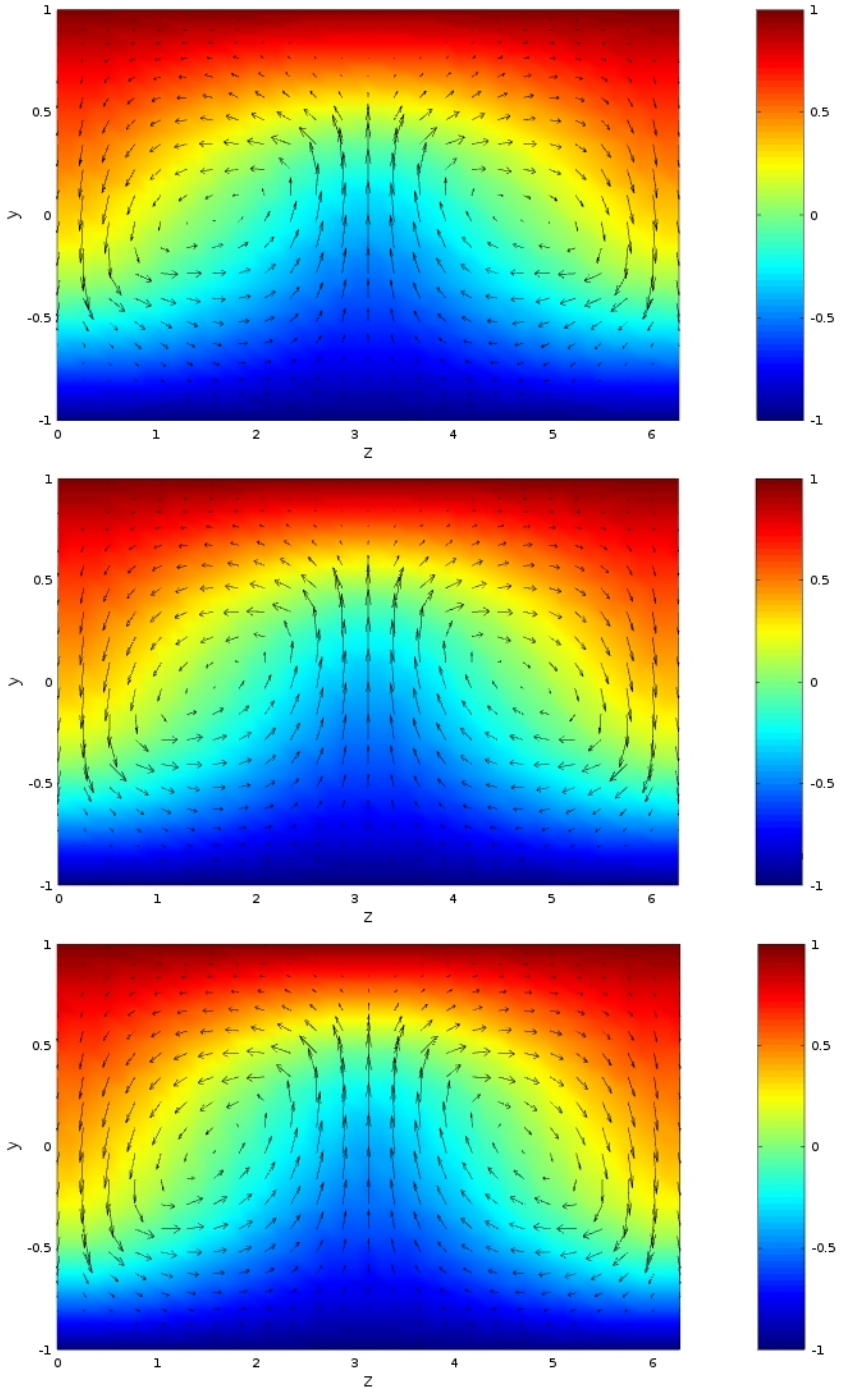


Figure 4.6: The vortex velocity field made up of a streak u and rolls v, w. The colour scale refers to the streak and rolls are depicted by arrows. $\alpha = 0.8, 1.0, 1.2$ in the top, middle and bottom plots respectively. $R = 10000$.

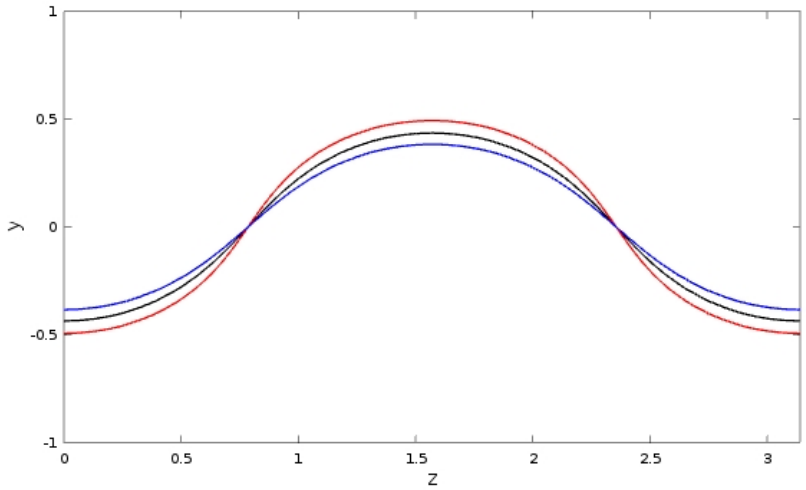


Figure 4.7: The equilibrium critical layers $y = f(z)$ where the streak velocity equals the wavespeed $u = c$, which equal zero in this situation. $\alpha = 0.8$ is the blue line, $\alpha = 1.0$ is the black line, and $\alpha = 1.2$ is the red line. $R = 10000$.

they showed that for small wavenumbers there is a proportional relationship of $\rho \propto \alpha^{5/6}$. Deguchi & Hall found the wall drag for equilibrium solutions for several values of the Reynolds number in their Figure 1. Table 4.2 presents the data from Deguchi & Hall for $R = 10000$ against the results found from the model developed for this thesis. The wall drag is calculated here in a similar way to Deguchi & Hall, which is to average the streamwise velocity gradient in the spanwise direction. The data from the model developed for this thesis matches well to the results in previous research.

α	ρ	Wall drag	Wall drag (D&H)
0.5	0.44	1.14	1.16
0.8	0.69	1.22	1.24
1.0	0.92	1.31	1.32
1.2	1.25	1.42	1.43

Table 4.2: The lower branch equilibrium amplitude ρ and the wall drag as a function of α calculated for this thesis compared to the wall drag calculated by Deguchi & Hall[9]. $R = 10000$.

For the lower branch solutions, which Table 4.2 is concerned with, the wall drag increases as α increases. This can be justified by considering that a larger α requires a larger forcing to achieve equilibrium, and this stronger

wave drives a more angled roll. Finally, this angled roll increases the gradients in the streak and the wall drag. This effect can been seen in Figure 4.6.

In the formulation of this problem, unlike those before it, the time derivative was kept in the vortex system. Previous studies assumed the steady solution was possible but here it is shown that the equilibrium solutions do indeed converge to a steady state through marching forward in time. Figure 4.8 shows that after only a few small time steps the wave amplitude is close to the converged value. This large time value for ρ is the one used in Table 4.2 and compared to previous results.

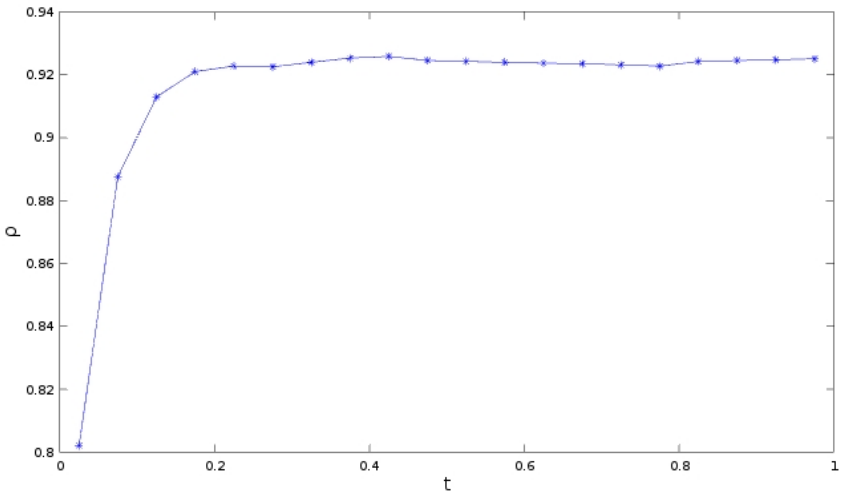


Figure 4.8: Convergence in time of the wave amplitude ρ for the lower branch steady solution. $\alpha = 1.0$, $R = 10000$.

It remains to describe what the wave field looks like for the lower branch equilibrium solutions and how it compares to previous work. Figure 7 in Hall & Sherwin[22] shows the axial and spanwise components of the wave for various α in the half spanwise period. The symmetries in the wave and the flow mean that all the characteristics are captured in the half period. Similar plots have been produced here in Figure 4.9. The three plots, for the longitudinal, radial and spanwise components, show the localisation of the disturbance velocity around the critical layer. It can now be clearly seen how the wave drives the roll.

It was shown by Deguchi & Hall[9] that the upper branch equilibrium solutions

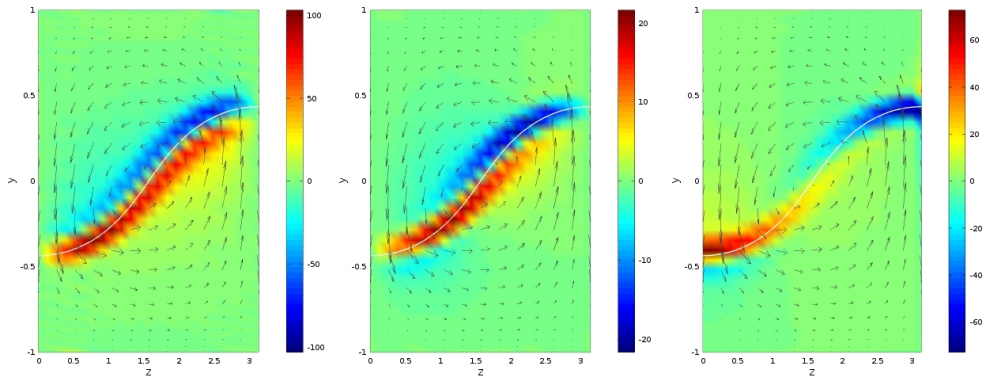


Figure 4.9: Longitudinal (left), radial (middle) and spanwise (right) disturbance velocity components in half spanwise period. The arrows describe the vortex roll and the white line is the critical layer.

are distinct from the lower branch solutions but can be captured with the same scalings and methodology. This is true of the approach developed here using the unsteady equations and, like the lower branch solutions, the steady upper branch equilibrium is found as the solution is marched forward in time.

The visible difference between the lower and upper branch solutions is the non-unique, multivalued critical layer in the spanwise direction. Figure 3 in Deguchi & Hall[9] compared solutions of both branches for three α values and a similar plot has been generated in Figure 4.11.

Once again the similarity in the results between this investigation and previous research is very close. In each of the four panels in Figure 4.11 $(a) - (d)$ the upper plot is the vortex system while the lower plot is the magnitude of the wave Reynolds stress. Panels (c) and (d), for the lower branch, show what has been described before: the increasing movement of the critical layer away from the horizontal, making the rolls more arched and the gradients in the streak greater. The opposite trend is happening in the upper branch, panels (a) and (b). The equilibrium solution has less distortion of the critical layer when α is higher. Figure 1 in Deguchi & Hall[9] plots this equilibrium neutral curve and there is a turning point at around $\alpha = 1.3$. As mentioned before, the critical layer in the upper branch has inflections points but there is the further difference that some of the higher-magnitude Reynolds stresses appear removed from the critical layer.

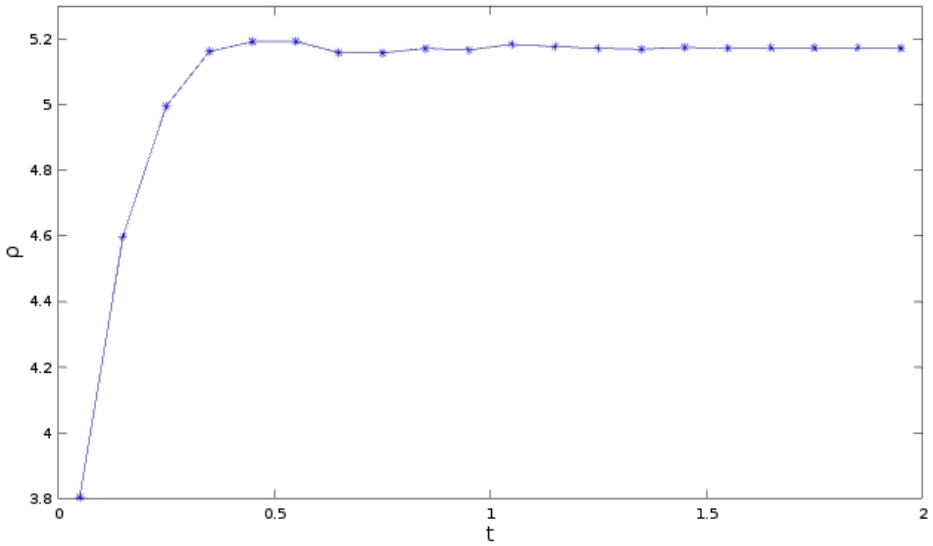


Figure 4.10: Convergence in time of the wave amplitude ρ for the upper branch steady solution. $\alpha = 1.0$, $R = 10000$.

Table 4.3 details the important metrics for comparison. For the same α, the ρ required to drive the whole system to the upper branch equilibrium is much greater. The wall drag is also vastly increased and this is intuitive from the plots, where it can be seen that the streak is now deformed even further from plane Couette flow. The upper branch solution is becoming more deformed for lower α and this makes the phenomenon harder to capture numerically as more resolution is required to generate a sufficiently accurate solution. These results compare very well to those in Deguchi & Hall[9].

Branch	α	ρ	Wall drag	Wall drag (D&H)
Lower	1.0	0.92	1.31	1.32
Upper	1.0	5.17	2.98	2.82
Lower	1.2	1.25	1.42	1.43
Upper	1.2	3.74	2.38	2.30

Table 4.3: The amplitude ρ and the wall drag for lower and upper branch vortex-wave interaction equilibrium solutions as a function of α. The results calculated for this thesis are compared against the wall drag calculated by Deguchi & Hall[9] which were shared in a private communication. $R = 10000$.

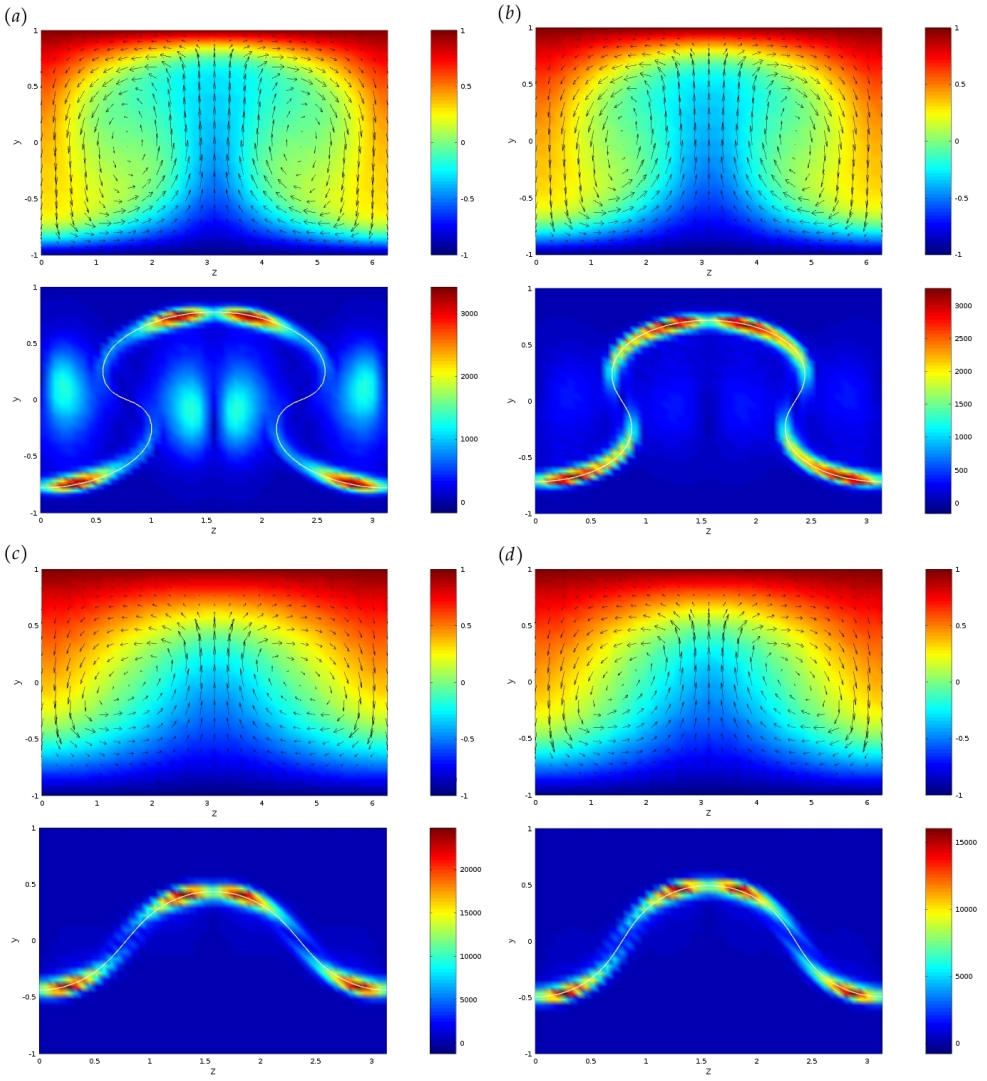


Figure 4.11: Panel (a) is the upper branch equilibrium solution for $\alpha = 0.8$. Panel (b) is the upper branch for $\alpha = 1.0$. Panel (c) is the lower branch for $\alpha = 0.8$. Panel (d) is the lower branch for $\alpha = 1.0$. Upper plots: vortex system, with the colour scale for the streak u and the arrows for the rolls v, w. Lower plots: magnitude of the wave Reynolds stress. $R = 10000$.

4.2.9 Time periodic solutions

So far this chapter has been concerned with stationary, steady solutions of the vortex-wave interaction equations but time periodic solutions and travelling waves have also been shown to exist by Deguchi & Hall[10]. Travelling waves, where the wave speed c is non-zero, are known to be solutions of these equations but they are harder to capture numerically. Time periodic solutions can still have $c = 0$, and therefore have zero growth and zero wave speed, but the amplitude of the wave oscillates in time and these are worth further consideration here.

The paper by Deguchi & Hall[10] discussed a similar configuration of the vortex-wave interaction equations as in this chapter and found time periodic solutions that existed near to the bifurcation between the lower and upper branch solutions. The periodic solutions have a wave amplitude, ρ, roughly half way between the steady equilibrium solutions for the lower and upper branches. The new solutions that were detected varied as a function of ρ in the periodicity and the amplitude of the oscillations, and these are depicted in Figure 16 of Deguchi & Hall.

The authors found that the rapidly oscillating solution was probably associated with a bifurcation from the lower branch equilibrium solutions. The oscillations here are small and the solution is almost steady in nature. This solution shares many characteristics with the lower branch mode. Deguchi & Hall[10] found it highly likely that this high Reynolds number solution corresponds to Kawahara & Kida's[31] 'gentle solution' which follows a bifurcation from the steady lower branch equilibrium solutions for smaller Reynolds numbers. For the time periodic solutions with large, slow oscillations Deguchi & Hall suggested that these are connected to the upper branch equilibrium solutions.

To find time periodic solutions Deguchi & Hall[10] used direct numerical simulations around the region of the steady solutions. The authors assumed all the symmetries suggested by Hall & Sherwin[22], and also used in this thesis, and the initial conditions were chosen in a precise way such that the solution would converge to the edge of the laminar and turbulent attractors. This so-

lution is therefore unstable and difficult to find with a less exact method. It remains to be seen if a more theoretical and less computationally demanding method can find these time periodic solutions.

Two approaches were used to find these periodic solutions with the methodology established in this chapter. The first attempt involved substantially increasing the equilibrium amplitude from the converged, steady lower branch solution, or decreasing the equilibrium amplitude from the upper branch solution, and marching forward in time. This approach only served to increase or decrease the growth rate of the wave and no new eigenvalues were detected. The second approach involved revisiting the initial artificial forcing and carefully varying the initial amplitude in the region where it might be expected to detect periodic solutions. This careful modification of the initial conditions still only found the lower and upper branch solutions. The results of this part of the investigation are disappointing but are believed to be a result of the unstable nature of the time periodic solutions.

Numerical validity and convergence

In the formulation of the vortex-wave interaction equations there is a requirement for the Reynolds number to be asymptotically large to allow the scales and assumptions to make sense. Table 4.4 provides assurances that when the Reynolds number is increased the wave amplitude converges.

Reynolds number	ρ
2000	0.74171
5000	0.83735
10000	0.92509
15000	0.95746
20000	0.96990
25000	0.93016

Table 4.4: The converged amplitude ρ for the lower branch equilibrium solutions to the vortex-wave interaction equations against the Reynolds number. $\alpha = 1.0$.

In Table 4.4 the Reynolds number is varied while the rest of the parameters remain the same. It can be seen that when the Reynolds number is larger

than 10000 the converged value of the amplitude parameter ρ changes less. As the Reynolds number increases the disturbance becomes more localised around the critical layer making high accuracy results harder to achieve with the same number of collocation points. The reason why most of the plots and results shown in this chapter are for $R = 10000$ is because this value seems to be large enough in the asymptotic sense but not so large that numerical calculations require a prohibitively small grid size.

The results presented in this section are with 50 points in the wall normal direction and 24 in the spanwise direction. A study of the numerical convergence was presented in the Numerical methods Chapter 2 but the plots for the wave Reynolds stresses with different number of grid points can be found in Figures 4.12 and 4.13 for the lower branch solutions. The plots are virtually identical and only a slight change in the 'pixellation' of the plot can be seen when there is a rapid change in magnitude. When the upper branch solutions are depicted results are very similar again and Figures 4.14 and 4.15 contain these plots.

4.2.10 Conclusions

This section considered a channel flow with the dominant characteristic being a pair of longitudinal vortices. The specific flow under investigation was Couette flow, as has been studied many times before as the prototype channel flow. The method of analysis for this flow field was the theory of vortex-wave interactions. This theory was developed through several papers over the last thirty years. It draws on the results from experiments that showed that these vortex structures can be maintained in time and are persistent in the transition to turbulence and even in turbulent flows.

Vortex-wave interaction theory is analogous to the large Reynolds solutions from the numerical research into self-sustained processes. In these processes a pair of streamwise rolls drive a streaky flow. On this streak there is wave instability and this wave drives the rolls. For this system to be observed in time it must be in equilibrium to ensure that there isn't a breakdown of the base flow.

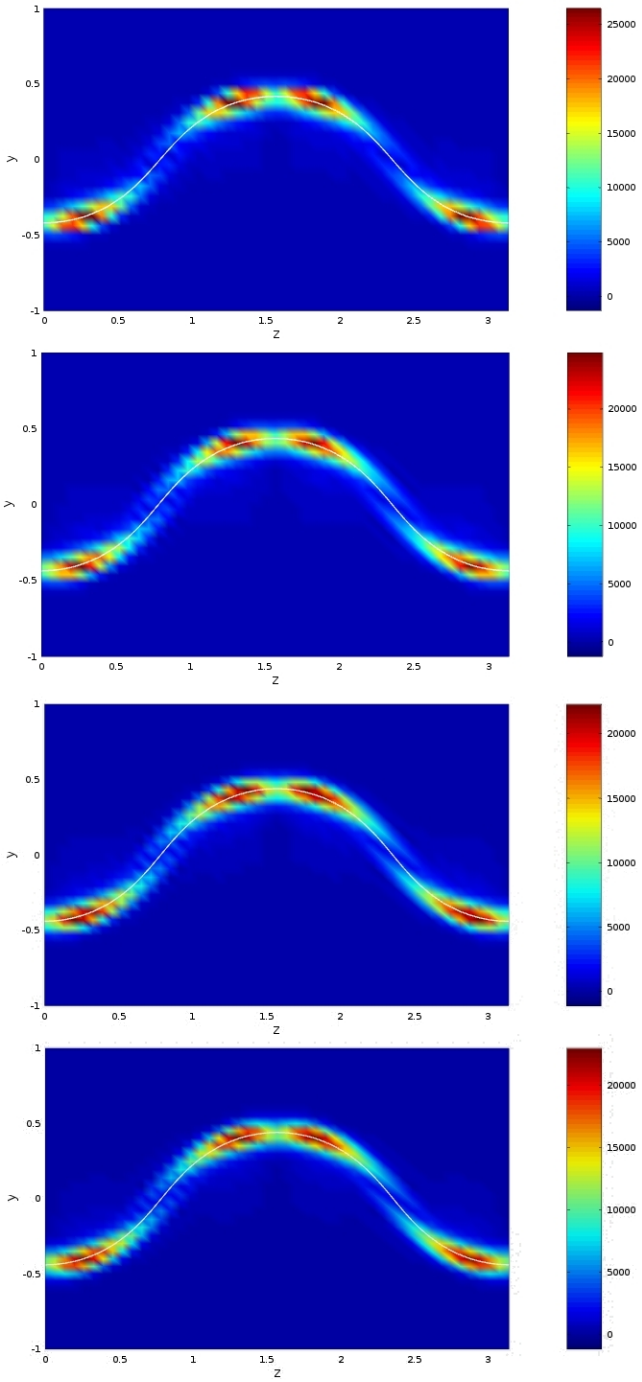


Figure 4.12: Plots of the magnitude of the wave Reynolds stress for converged lower branch equilibrium solutions with varying number of collocation points in the wall normal direction. From top to bottom: 46 points, 50, 54, 58. 24 points in the spanwise direction. $\alpha = 1.0$, $R = 10000$.

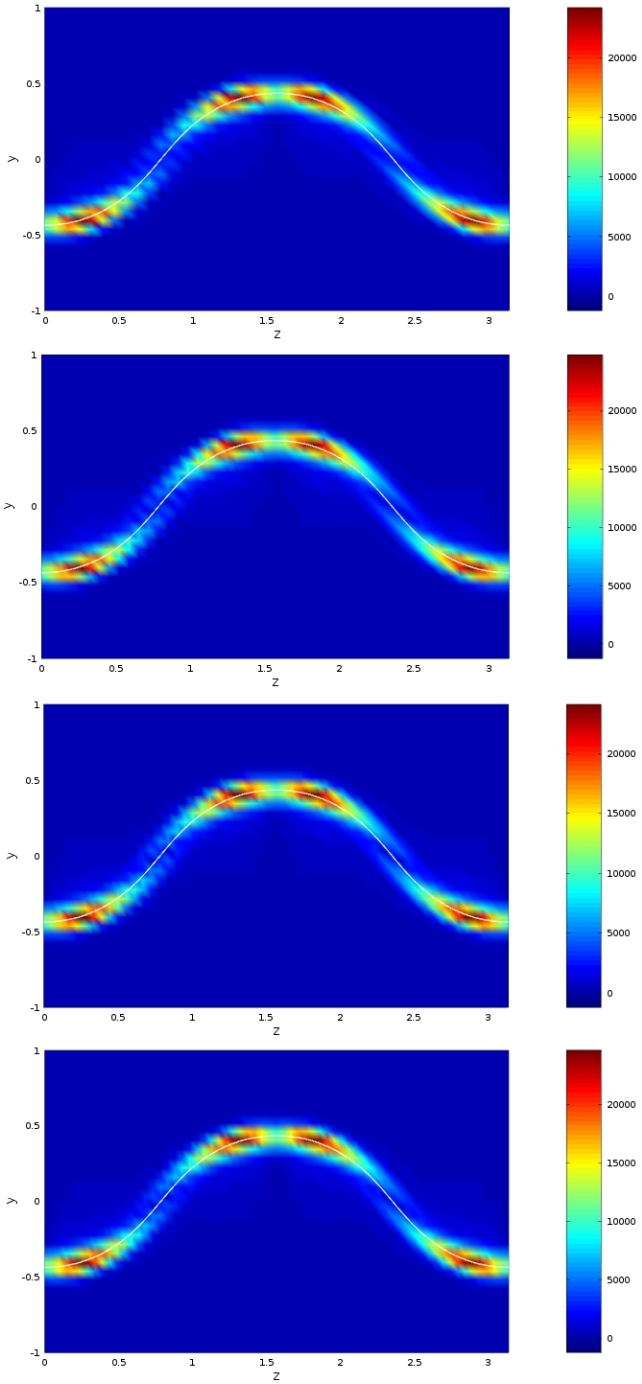


Figure 4.13: Plots of the magnitude of the wave Reynolds stress for converged lower branch equilibrium solutions with varying number of collocation points in the spanwise direction. From top to bottom: 20 points, 24, 28, 32. 50 points in the wall normal direction. $\alpha = 1.0$, $R = 10000$.

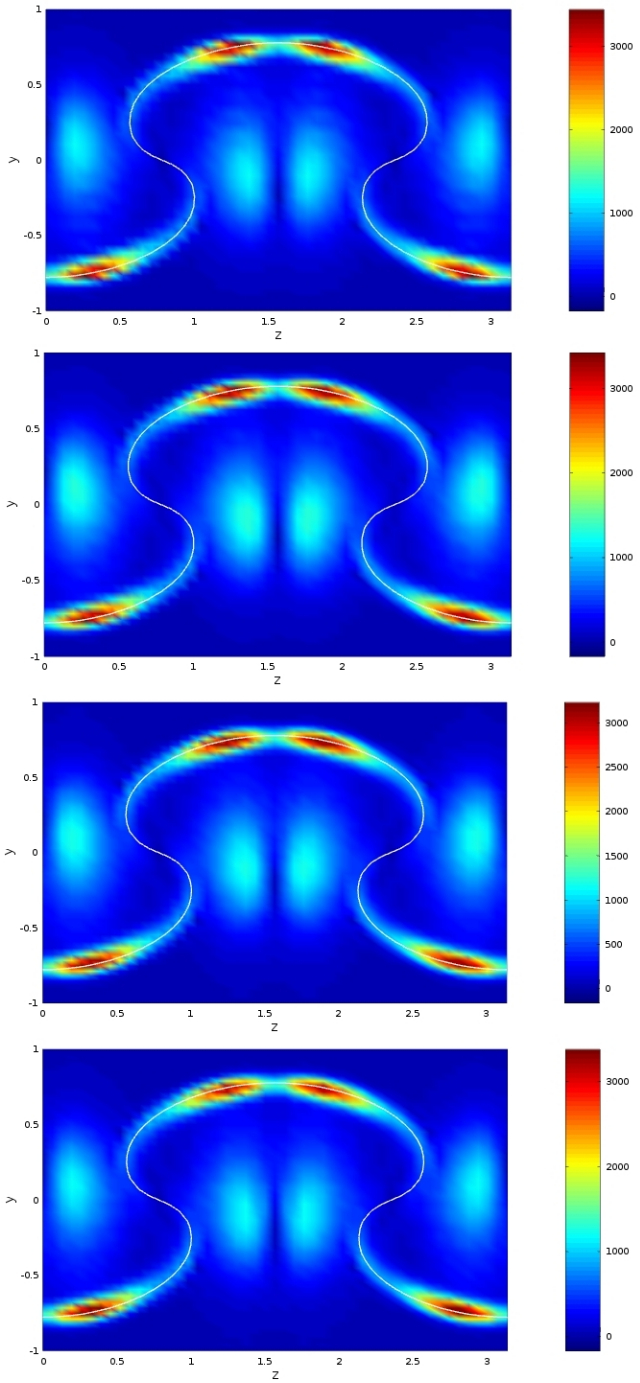


Figure 4.14: Plots of the magnitude of the wave Reynolds stress for converged upper branch equilibrium solutions with varying number of collocation points the wall normal direction. From top to bottom: 46 points, 50, 54, 58. 24 points in the spanwise direction. $\alpha = 1.0$, $R = 10000$.

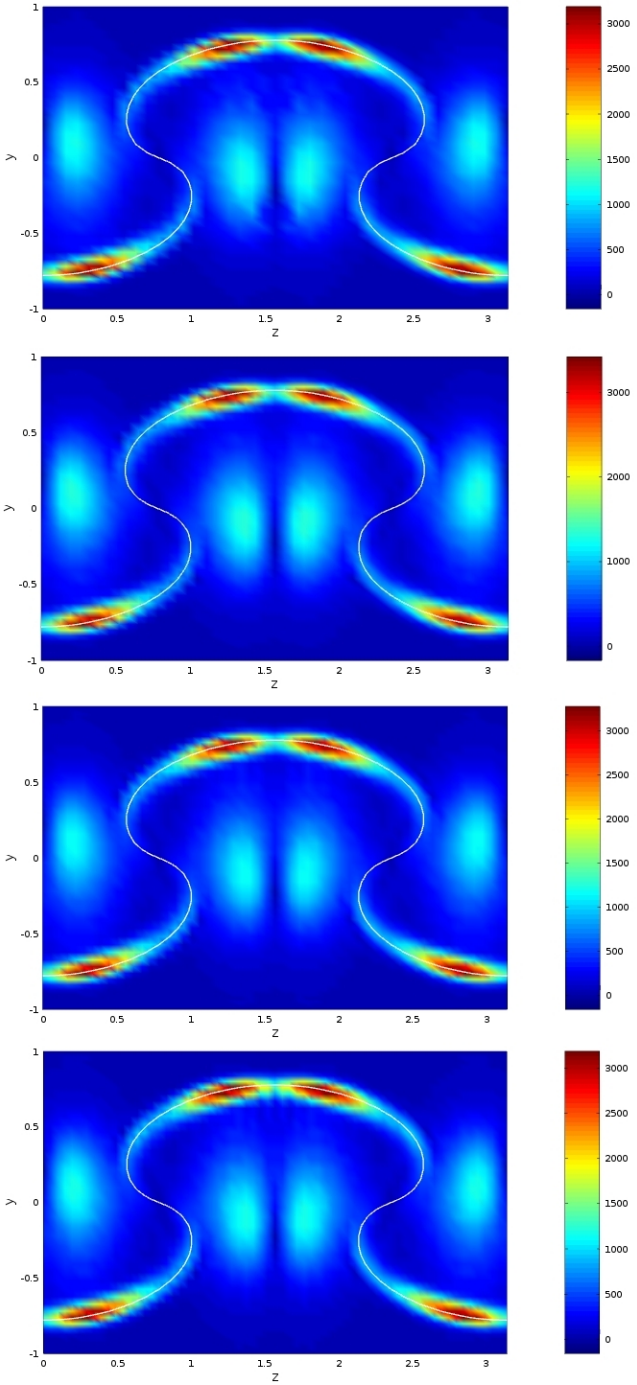


Figure 4.15: Plots of the magnitude of the wave Reynolds stress for converged upper branch equilibrium solutions with varying number of collocation points the spanwise direction. From top to bottom: 20 points, 24, 28, 32. 50 points in the wall normal direction. $\alpha = 1.0$, $R = 10000$.

Instead of solving the full Navier-Stokes equations the problem can be considered as flow components on different scales which interact. In vortex-wave interaction theory the Reynolds number is taken to be asymptotically large and the scales are associated to this nondimensional constant. It is possible to capture many, if not all, characteristics of these vortex systems through this asymptotic derivation and the theory has been shown to be accurate even down to quite small Reynolds numbers.

In this thesis the vortex-wave equations are taken in the special case where the wave is not fully time-dependent. The wave instability is composed of a shape profile and a wave-like part, and this profile is not changing in time. The type of instability investigated here is of Tollmien-Schlichting type and specifically the so-called sinuous mode which is known to be the most pervasive and dominant. For the interaction between the wave and the roll a hybrid computational method is employed, which uses the wave's Reynolds stresses as forcing terms. A wave solution is sought that is neutral, otherwise the wave will experience exponential growth or decay.

To ensure the restriction on the wave shapes is maintained the wave solutions would have to be stationary. It has been shown that if a stationary wave is required the numerical system must be subject to certain symmetries. These symmetries in the periodic spanwise channel are enforced in this study. The stationary wave in Couette flow has lower and upper branch solutions and these are associated to different states and different shape structure. The lower branch is an edge state disturbance between laminar and transitioning flow, while the upper branch is an attractor for turbulent flow. The aim of this section was to show it is possible to replicate the lower and upper branch stationary results of previous studies with this formulation and investigate solutions that have a periodic wave amplitude.

The vortex flow was generated and plotted in this section and it was shown that where there is a sinuous instability mode the slow streamwise flow near the centre of the channel is forced upwards. As the wave amplitude is increased the critical layer becomes more extreme and the rolls are forced into a more arched shape. It was also demonstrated that the equilibrium solutions are independent of the Reynolds number when it is sufficiently large.

This is a necessary requirement for the formulation to be correct and gives an indication of the limits of the asymptotic formulation.

It was possible to replicate the lower branch solutions that have been shown by various authors with several approaches. For the lower branch it is clear that increasing the streamwise wavenumber, α, means the wave amplitude must be increased to ensure the system is at equilibrium. Increasing the wave amplitude results in higher wall drag and several plots and tables in this section confirm the results against previous publications. It was also possible to find upper branch solutions near the turning point in the curve of the streamwise wavenumber against wall drag. The opposite relationship is true for the upper branch: decreasing the wave amplitude results in higher wall drag.

It was found that it is not possible to replicate the periodic wave amplitude solutions. These solutions are known to be unstable and are not found by this method. Finally, the code used here was validated for numerical stability and consistency.

5

Conclusion

This thesis is concerned with furthering the understanding of instabilities in shear flows. Many unknowns still remain in transition and turbulent flow and there are several large fields of active investigation. In this research two significant problems are tackled: instability of pipe flows and vortex-wave interaction theory for Couette flow. The first problem addresses the deficiencies in the assumption of parallel flow in a pipe and in linear stability theory. The second problem builds on the analytical analysis of nonlinear interactions between vortex flows and waves. Linear hydrodynamic stability is important for understanding primary mode growth and it is a starting point for all the problems in this thesis. However, further analysis is required for these problems and weakly nonlinear stability theory is considered for the pipe flow problem, while nonlinear equilibrium solutions are followed in time for the flow between parallel plates.

The first chapter in this thesis considers spatial stability of fully developed flow in a pipe driven by a pressure gradient. The chapter begins by reproducing several results for Hagen-Poiseuille flow. The flow is parallel and known to be linearly stable and this characteristic is shown to hold true even for non-axisymmetric disturbances. It is found that the eigenmode associated

with the $n = 1$ Fourier mode is always the least stable and this property is related to the non-zero velocity of the radial and azimuthal disturbance at the centre of the pipe for this Fourier mode. This is the only Fourier mode for which the radial and azimuthal disturbance velocities are non-zero. Although the linear spatial stability results generated here are consistent with previous literature they are at odds with results from experiments which show pipe flow becoming unstable and transitioning for Reynolds numbers greater than some critical value. This discrepancy is related to linear stability theory where there isn't the scope for small disturbances to interact with the mean flow but also with the assumption of parallel flow.

The second half of the first chapter seeks to addresses these deficiencies. Periodic suction on the pipe wall boundary is introduced and this causes the base flow to become non-parallel. The investigation focuses on the 2π-periodic suction condition. It is found that this suction moves the maximum of the axial velocity away from the centre of the pipe in the direction of the suction and this maximum is reduced as the suction is increased. The suction also destabilises the flow and now a critical Reynolds number exists. It is shown that the neutral curves for a range of suction coefficients collapse on to one curve and the critical number of these curves is about 4000. This result implies that for any flow in a pipe that is not perfectly axisymmetric, which would be all real world flows, there is a critical Reynolds number and this can be found with linear stability theory.

Several other results are also revealed for this flow. The disturbance is localised around the area where $\alpha_r u = \omega$, with α_r being the axial wavenumber, u the streamwise velocity and ω the wave frequency. This is common in models of this type and is related to a change in the sign of the term that connects the temporal derivative with the spatial derivative in the Navier-Stokes equations. It is shown that the wavenumber is proportional to the wave frequency and therefore the phase velocity is constant and equal to the group velocity. The phase velocity also has a linear relationship with the maximum of the axial velocity. More research into these relationships would generate a better understanding of the significances here. A weakly nonlinear stability analysis of this non-parallel pipe flow establishes several analytical

results that are similar to previously published work. The important result here is that the weakly nonlinear problem is solved numerically and solutions exist that show there is a valid supercritical equilibrium solution for small disturbances. This finding completes the connection of results in experiments with analytics.

The second chapter starts with a temporal stability analysis of Couette flow between two concentric cylinders. This problem acts as a bridge between the spatial stability analysis of pipe flows in the first chapter and the vortex-wave interactions in Couette flow later in the second chapter. The flow in this problem is driven by a rotating inner cylinder and the static outer cylinder is positioned a small distance away. Once again the linear stability problem is tackled first and the minimum critical Taylor number is found to be 3389.9 and occurring when the axial wavenumber is 3.1266. These results tally with previous findings and the cellular toroidal vortices spaced along cylinder axis are also found. The linear stability results display exponential growth and decay when the system is not in equilibrium but the nonlinear results are more realistic. For subcritcal Taylor numbers the disturbances still decay to zero but in the supercritical region the disturbances attain a finite equilibrium solution. The nonlinear results reveal the importance of the nonlinear terms in the model.

The final but perhaps the most significant problem in this thesis is concerned with Couette flow in a parallel plate channel with a sinuous wave disturbance. The model developed in this thesis differs from those in previous papers as the vortex flow is fully time dependent and the problem is solved at each time-step and then marched forward. The wave is allowed to grow or decay but the shape of the wave is not dependent on time. This model is designed to specifically seek stationary waves. The model successfully recovers the longitudinal vortices that are synonymous with vortex-wave interactions and the slow longitudinal flow is drawn up between the rolls. The wave amplitude is modified to drive the rolls, which creates a streak and this has a wave which is neutral in growth in time. These equilibrium solutions are then followed to large time. The lower and upper branch solutions are found and shown to have close agreement with previous work.

These results show that the numerical investigations of 'self-sustained processes' are finite Reynolds number solutions analogous to vortex-wave interactions. These analytical solutions also represent important structures that appear in transitioning and turbulent flow and which are now better understood. Although this reduced version of the vortex-wave interactions was able to capture stationary results it was not possible to find time periodic solutions where the wave amplitude changes. These solutions have been found by numerical methods but attempts to find them here were unsuccessful. Further consideration of the model developed in this thesis could yield results in this area too.

A

Weakly nonlinear equations

The weakly nonlinear equations are the Navier-Stokes equations for a small disturbance that has been expanded into several amplitudes and harmonics. These equations are considered at each amplitude and harmonic separately, and the solution at each amplitude is used in the problem at the next order of amplitude. The disturbances are taken to be small, like in linear stability analysis, and the problem described below is for conditions close to the neutral stability curve.

The linear disturbance problem for the nonlinear pipe flow described in Chapter 3 is set in a cylinderical coordinate system, (x, r, θ), where x is in the streamwise direction, r the radial direction and θ the azimuthal direction. The equations from Chapter 3 that describe this problem, (3.33-3.36), are reproduced below,

$$\begin{aligned} &i\alpha uU - i\omega U + V\frac{\partial u}{\partial r} + \frac{W}{r}\frac{\partial u}{\partial \theta} + \frac{1}{R}\left[v\frac{\partial U}{\partial r} + \frac{w}{r}\frac{\partial U}{\partial \theta}\right] \\ &\quad = -\alpha i P + \frac{1}{R}\left[\frac{1}{r}\frac{\partial U}{\partial r} + \frac{\partial^2 U}{\partial r^2} + \frac{1}{r^2}\frac{\partial^2 U}{\partial \theta^2} - \alpha^2 U\right], \end{aligned} \tag{A.1}$$

$$i\alpha uV - i\omega V + \frac{1}{R}\left[V\frac{\partial v}{\partial r} + v\frac{\partial V}{\partial r} - \frac{2wW}{r} + \frac{w}{r}\frac{\partial V}{\partial \theta} + \frac{W}{r}\frac{\partial v}{\partial \theta}\right]$$
$$= -\frac{\partial P}{\partial r} + \frac{1}{R}\left[\frac{1}{r}\frac{\partial V}{\partial r} + \frac{\partial^2 V}{\partial r^2} + \frac{1}{r^2}\frac{\partial^2 V}{\partial \theta^2} - \frac{V}{r^2} - \frac{2}{r^2}\frac{\partial W}{\partial \theta} - \alpha^2 V\right], \quad \text{(A.2)}$$

$$i\alpha uW - i\omega W + \frac{1}{R}\left[V\frac{\partial w}{\partial r} + v\frac{\partial W}{\partial r} + \frac{wV}{r} + \frac{vW}{r} + \frac{w}{r}\frac{\partial W}{\partial \theta} + \frac{W}{r}\frac{\partial w}{\partial \theta}\right]$$
$$= -\frac{1}{r}\frac{\partial P}{\partial \theta} + \frac{1}{R}\left[\frac{1}{r}\frac{\partial W}{\partial r} + \frac{\partial^2 W}{\partial r^2} + \frac{1}{r^2}\frac{\partial^2 W}{\partial \theta^2} - \frac{W}{r^2} + \frac{2}{r^2}\frac{\partial V}{\partial \theta} - \alpha^2 W\right], \quad \text{(A.3)}$$

$$i\alpha U + \frac{1}{r}V + \frac{\partial V}{\partial r} + \frac{1}{r}\frac{\partial W}{\partial \theta} = 0. \quad \text{(A.4)}$$

Where the flow disturbance is $\mathbf{\Psi} = (U(r,\theta), V(r,\theta), W(r,\theta))\, E(x,t) + c.c.$, the basic flow is $\mathbf{u} = \left(u(r,\theta), \frac{v(r,\theta)}{R}, \frac{w(r,\theta)}{R}\right)$, $E = e^{i(\alpha x - \omega t)}$, α is the wavenumber and ω is the frequency. The pressure is taken to be $p = -\frac{4x}{R} + \epsilon(P(r,\theta)E(x,t) + c.c.)$, with ϵ an arbitrary small constant. This system of equations (A.1-A.4) can be represented as a matrix operator, L, on the disturbance vector, $\boldsymbol{\delta} = (U, V, W, P)$, such that $L\boldsymbol{\delta} = 0$.

$$L\boldsymbol{\delta} = \left(\begin{bmatrix} a_0 & a_1 \\ 0 & I \end{bmatrix} + \alpha \begin{bmatrix} 0 & a_2 \\ -I & 0 \end{bmatrix}\right)\begin{pmatrix} \boldsymbol{\delta} \\ \alpha\boldsymbol{\delta} \end{pmatrix} = \begin{pmatrix} 0 \end{pmatrix}, \quad \text{(A.5)}$$

where

$$a_0 = \begin{bmatrix} M & \frac{\partial u}{\partial r} & \frac{1}{r}\frac{\partial u}{\partial \theta} & 0 \\ 0 & \frac{1}{R}\left[\frac{\partial v}{\partial r} + \frac{1}{r^2}\right] + M & \frac{1}{R}\left[\frac{1}{r}\frac{\partial v}{\partial \theta} - \frac{2w}{r} + \frac{2}{r^2}\frac{\partial}{\partial \theta}\right] & \frac{\partial}{\partial r} \\ 0 & \frac{1}{R}\left[\frac{\partial w}{\partial r} + \frac{w}{r} - \frac{2}{r^2}\frac{\partial}{\partial \theta}\right] & \frac{1}{R}\left[\frac{v}{r} + \frac{1}{r}\frac{\partial w}{\partial \theta} + \frac{1}{r^2}\right] + M & \frac{1}{r}\frac{\partial}{\partial \theta} \\ 0 & \frac{1}{r} + \frac{\partial}{\partial r} & \frac{1}{r}\frac{\partial}{\partial \theta} & 0 \end{bmatrix}, \quad \text{(A.6)}$$

$$a_1 = \begin{bmatrix} iu & 0 & 0 & i \\ 0 & iu & 0 & 0 \\ 0 & 0 & iu & 0 \\ i & 0 & 0 & 0 \end{bmatrix}, \tag{A.7}$$

$$a_2 = \begin{bmatrix} \frac{1}{R} & 0 & 0 & 0 \\ 0 & \frac{1}{R} & 0 & 0 \\ 0 & 0 & \frac{1}{R} & 0 \\ 0 & 0 & 0 & 0 \end{bmatrix}, \tag{A.8}$$

$$M = -\omega i - \frac{1}{R}\left[-v\frac{\partial}{\partial r} - \frac{w}{r}\frac{\partial}{\partial \theta} + \frac{1}{r}\frac{\partial}{\partial r} + \frac{\partial^2}{\partial r^2} + \frac{1}{r^2}\frac{\partial^2}{\partial \theta^2}\right], \tag{A.9}$$

The weakly nonlinear expanded description of the small, $\mathcal{O}(\epsilon)$, perturbation, $\boldsymbol{\Psi}$, and its harmonics are described in (A.10).

$$\boldsymbol{\Psi} = \boldsymbol{\delta_1} e^{i(\alpha x - \omega t)} + \overline{\boldsymbol{\delta_1}} e^{-i(\overline{\alpha} x - \omega t)} + \epsilon \boldsymbol{\delta_0} + \epsilon \boldsymbol{\delta_2} e^{2i(\alpha x - \omega t)} + \epsilon \overline{\boldsymbol{\delta_2}} e^{-2i(\overline{\alpha} x - \omega t)} + \text{higher harmonics.} \tag{A.10}$$

The $\boldsymbol{\delta_j} = (U_j(r,\theta), V_j(r,\theta), W_j(r,\theta), P_j(r,\theta))$ terms, where $j = 0, 1, 2$, are the shape functions for the zeroth, first and second harmonics respectively, and the superscript 'overline' represents the complex conjugate. The first harmonic is largest, as the disturbance wave could always be rescaled in such a way that this is true, and the choice of the relative scalings of the other harmonics follows the work of Stuart[46] and Watson[56]. Continuing the path of their formulation, a complex amplitude A is introduced to the problem such that the unknown first harmonic disturbance shape can be represented as $\boldsymbol{\delta_1} = A\boldsymbol{\phi_1}$. In the problem presented here, where spatial stability analysis is the concern, A is taken to be a function of the streamwise coordinate, $A = A(X)$, where $X = \epsilon^2 x$ is a short streamwise length scale. It remains to define $\boldsymbol{\delta_0}$ and $\boldsymbol{\delta_2}$ in terms of A. This isn't a restricted choice at this point and the appropriate amplitude will be determined in due course. This weakly

nonlinear solution is only valid near the linear neutral stability curve, as the disturbances are still taken to be small, and to find new equilibrium solutions the starting point is the known equilibrium solution from the linear problem. If this solution is considered as the leading order term in the expansion of the first harmonic disturbance shape, and is denoted $\boldsymbol{\delta_{10}}$, then $\boldsymbol{\delta_1} = \boldsymbol{\delta_{10}} + \epsilon^2 \boldsymbol{\delta_{11}}$.

The linear stability solution when the growth rate is zero is known and the Reynolds number at this point is called the critical Reynolds number, R_c, and the spatial eigenvalue, $\alpha = \alpha_c$, is real. In the weakly nonlinear setup the goal is equilibrium solutions but a small amount of growth or decay is allowed. This growth or decay is contained within the amplitude term, A, which is dependent on X, and is therefore not exponential. These solutions may be slightly different to the linear solutions and for that reason the Reynolds number used in the nonlinear problem is different to the critical Reynolds number, $R = R_c + \epsilon^2 R_1$. When R is varied in this way there will be an amplifing or decaying growth rate and this is now contained in the amplitude term, A, which is dependent on X. This variable will also include any changes to the wavenumber. Upon substitution of the new expansions and disturbance harmonics to the Navier-Stokes equations, equations (3.4) and (3.5), a number of different orders of magnitude and harmonics appear. These should be resolved separately, and at the $\mathcal{O}(\epsilon)$ level the linear perturbation problem for $\boldsymbol{\phi_{10}}(r,\theta) = (U_1, V_1, W_1, P_1)$, as described in equations (A.1-A.4), is recovered. At the next level, $\mathcal{O}(\epsilon^2)$, there are zeroth and second harmonic perturbation problems. Without loss of generality, take $\boldsymbol{\delta_0} = f_1(A)\boldsymbol{\phi_0}(r,\theta)$ and $\boldsymbol{\delta_2} = f_2(A)\boldsymbol{\phi_2}(r,\theta)$, where $\boldsymbol{\phi_0}(r,\theta) = (U_0, V_0, W_0, P_0)$ and $\boldsymbol{\phi_2}(r,\theta) = (U_2, V_2, W_2, P_2)$, and f_1 and f_2 are functions used to balance the $\mathcal{O}(\epsilon^2)$ problems and are yet to be determined.

A.1 The zeroth harmonic

The zeroth harmonic terms are the mean flow correction and when they are grouped together the equations of momentum and the continuity equation at $\mathcal{O}(\epsilon^2)$ become:

$$f_1(A)\left(V_0\frac{\partial u}{\partial r}+\frac{W_0}{r}\frac{\partial u}{\partial \theta}+v\frac{\partial U_0}{\partial r}+\frac{w}{r}\frac{\partial U_0}{\partial \theta}-\frac{1}{R_c}\left[\frac{1}{r}\frac{\partial U_0}{\partial r}+\frac{\partial^2 U_0}{\partial r^2}+\frac{1}{r^2}\frac{\partial^2 U_0}{\partial \theta^2}\right]\right)$$
$$=-|A|^2\left(\overline{V_1}\frac{\partial U_1}{\partial r}+V_1\frac{\partial \overline{U_1}}{\partial r}+\frac{\overline{W_1}}{r}\frac{\partial U_1}{\partial \theta}+\frac{W_1}{r}\frac{\partial \overline{U_1}}{\partial \theta}+(i\alpha_c-i\overline{\alpha_c})\overline{U_1}U_1\right), \tag{A.11}$$

$$\begin{aligned}f_1(A)\Bigg(&V_0\frac{\partial v}{\partial r}+v\frac{\partial V_0}{\partial r}-\frac{2wW_0}{r}+\frac{w}{r}\frac{\partial V_0}{\partial \theta}+\frac{W_0}{r}\frac{\partial v}{\partial \theta}+\frac{\partial P_0}{\partial r}\\&-\frac{1}{R_c}\left[\frac{1}{r}\frac{\partial V_0}{\partial r}+\frac{\partial^2 V_0}{\partial r^2}+\frac{1}{r^2}\frac{\partial^2 V_0}{\partial \theta^2}-\frac{V_0}{r^2}-\frac{2}{r^2}\frac{\partial W_0}{\partial \theta}\right]\Bigg)\\&=-|A|^2\Bigg(\overline{V_1}\frac{\partial V_1}{\partial r}+V_1\frac{\partial \overline{V_1}}{\partial r}+\frac{\overline{W_1}}{r}\frac{\partial V_1}{\partial \theta}\\&+\frac{W_1}{r}\frac{\partial \overline{V_1}}{\partial \theta}+i\alpha_c\overline{U_1}V_1-i\overline{\alpha_c}U_1\overline{V_1}-\frac{2W_1\overline{W_1}}{r}\Bigg),\end{aligned} \tag{A.12}$$

$$\begin{aligned}f_1(A)\Bigg(&V_0\frac{\partial w}{\partial r}+v\frac{\partial W_0}{\partial r}+\frac{wV_0}{r}+\frac{vW_0}{r}+\frac{w}{r}\frac{\partial W_0}{\partial \theta}+\frac{W_0}{r}\frac{\partial w}{\partial \theta}+\frac{1}{r}\frac{\partial P_0}{\partial \theta}\\&-\frac{1}{R_c}\left[\frac{1}{r}\frac{\partial W_0}{\partial r}+\frac{\partial^2 W_0}{\partial r^2}+\frac{1}{r^2}\frac{\partial^2 W_0}{\partial \theta^2}-\frac{W_0}{r^2}+\frac{2}{r^2}\frac{\partial V_0}{\partial \theta}\right]\Bigg)\\&=-|A|^2\Bigg(\overline{V_1}\frac{\partial W_1}{\partial r}+V_1\frac{\partial \overline{W_1}}{\partial r}+\frac{\overline{W_1}}{r}\frac{\partial W_1}{\partial \theta}+\frac{W_1}{r}\frac{\partial \overline{W_1}}{\partial \theta}\\&+i\alpha_c\overline{U_1}W_1-i\overline{\alpha_c}U_1\overline{W_1}+\frac{V_1\overline{W_1}}{r}+\frac{\overline{V_1}W_1}{r}\Bigg),\end{aligned} \tag{A.13}$$

$$\frac{1}{r}V_0+\frac{\partial V_0}{\partial r}+\frac{1}{r}\frac{\partial W_0}{\partial \theta}=0. \tag{A.14}$$

It can be seen immediately that f_1 must be equal to $|A|^2$ in order to balance the equations, and therefore $\boldsymbol{\delta_0} = |A|^2\boldsymbol{\phi_0}(r,\theta)$. Although the small order term in the Reynolds number expansion is order ϵ^2, and the $\mathcal{O}(1)$ mean flow

terms have no harmonic, the product of these terms do not appear in the equations above. This is because the $\epsilon^2 R_1/R_c$ terms could be absorbed into the mean flow by the definition of the normalisation. The right hand side of equations (A.11-A.14) are known from the solutions of (A.1-A.4) and the system of linear equations can be solved directly. The boundary conditions, which need special consideration because of the coordinate system singularity at the centre of the pipe, are the same as the conditions for the linear problem that were described in the Numerical methods Chapter in subsection 2.3.

A.2 The second harmonic

For the second harmonic the equations of momentum and the continuity equation take the following form,

$$\begin{aligned} f_2(A)\Bigg(&2i\alpha_c u U_2 - 2i\omega U_2 + V_2\frac{\partial u}{\partial r} + \frac{W_2}{r}\frac{\partial u}{\partial \theta} + v\frac{\partial U_2}{\partial r} + \frac{w}{r}\frac{\partial U_2}{\partial \theta} + 2i\alpha_c P_2 \\ &-\frac{1}{R_c}\left[\frac{1}{r}\frac{\partial U_2}{\partial r} + \frac{\partial^2 U_2}{\partial r^2} + \frac{1}{r^2}\frac{\partial^2 U_2}{\partial \theta^2} - 4\alpha_c^2 U_2\right]\Bigg) \\ &= -A^2\left(V_1\frac{\partial U_1}{\partial r} + \frac{W_1}{r}\frac{\partial U_1}{\partial \theta} + i\alpha_c U_1^2\right), \end{aligned} \tag{A.15}$$

$$\begin{aligned} f_2(A)\Bigg(&2i\alpha_c u V_2 - 2i\omega V_2 + V_2\frac{\partial v}{\partial r} + v\frac{\partial V_2}{\partial r} - \frac{2wW_2}{r} + \frac{w}{r}\frac{\partial V_2}{\partial \theta} + \frac{W_2}{r}\frac{\partial v}{\partial \theta} + \frac{\partial P_2}{\partial r} \\ &-\frac{1}{R_c}\left[\frac{1}{r}\frac{\partial V_2}{\partial r} + \frac{\partial^2 V_2}{\partial r^2} + \frac{1}{r^2}\frac{\partial^2 V_2}{\partial \theta^2} - \frac{V_2}{r^2} - \frac{2}{r^2}\frac{\partial W_2}{\partial \theta} - 4\alpha_c^2 V_2\right]\Bigg) \\ &= -A^2\left(V_1\frac{\partial V_1}{\partial r} + \frac{W_1}{r}\frac{\partial V_1}{\partial \theta} + i\alpha_c U_1 V_1 - \frac{W_1^2}{r}\right), \end{aligned} \tag{A.16}$$

$$
\begin{aligned}
f_2(A)\Bigg(&2i\alpha_c u W_2 - 2i\omega W_2 + V_2\frac{\partial w}{\partial r} + v\frac{\partial W_2}{\partial r} + \frac{wV_2}{r} \\
&+\frac{vW_2}{r} + \frac{w}{r}\frac{\partial W_2}{\partial \theta} + \frac{W_2}{r}\frac{\partial w}{\partial \theta} + \frac{1}{r}\frac{\partial P_2}{\partial \theta} \\
-\frac{1}{R_c}&\left[\frac{1}{r}\frac{\partial W_2}{\partial r} + \frac{\partial^2 W_2}{\partial r^2} + \frac{1}{r^2}\frac{\partial^2 W_2}{\partial \theta^2} - \frac{W_2}{r^2} + \frac{2}{r^2}\frac{\partial V_2}{\partial \theta} - 4\alpha_c^2 W_2\right]\Bigg) \\
&= -A^2\left(V_1\frac{\partial W_1}{\partial r} + \frac{W_1}{r}\frac{\partial W_1}{\partial \theta} + i\alpha_c U_1 W_1 + \frac{V_1 W_1}{r}\right),
\end{aligned}
\tag{A.17}
$$

$$
2i\alpha_c U_2 + \frac{1}{r}V_2 + \frac{\partial V_2}{\partial r} + \frac{1}{r}\frac{\partial W_2}{\partial \theta} = 0. \tag{A.18}
$$

In this case the nonlinear terms on the right hand side have the amplitude A^2, implying that $\boldsymbol{\delta_2} = A^2\boldsymbol{\phi_2}(r,\theta)$. Once again the right hand side of the equations, (A.15-A.18), are known and the system of linear equations can be solved directly. The boundary conditions are also the same as in the linear problem.

A.3 The first harmonic correction

Now that $\boldsymbol{\phi_0}$ and $\boldsymbol{\phi_2}$ have been found the first harmonic problem at the $\mathcal{O}(\epsilon^3)$ level can be considered. These equations will provide the solution to the linear disturbance correction terms, $\boldsymbol{\phi_{11}}$, where $\boldsymbol{\delta_1} = A\boldsymbol{\phi_1} = A\boldsymbol{\phi_{10}} + A\epsilon^2\boldsymbol{\phi_{11}}$. The problem can be written $L\boldsymbol{\phi_{11}} = -\boldsymbol{h}(\boldsymbol{\phi_{10}}, \boldsymbol{\phi_0}, \boldsymbol{\phi_2})$, where L is the matrix operator from equation (A.5) and $\boldsymbol{h} = (h_x, h_r, h_\theta, h_c)$. $\boldsymbol{h}$ is described by the equations (A.19-A.22).

$$
\begin{aligned}
h_x = \frac{\partial A}{\partial X}\left(uU_1 + P_1 - \frac{2}{R_c}i\alpha_c U_1\right) \\
+\frac{AR_1}{R_c}\left(i\alpha_c u U_1 - i\omega U_1 + V_1\frac{\partial u}{\partial r} + \frac{W_1}{r}\frac{\partial u}{\partial \theta} + v\frac{\partial U_1}{\partial r} + \frac{w}{r}\frac{\partial U_1}{\partial \theta} + i\alpha_c P_1\right) \\
+A|A|^2\left(V_1\frac{\partial U_0}{\partial r} + V_0\frac{\partial U_1}{\partial r} + \frac{W_1}{r}\frac{\partial U_0}{\partial \theta} + \frac{W_0}{r}\frac{\partial U_1}{\partial \theta} + i\alpha_c U_1 U_0\right. \\
\left.+\overline{V_1}\frac{\partial U_2}{\partial r} + V_2\frac{\partial \overline{U_1}}{\partial r} + \frac{\overline{W_1}}{r}\frac{\partial U_2}{\partial \theta} + \frac{W_2}{r}\frac{\partial \overline{U_1}}{\partial \theta} + i(2\alpha_c - \overline{\alpha_c})\overline{U_1}U_2\right),
\end{aligned}
\tag{A.19}
$$

$$
\begin{aligned}
h_r = \frac{\partial A}{\partial X}\left(uV_1 - \frac{2}{R_c}i\alpha_c V_1\right) \\
+\frac{AR_1}{R_c}\left(i\alpha_c u V_1 - i\omega V_1 + V_1\frac{\partial v}{\partial r} + v\frac{\partial V_1}{\partial r} - \frac{2wW_1}{r} + \frac{w}{r}\frac{\partial V_1}{\partial \theta} + \frac{W_1}{r}\frac{\partial v}{\partial \theta} + \frac{\partial P_1}{\partial r}\right) \\
+A|A|^2\left(V_0\frac{\partial V_1}{\partial r} + V_1\frac{\partial V_0}{\partial r} + \frac{W_0}{r}\frac{\partial V_1}{\partial \theta} + \frac{W_1}{r}\frac{\partial V_0}{\partial \theta} + i\alpha_c U_0 V_1 - \frac{2W_1W_0}{r}\right. \\
\left.+\overline{V_1}\frac{\partial V_2}{\partial r} + V_2\frac{\partial \overline{V_1}}{\partial r} + \frac{\overline{W_1}}{r}\frac{\partial V_2}{\partial \theta} + \frac{W_2}{r}\frac{\partial \overline{V_1}}{\partial \theta} + 2i\alpha_c\overline{U_1}V_2 - i\overline{\alpha_c}U_2\overline{V_1} - \frac{2W_2\overline{W_1}}{r}\right),
\end{aligned}
\tag{A.20}
$$

$$
\begin{aligned}
h_\theta = \frac{\partial A}{\partial X}\left(uW_1 - \frac{2}{R_c}i\alpha_c W_1\right) \\
+\frac{AR_1}{R_c}\left(i\alpha_c u W_1 - i\omega W_1 + V_1\frac{\partial w}{\partial r} + v\frac{\partial W_1}{\partial r} + \frac{wV_1}{r} + \frac{vW_1}{r}\right. \\
\left.+\frac{w}{r}\frac{\partial W_1}{\partial \theta} + \frac{W_1}{r}\frac{\partial w}{\partial \theta} + \frac{1}{r}\frac{\partial P_1}{\partial \theta}\right) \\
+A|A|^2\left(V_0\frac{\partial W_1}{\partial r} + V_1\frac{\partial W_0}{\partial r} + \frac{W_0}{r}\frac{\partial W_1}{\partial \theta} + \frac{W_1}{r}\frac{\partial W_0}{\partial \theta}\right. \\
+i\alpha_c U_0 W_1 + \frac{V_1W_0}{r} + \frac{V_0W_1}{r} + \overline{V_1}\frac{\partial W_2}{\partial r} + V_2\frac{\partial \overline{W_1}}{\partial r} + \frac{\overline{W_1}}{r}\frac{\partial W_2}{\partial \theta} + \frac{W_2}{r}\frac{\partial \overline{W_1}}{\partial \theta} \\
\left.+2i\alpha_c\overline{U_1}W_2 - i\overline{\alpha_c}U_2\overline{W_1} + \frac{V_2\overline{W_1}}{r} + \frac{\overline{V_1}W_2}{r}\right),
\end{aligned}
\tag{A.21}
$$

$$h_c = \frac{dA}{dX} U_1. \tag{A.22}$$

To progress in solving this problem the differential equation for the amplitude of the nonlinear terms, $\boldsymbol{h}$, must be considered. The bounded matrix operator on the function $\boldsymbol{\phi_{11}}$, denoted as L, has the adjoint operator L^* and there is an adjoint function, $\hat{\mathbf{\Phi}}$, such that $L^*\hat{\mathbf{\Phi}} = 0$. Consider multipling $L\boldsymbol{\phi_{11}}$ by $\hat{\mathbf{\Phi}}$ and taking the integral over the area of the pipe. The properties of this bounded matrix operator are such that the integral is equal to $\boldsymbol{\phi_{11}}$ multiplied by $L^*\hat{\mathbf{\Phi}}$, which is known to be zero.

$$\int\int \hat{\mathbf{\Phi}} \cdot L\boldsymbol{\phi_{11}} r \partial r \partial\theta = \int\int \boldsymbol{\phi_{11}} \cdot L^*\hat{\mathbf{\Phi}} r \partial r \partial\theta = 0. \tag{A.23}$$

It follows that there is only a valid solution if the solvability property (A.24) is satisfied,

$$\int\int \hat{\mathbf{\Phi}} \cdot \boldsymbol{h} r \partial r \partial\theta = 0. \tag{A.24}$$

A.4 The adjoint problem and the solvability condition

Calculating the adjoint operator is an exercise in integrating by parts and below are the four equations that comprise the problem $L^*\hat{\mathbf{\Phi}} = 0$, with $\hat{\mathbf{\Phi}}(r,\theta) = (\hat{u}(r,\theta), \hat{v}(r,\theta), \hat{w}(r,\theta), \hat{p}(r,\theta))$.

$$\begin{aligned} &-i\overline{\alpha_c} u\hat{u} + i\overline{\omega}\hat{u} - \hat{u}\frac{\partial v}{\partial r} - v\frac{\partial \hat{u}}{\partial r} - \frac{\hat{u}}{r}\frac{\partial w}{\partial \theta} - \frac{w}{r}\frac{\partial \hat{u}}{\partial \theta} \\ &= \overline{\alpha_c} i\hat{p} + \frac{1}{R_c}\left[\frac{\partial^2 \hat{u}}{\partial r^2} - \frac{1}{r}\frac{\partial \hat{u}}{\partial r} + \frac{1}{r^2}\frac{\partial^2 \hat{u}}{\partial \theta^2} + \frac{\hat{u}}{r^2} - \overline{\alpha_c}^2 \hat{u}\right], \end{aligned} \tag{A.25}$$

$$\hat{u}\frac{\partial u}{\partial r} - i\overline{\alpha_c}u\hat{v} + i\overline{\omega}\hat{v} - v\frac{\partial \hat{v}}{\partial r} - \frac{w}{r}\frac{\partial \hat{v}}{\partial \theta} - \frac{\hat{v}}{r}\frac{\partial w}{\partial \theta} + \hat{w}\frac{\partial w}{\partial r} + \frac{w\hat{w}}{r}$$
$$= \frac{\partial \hat{p}}{\partial r} - \frac{\hat{p}}{r} + \frac{1}{R_c}\left[\frac{\partial^2 \hat{v}}{\partial r^2} - \frac{1}{r}\frac{\partial \hat{v}}{\partial r} + \frac{1}{r^2}\frac{\partial^2 \hat{v}}{\partial \theta^2} - \frac{2}{r^2}\frac{\partial \hat{w}}{\partial \theta} - \overline{\alpha_c}^2\hat{v}\right], \tag{A.26}$$

$$\frac{\hat{u}}{r}\frac{\partial u}{\partial \theta} - i\overline{\alpha_c}u\hat{w} + i\overline{\omega}\hat{w} + \frac{\hat{v}}{r}\frac{\partial v}{\partial \theta} - \hat{w}\frac{\partial v}{\partial r} - v\frac{\partial \hat{w}}{\partial r} - \frac{2w\hat{v}}{r} + \frac{v\hat{w}}{r} - \frac{w}{r}\frac{\partial \hat{w}}{\partial \theta}$$
$$= \frac{1}{r}\frac{\partial \hat{p}}{\partial \theta} + \frac{1}{R_c}\left[\frac{\partial^2 \hat{w}}{\partial r^2} - \frac{1}{r}\frac{\partial \hat{w}}{\partial r} + \frac{1}{r^2}\frac{\partial^2 \hat{w}}{\partial \theta^2} + \frac{2}{r^2}\frac{\partial \hat{v}}{\partial \theta} - \overline{\alpha_c}^2\hat{w}\right], \tag{A.27}$$

$$-i\overline{\alpha_c}\hat{u} - \frac{\partial \hat{v}}{\partial r} - \frac{1}{r}\frac{\partial \hat{w}}{\partial \theta} = 0. \tag{A.28}$$

The boundary conditions must ensure that the coordinate conditions are met and the concomitant is equal to zero. In this case those conditions are $\hat{u}, \hat{v}, \hat{w} = 0$ at $r = 0$ and $r = 1$. $\hat{p} = 0$ at the centre of the pipe but at the pipe wall the streamwise momentum equation becomes

$$\overline{\alpha_c}i\hat{p} + \frac{1}{Re}\frac{\partial^2 \hat{u}}{\partial r^2} = -\frac{\partial \hat{u}}{\partial r}\left(\overline{v} - \frac{1}{R_c}\right). \tag{A.29}$$

By solving the adjoint problem, $L^*\hat{\mathbf{\Phi}} = 0$, a linear system of equations, the unknown adjoint function is found. This solution enables progress to be made in finding the amplitude of the disturbances, A, via the integral solvability condition (A.24), $< \hat{\mathbf{\Phi}}, \boldsymbol{h} >= 0$.

References

[1] Bansal, J. L. 1966. Laminar flow through a uniform circular pipe with small suction. *Proc. Indian Nat. Sci. Aca.* vol. 32A, art. 06.

[2] Batchelor, G. K., Gill, A. E. 1962. Analysis of the stability of axisymmetric jets. *J. Fluid Mech.* vol. 14, pp 529-550.

[3] Blackburn, H. M, Hall, P., Sherwin, S. J 2013. Lower branch equilibria in Couette flow: the emergence of canonical states for arbitrary shear flows. *J. Fluid Mech. Rapids* vol. 726.

[4] Boyd, J. P. 2000. Chebyshev and Fourier Spectral Methods. *Dover Publications.*

[5] Davey, A. 1962. The growth of Taylor vortices in flow between rotating cylinders. *J. Fluid Mech.* vol. 14, pp 336-368.

[6] Davey, A. 1978. On Itohs finite amplitude stability theory for pipe flow. *J. Fluid Mech.* vol. 86, part 4, pp 695-703.

[7] Davey, A., Drazin, P. G. 1969. The stability of Poiseuille flow in a pipe. *J. Fluid Mech.* vol. 36, pp 209-218.

[8] Davey, A., Nguyen, H. P. F. 1971. Finite-amplitude stability of pipe flow. *J. Fluid Mech.* vol. 45, part 4, pp 701-720.

[9] Deguchi, K., Hall, P. 2014. The high-Reynolds-number asymptotic development of nonlinear equilibrium states in plane Couette flow. *J. Fluid Mech.* vol. 750, pp 99-112.

[10] Deguchi, K., Hall, P. 2016. On the instability of vortex-wave interaction states. *J. Fluid Mech.* vol. 802, pp 634-666.

[11] Donnelly, R. J, Simon, N. J 1960. An empirical torque relation for supercritical flow between rotating cylinders. *J. Fluid Mech.* vol. 7, pp 401-418.

[12] Faisst, H., Eckhardt, B. 2003. Traveling waves in pipe flow. *Phys. Rev. Lett.* vol. 91, 224502.

[13] Farrell, B. F, Ioannou, P. J 2012. Dynamics of streamwise rolls and streaks in turbulent wall-bounded shear flow. *J. Fluid Mech.* vol. 708, pp 149-196.

[14] Gaster, M. 1974. On the effects of boundary-layer growth on flow stability. *J. Fluid Mech.* vol. 66, pp 465-480.

[15] Garg, V. K., Rouleau, W. T. 1972. Linear spatial stability of pipe Poiseuille flow. *J. Fluid Mech.* vol. 54, pp 113-127.

[16] Gill, A. E. 1965. On the behaviour of small disturbances to Poiseuille flow in a circular pipe. *J. Fluid Mech.* vol. 21, part 1, pp 145-172.

[17] Hagen, G. H. L. 1839. Über die Bewegung des Wassers in engen cylindrischen Röhren. *Annalen der Physik und Chemie* vol. 16, pp 423.

[18] Hall, P. 1975. The stability of unsteady cylinder flows. *J. Fluid Mech.* vol. 67, part 1, pp 29-63.

[19] Hall, P. 1982. Taylor-Gortler vortices in fully developed or boundary-layer flows: linear theory. *J. Fluid Mech.* vol. 124, pp 475-494.

[20] Hall, P. 1983. The linear development of Görtler vortices in growing boundary layers. *J. Fluid Mech.* vol. 130, pp 41-58.

[21] Hall, P., Horseman, N. J. 1991. The linear inviscid secondary instability of longitudinal vortex structures in boundary layers. *J. Fluid Mech.* vol. 232, pp 357-375.

[22] Hall, P., Sherwin, S. 2010. Streamwise vortices in shear flows: harbingers of transition and the skeleton of coherent structures. *J. Fluid Mech.* vol. 661, pp 178-205.

[23] Hall, P., Smith, F. T. 1988. The nonlinear interaction of Tollmien-Schlichting waves and Taylor-Görtler vortices in curved channel flows. *Proc. R. Soc. Lond.* vol. 417, pp 255-282.

[24] Hall, P., Smith, F. T. 1989. Nonlinear Tollmien-Schlichting/vortex interaction in boundary layers. *Eur. J. Mech.* B8, pp 179-205.

[25] Hall, P., Smith, F. T. 1990. Near planar TS waves and longitudinal vortices in channel flow: nonlinear interaction and focusing. *ICASE Rep.* pp 5-39.

[26] Hall, P., Smith, F. T. 1991. On strongly nonlinear vortex-wave interactions in boundary-layer transition. *J. Fluid Mech.* vol. 227, pp 641-666.

[27] Isoni, A. 2014. Vortex wave interaction theory to understand self-sustaining processes in transitional flows. *PhD thesis.*

[28] Itoh, N. 1977. Nonlinear stability of parallel flows with subcritical Reynolds numbers. Part 1. An asymptotic theory valid for small amplitude disturbances. *J. Fluid Mech.* vol. 82, part 3, pp 465-467.

[29] Itoh, N. 1977. Nonlinear stability of parallel flows with subcritical Reynolds numbers. Part 2. Stability of pipe Poiseuille flow to finite axisymmetric disturbances. *J. Fluid Mech.* vol. 82, part 3, pp 469-479.

[30] Karniadakis, G., Sherwin, S. 2005. Spectral/hp element methods for computational fluid dynamics. *Oxford University Press* 2nd edition.

[31] Kawahara, G., Kida, S. 2001. Periodic motion embedded in plane Couette turbulence: regeneration cycle and burst. *J. Fluid Mech.* vol. 449, pp 291-300.

[32] Landau, L. D. 1944. On the problem of turbulence. *C.R. Acad. Sci. U.S.S.R.* vol. 44, pp 311-314.

[33] Mack, L. M. 1976. A numerical study of the temporal eigenvalue spectrum of the Blasius boundary layer. *J. Fluid Mech.* vol. 73, Issue 03, pp 497-520.

[34] Nagata, M. 1990. Three-dimensional finite-amplitude solutions in plane Couette flow: bifurcation from infinity. *J. Fluid Mech.* vol. 217, pp 519-527.

[35] Neiland, V. Y. 1969. Theory of laminar boundary layer separation in supersonic flow. *Izv. AN SSSR. Mekhanika Zhidkosti i Gaza* vol. 4 (4), pp 53-57.

[36] Orszag, S. A. 1971. Accurate solution of the Orr-Sommerfeld stability equation. *J. Fluid Mech.* vol. 50, part 4, pp 659-703.

[37] Ozcakir, O. 2014. Vortex-Wave Solutions of Navier-Stokes Equations in a Cylindrical Pipe. *PhD Thesis, The Ohio State University.*

[38] Ozcakir, O., Tanveer, S., Hall, P., Overman, E. A. 2016. Travelling wave states in pipe flow. *J. Fluid Mech.* vol. 791, pp 284-328.

[39] Poiseuille, J. L. M. 1840. Recherches experimentelles sur les mouvement des liquides dans les tubes de tres petits diametres. *C. R. Acad. Sci.* vol. 11, pp 961.

[40] Prandtl, L. 1904. Über Flüssigkeitsbewegung bei sehr kleiner. *Proc. Third. Int. Congr. Math.* (Heidelberg), pp. 484-491.

[41] Reynolds, O. F. R. S. 1883. An experimental investigation of the circumstances which determine whether the motion of water shall be direct or sinuous, and of the law of resistance in parallel channels. *Phil. Trans. R. Soc.* vol. 174, pp935-982.

[42] Saric, W. S., Nayfeh, A. H. 1975. Non-parallel stability of boundary-layer flows. *Phys. Fluids* vol. 18.

[43] Smith, F. T. 1979. Instability of flow through pipes of general cross-section. Part 1. *Mathematika* vol. 26, pp 187-210.

[44] Squire, H. B. 1933. On the stability for three-dimensional disturbances of viscous fluid flow between parallel plates. *Proc. R. Soc.* vol. 142, issue 847, pp. 621-628.

[45] Stewartson, K., Williams, P. G. 1969. Self-induced separation. *Proc. Roy. Soc. A.* vol. 312, pp 181-206.

[46] Stuart, J. T. 1960. On the non-linear mechanics of wave disturbances in stable and unstable parallel flows. Part 1. The basic behaviour in plane Poiseuille flow. *J. Fluid Mech.* vol. 9, pp 353-370.

[47] Stuart, J. T. 1971. Nonlinear stability theory. *Annu. Rev Fluid Mech.* vol. 3, pp 347-370.

[48] Swearingen, J. D., Blackwelder, R. F. 1960. The growth and breakdown of streamwise vortices in the presence of a wall. *J. Fluid Mech.* vol. 182, pp 255-290.

[49] Taylor, G. I., 1923. Stability of a Viscous Liquid contained between Two Rotating Cylinders. *Phil. Trans. R. Soc.* vol. 223, pp. 289-343.

[50] Taylor, G. I., 1936. Fluid Friction between Rotating Cylinders. I. Torque Measurements. *Proc. R. Soc.* vol. 157, pp. 546-564.

[51] Thomas, V. L., Lieu, B. K, Jovanović, M. R, Farrell, B. F, Ioannou, P. J, Gayme1, D. F , 2014. Self-sustaining turbulence in a restricted nonlinear model of plane Couette flow. *Phys. Fluids* vol. 26, issue 10.

[52] Waleffe, F. 1997. On a self-sustaining process in shear flows. *Phys. Fluids* vol. 9, pp. 883-900.

[53] Waleffe, F. 2001. Exact coherent structures in channel flow. *J. Fluid Mech.* vol. 435, pp 93-102.

[54] Waleffe, F. 2003. Homotopy of exact coherent structures in plane shear flows. *Phys. Fluids* vol. 15, no. 6, pp. 1517-1534.

[55] Wang, J., Gibson, J., Waleffe, F. 2007. Lower Branch Coherent States in Shear Flows: Transition and Control. *Phys. Rev. Lett.* vol. 98 (20), 204501.

[56] Watson, J. 1960. On the non-linear mechanics of wave disturbances in stable and unstable parallel flows. Part 2. The development of a solution

for plane Poiseuille flow and for plane Couette flow. *J. Fluid Mech.* vol. 9, pp 371-389.

[57] Wedin, H., Kerswell, R. R. 2004. Exact coherent structures in pipe flow: travelling wave solutions. *J. Fluid Mech.* vol. 508, pp 333-371.

[58] Zaturska, M. B., Banks, W. H. H. 1995. Flow in a pipe driven by suction at an accelerating wall. *Acta Mechanica* vol. 110, pp 111-121.